Rheology and deformation of glass under extreme conditions

Dissertation
Zur Erlangung des akademischen Grades

"Doktor der Naturwissenschaften"
Im Promotionsfach Geologie/Paläontologie

Am Fachbereich 09 für Chemie, Pharmazie und Geowissenschaften
der Johannes Gutenberg-Universität Mainz

von

Linfeng Ding

geboren in Zhejiang, China

JOHANNES GUTENBERG UNIVERSITÄT MAINZ

JG|U

Mainz, 2018

Dekan:

1. Berichterstatter:

2. Berichterstatter:

Datum der mündlichen Prüfung: 29.06.2018

Declaration

I hereby declare that the contents of this dissertation are original and have not been submitted in whole or in part for consideration for any other degree or qualification in this, or any other University. This dissertation is the result of my own work, except where specifically indicated in the text.

Erklärung

Ich versichere hiermit gemäß §10 Abs. 3d der Promotionsordnung des Fachbereichs 09 (Chemie, Pharmazie und Geowissenschaften) der Johannes Gutenberg-Universität Mainz vom 24.07.2007, die als Dissertation vorgelegte Arbeit selbständig und nur unter Verwendung der in der Arbeit angegebenen Hilfsmittel verfasst zu haben. Ich habe oder hatte die hier als Dissertation vorgelegte Arbeit nicht als Prüfungsarbeit für eine staatliche oder andere wissenschaftliche Prüfung eingereicht. Ich hatte weder die jetzt als Dissertation vorgelegte Arbeit noch Teile davon bei einer anderen Fakultät bzw. einem anderen Fachbereich als Dissertation eingereicht.

_____

(Linfeng Ding)
Mainz, 20. 05. 2018

Abstract

Hardness measurements performed at room temperature have proven that glass can flow under elevated pressure. During industrial glass production processes, the actual distribution of stress components in the glass during scribing remains, to date, poorly quantified, and thus continues to be challenging to model numerically. To better quantify the viscous contribution to the rheology of glass, the effect of pressure on the viscosity and structural relaxation of glass, needs to be quantified experimentally by *in situ* deformation measurements.

In this thesis, I performed experiments and models to study: (i) the volumetric relaxation of glass after high-pressure treatment above the glass transition region in Piston-cylinder apparatus and volume recovery measurements; (ii) the uniaxial deformation of glass under high pressure in Paterson press; (iii) the deviatoric torsional deformation of glass in high-pressure torsion apparatus.

In Chapter 3, I developed a simplified and effective pressure cell together with an experimental procedure to compress samples of SCHOTT N-BK7® glass under static high pressures in a piston-cylinder apparatus. Results from the density and volume recovery measurements show that the glass samples were effectively densified in piston-cylinder apparatus with the density at room temperature increases linearly with frozen-in pressure. To explain the experimental data, a mathematical model was developed based on a suggestion by Gupta (1988) with two internal parameters, named fictive temperature (T_f) and fictive pressure (P_f), which fits the experimental data well.

In Chapter 4, I experimentally quantified the effect of pressure and temperature on the viscosity of SCHOTT N-BK7® glass, by performing *in situ* deformation experiments at temperatures between 550 and 595 °C and confining pressures between 100 MPa and 300 MPa. Experiments were performed at constant displacement rates to produce almost constant strain rates between 9.70×10^{-6} s^{-1} and 4.98×10^{-5} s^{-1}. The resulting net axial stresses range from 81 MPa to 802 MPa, and the finite strains range from 1.4 % to 8.9 %. The mechanical results show that the SCHOTT N-BK7® glass is viscoelastic near the glass transition temperature at 300 MPa of confining pressure. To elucidate the data, we incorporated both 1-element and 2-element generalized Maxwell viscoelastic models in an inversion approach, for which we provide MATLAB scrips. Results show that the 2-element Maxwell model fits the experimental data well. The stress decreases with increasing temperature at 300 MPa and the temperature dependence yields a similar activation energy (601±10 $kJ \cdot mol^{-1}$ or $\Delta H/R = 7.2 \times 10^4$ K) to a

previously reported value at 1-atm (615 kJ·mol^{-1} or $\Delta H/R = 7.4\times10^4$ K). The SCHOTT N-BK7® glass shows a limited linear increase of viscosity with increasing pressure of ~0.1 $\log_{10}$(Pa·s)/100 MPa, which is in agreement with the results from Chapter 3.

Finally, in Chapter 5, I applied a high-pressure torsion (HPT) apparatus to deform SCHOTT SF6® glass and attempted to quantify the effect of pressure and temperature on the shear deformation of glass subjected to pressures from 0.3 GPa to 7 GPa and temperatures from 25 ℃ to 496 ℃. Results show that the plastic yield deformation was occurring during the HPT experiments on the SF6 glass at elevated temperature from 350 ℃ to 496 ℃. The yield stress of SF6 glass decreases with increasing temperature and decreasing pressure. An extended Arrhenius model with one set of parameters, namely infinite yield stress Y_0=0.17±0.1 GPa, activation energy E_a=4.8±0.5 kJ·mol^{-1} and activation volume V_a=1.4±0.2 cm^3·mol^{-1}, can explain the experimental results well.

Overall, this work demonstrates the significance of studying the pressure dependence of the rheology of glass. The experiments and models presented can benefit to the understanding on the rheology of glass under extreme conditions. Yet, linking yield stress and viscosity remains an open question.

Kurzfassung

Härte-Messungen bei Raumtemperatur haben gezeigt, dass Glas unter erhöhtem Druck fließen kann. Die genaue Spannungsverteilung beim Anritzen von industriell gefertigtem Glas ist bisher nicht ausreichend verstanden. Um den Einfluss viskoser Eigenschaften auf die Rheologie von Glas zu verstehen, muss der Effekt von Druck auf die Viskosität sowie die strukturelle Relaxation experimentell durch in situ Deformations-Messungen quantifiziert werden.

In dieser Arbeit werden verschiedene Experimente und Modellierungen durchgeführt, um folgendes genauer zu untersuchen: (i) Die volumetrische Relaxation von Glas nach einer oberhalb des Übergangsbereichs ausgeführten Hochdruck-Behandlung im Piston-Zylinder und Volume-Recovery-Messungen; (ii) Die einachsige Deformation von Glas in einem Hochdruck Peterson-Presse; (iii) Die deviatorisch-torsionale Deformation von Glas in einem Hochdruck Torsions-Apparat.

Zunächst wird in Kapitel 3 eine vereinfachte, effektive Druck-Zelle entwickelt und eine experimentelle Prozedur erarbeitet, um Proben von SCHOTT N-BK7® Glas unter statischem Hochdruck in einem Piston-Zylinder zu verdichten. Die Ergebnisse der Dichte- und Volume-Recovery-Messungen haben gezeigt, dass die Glas-Proben effektiv im Piston-Zylinder verdichtet wurden, wobei die Dichte bei Raumtemperatur linear zum Druck ansteigt. Um diese Experimente erklären zu können, wurde ein mathematisches Modell auf Grundlage von Gupta (1988) mit zwei internen Parametern - fiktive Temperatur (T_f) und fiktiver Druck (P_f) - entwickelt, das die experimentellen Daten hinreichend beschreibt.

In Kapitel 4 wird der Effekt von Druck und Temperatur auf die Viskosität von SCHOTT N-BK7® Glas über in situ Deformations-Experimente bei Temperaturen zwischen 550 bis 595 °C und Drücken von 100 bis 300 MPa quantifiziert. Dabei wurde die experimentelle Verformungs -Rate konstant gehalten, was in nahezu konstanten Verformungs-Raten zwischen 9.70×10^{-6} s^{-1} und 4.98×10^{-5} s^{-1} resultiert. Die dabei entstehenden axialen Spannungen reichen von 81 bis 802 MPa bei Verformungen von 1.4 bis 8.9 %. Diese Resultate zeigen, dass sich SCHOTT N-BK7® Glas nahe dem Glas-Übergangsbereich bei 300 MPa Außendruck visko-elastisch verhält. Um dies plausibilisieren zu können, wurden 1-Element sowie 2-Element Maxwell-Modelle in einen Inversions-Algorithmus eingebaut, für den MATLAB-Skripte zur Verfügung gestellt werden. Die Ergebnisse der Inversion zeigen, dass das 2-Element Maxwell-Model die experimentellen Daten gut beschreibt. Die Spannungsabnahme unter steigender Temperatur bei 300 MPa und die Temperaturabhängigkeit liefern eine ähnliche

Aktivierungsenergie (601±10 kJ·mol^{-1} oder $\Delta H/R = 7.2\times10^4$ K) wie bisherige Versuche bei 1 atm (615 kJ·mol^{-1} oder $\Delta H/R = 7.4\times10^4$ K). Die SCHOTT N-BK7® Glas-Probe weist einen limitierten linearen Anstieg der Viskosität bei steigendem Druck von ~0.1 log10(Pa·s)/100MPa auf, was mit den Resultaten aus Kapitel 3 übereinstimmt.

Zum Schluss werden in Kapitel 5 mehrere Proben von SCHOTT SF6® Glas in einem Hochdruck Torsions-Apparat (HPT) deformiert, um den Einfluss von Druck und Temperatur auf die Scherdeformation bei Drücken zwischen 0.3 und 7 GPa sowie Temperaturen von 25 bis 496 °C zu quantifizieren. Die Ergebnisse zeigen, dass plastische Deformation bei Temperaturen von 350 bis 496 °C auftritt und dass sich die maximale Fließspannung von SCHOTT SF6® Glas bei abnehmendem Druck und zunehmender Temperatur herabsetzt. Ein erweitertes Arrhenius-Model mit einem Parameter-Set, bestehend aus infiniter Fließspannung (Y_0=0.17±0.1 GPa), Aktivierungsenergie (E_a=4.8±0.5 kJ·mol^{-1}) und Aktivierungsvolumen (V_a=1.4±0.2 cm^3·mol^{-1}), beschreibt die experimentellen Resultate ausreichend gut.

Diese Arbeit hat gezeigt, wie wichtig die Untersuchung von Druckabhängigkeiten für Glas-Rheologie ist. Die präsentierten Experimente und Modelle können helfen, die Rheologie von Glas unter extremen Bedingungen zu verstehen. Jedoch bleibt die Verbindung von Fließspannung und Viskosität ist noch immer eine offene Frage.

Table of Contents

List of figures

List of tables

Chapter 1

1. General introduction

1.1 Rheology of glass

Rheology is the scientific study of the flow and deformation of materials (Schümmer, 1979). It was previously a study in a liquid state, while nowadays, the plastic yielding of solid is also concerned as a rheological study.

Glass lacks long-range order. It is cooled from the liquid state fast enough to avoid the crystalization. The temperature dependence of rheology of glass has been intensively studied, however, pressure also changes the properties and the mechanical behavior of glass even at room temperature which is not well understood yet (Zheng & Mauro, 2017). During industrial glass production processes, the actual distribution of stress components in the glass during scribing remains, to date, poorly quantified, and thus continues to be challenging to model numerically (Alkorta et al., 2005; Lee & Radok, 1960).

Moreover, rheology of glass (silicate melt) is also a key parameter to understand the birth of our earth (Christiansen & Drozdov, 2002) since geological silicate melts are continuously melted and solidified for millions of years.

The research on the rheology of glass under high pressure is important both for the industrial applications and geological processes.

1.2 Structural relaxation

Structural relaxation is a very important process for the rheological theories of glass. Fig.1.1 shows the glass formation during cooling and heating through the glass transition region. The relaxation of glass forming materials is highly temperature dependent. Firstly, at the temperature above the glass transition temperature, glass will behave like a liquid, in which the relaxation process is fast compared to the observation time (experimental time scale). Secondly, at the temperature near the glass transition temperature, glass will approach equilibrium within the observation time. Thirdly, at the temperature below glass transition temperature, the relaxation process is slow compared to the observation time. Moreover, the glass transition temperature (T_g) is influenced by the cooling rate, which indicates the time dependence.

Glass behaves viscoelastic near the glass transition region (Varshneya, 2013). For a hydrostatic deformation of glass near the glass transition region, the elastic part is governed by the bulk compliance $J_K=1/K$ (K is the bulk modulus). For a torsional deformation of glass near the glass transition region, the elastic part is governed by the shear compliance $J_G=1/G$ (G is the shear modulus), and the shear viscosity η_G can be calculated as

$$\eta_G = \frac{\sigma}{\dot{\varepsilon}} \qquad (1.1)$$

Where σ is the shear stress and $\dot{\varepsilon}$ is the shear strain rate. For a uniaxial deformation of glass near the glass transition region, the elastic part is governed by the uniaxial compliance $J_U=1/E$ (E is the Young's modulus), and the shear viscosity η_G after reaching steady state deformtion can be calculated as

$$\eta_G = \frac{\sigma_U}{3\dot{\varepsilon}_U} \qquad (1.2)$$

Glass in most situations is an isotropic material whose elastic moduli can be calculated according

$$E = 2G(1+\nu) = 3K(1-2\nu) \qquad (1.3)$$

Where ν is the Poission's ratio.

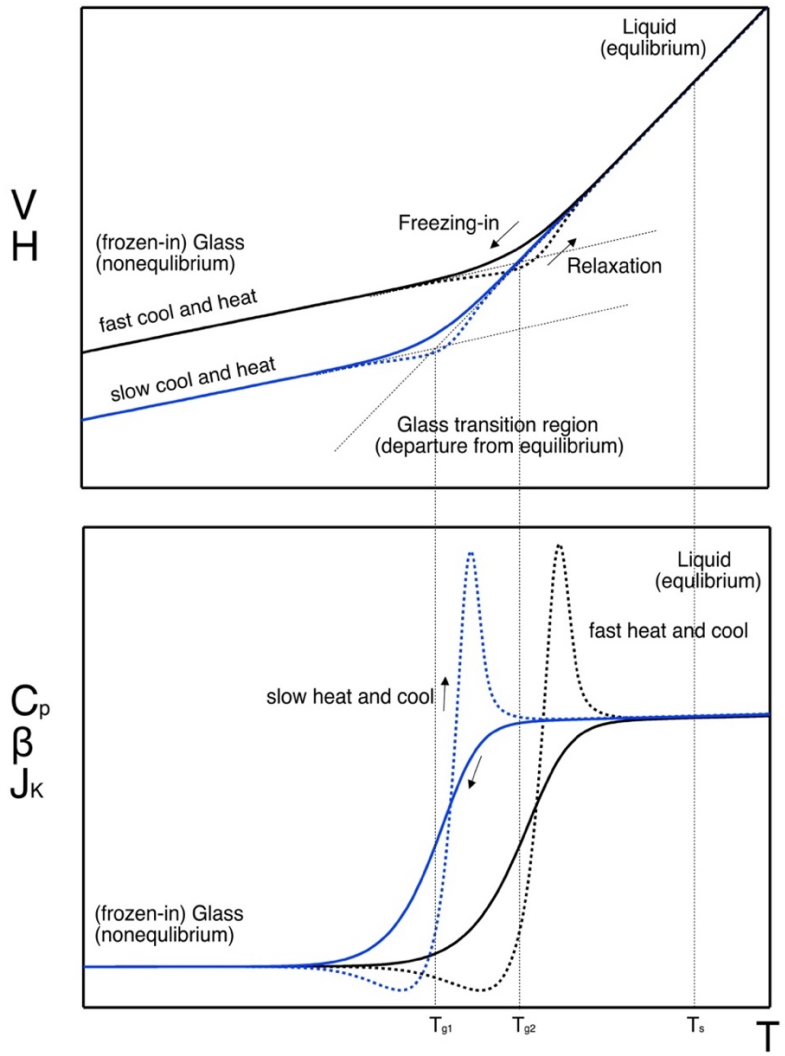

Fig. 1.1 *Temperature dependence volume (V), enthalpy (H), volumetric thermal expansion coefficient (β), heat capacity (C_p), and bulk compliance (J_K) curves for glass transition and relaxation. T_{g1} is the glass transition temperature for slow-cooled glass; T_{g2} is the glass transition temperature for fast-cooled glass; T_s is the melting temperature. The graph is based on the SCHOTT brochure of technical glasses.*

1.2.1 Structural relaxation measurement

There are many experimental methods to measure the glass relaxation, including the density and volume recovery measurement (Haruyama et al., 2010; Ritland, 1954; Scherer, G. W., 1986), the stress relaxation (creep) measurement (Barros et al., 1997; Rouxel et al., 2001; Shen et al., 2003), the refractive index measurement (Narayanaswamy, 1971; Scherer, 1984), the dielectric relaxation measurement(Barde et al., 2015; Fukao & Miyamoto, 2000; Stickel et al., 1995; Williams & Watts, 1970), etc.

Besides, Welch et al. (Welch et al., 2013) have also studied the structural relaxation of glass at ambient temperature. They performed an 18 months experiment on a large glass sheet (1050×1050×0.7 mm) by measuring the strain change as a function of time. The results show that the relaxation of glass at ambient condition can be fit to the stretched exponential model.

1.2.2 Static high-pressure treatment

Pressure changes the properties and the behavior of glass even at room temperature. Experimental examples are hardness measurement (Shang & Rouxel, 2005; Taylor, 1949) and scribing of glass. The static high-pressure treatments can be performed at several geological machines, e.g., Gas pressure vessels (up to ~1 GPa) (Paterson, 1970), Piston-Cylinder apparatus (up to ~4 GPa) (Boyd & England, 1960), Multi anvil apparatus (up to ~25 GPa) (Li et al., 1996), Diamond anvil cell (up to ~150 GPa) (Jayaraman, 1983), etc. Several experimental studies applied the static high-pressure treatment on the glass. For example, Bridgman and Simon (Bridgman & Simon, 1953) compressed thin samples of oxide glasses (SiO_2 and B_2O_3) and several mixed silicate glasses samples between two flat dies (uniaxial) made of carboloy at room temperature, and demonstrated that the vitreous SiO_2 had a density increase of almost 7.5% at 20 GPa, whereas the vitreous B_2O_3 has an asymptotic increase of density near 6% at pressures close to 20 GPa. An experimental study on a borosilicate glass with the pressure of up to 0.66 GPa and temperatures up to 300°C, showed that the density change was very small with only 0.05% at 0.66 GPa, 200°C and 24 hours (Anderson, 1956). A compilation of experimental data shows that there are significant differences in the manner in which different glass-types react to increases in pressure (Rouxel et al., 2008). Jin et al. (Jin et al., 2003) reported a 6 K/GPa change in T_g of a metallic glass by DSC measurements, and activation volume was suggested to describe the pressure dependence of glass relaxation in a free volume model.

1.2.3 Phenomenological model of structural relaxation

The phenomenological models are the most significant description of the glass transition and structural relaxation process (Scherer, 1990). Several phenomenological models (Grassia &

Simon, 2012; Hodge, 1994; Simon et al., 2002; Tribone et al., 1989) describe the time dependent frozen-in state and departure from equilibrium (δ) (Williams & Watts, 1970) of glass forming materials depending on temperature history (Moynihan et al., 1976; Narayanaswamy, 1971; Tool, 1946) and also pressure history (Grassia & Simon, 2012; Hodge, 1994; Simon et al., 2002; Tribone et al., 1989). Those models are based on the Tool-Narayanaswamy-Moynihan (Moynihan et al., 1976; Narayanaswamy, 1971; Tool, 1946) model and use one internal parameter named fictive temperature (T_f).

Fictive temperature is an artificial temperature used to describe the glassy state, firstly proposed by (Tool, 1946)

$$\frac{dT_f}{dt} = \frac{T - T_f}{\tau} \qquad (1.4)$$

where τ is the relaxation time. The frozen-in glass has the same structure as the supercooled liquid at temperature T_f. T_f acts like a map between the nonequilibrium glass state and the equilibrium liquid state. However, later index of refraction measurements performed by Ritland showed that one T_f is not sufficient to describe the glassy state.

Then, Narayanaswamy generalized Tool's model by introducing the nonlinearity parameter *x* and allowing a distribution of relaxation times. Narayanaswamy's relaxation model is based on the Arrhenius equation as

$$\tau = \tau_0 exp\left[\frac{x\Delta H}{RT} + \frac{(1-x)\Delta H}{RT_f}\right] \qquad (1.5)$$

If the relaxation function is described by the exponential decay term

$$M_p = \sum_{k=1}^{n} w_k \, exp\,(-\frac{t}{\tau_k}) \qquad (1.6)$$

where τ_k is the 'partial relaxation times'. Then the fictive temperature is the weighted sum of 'partial fictive temperatures'

$$T_f = \sum_{k=1}^{n} w_k \, T_{fk} \qquad (1.7)$$

where T_{fk} is individually obey Tool's theory with corresponding τ_k.

Moynihan et al. (Moynihan et al., 1976) described the relaxation function by using the stretched exponential term (Scherer, G. W., 1986)

$$M_p = exp\left[-\left(\frac{t}{\tau_k}\right)^{\beta}\right] \qquad (1.8)$$

where $0 < \beta < 1$ and a smaller β corresponds to a broader distribution of relaxation times. The exponent $0.6 < \beta < 0.9$ and the nonlinearity parameter $0.4 \leq x \leq 0.6$ are typically used. (Scherer, 1990)

The Tool-Narayanaswamy-Moynihan model has been widely tested and applied in the structural relaxation study of glass-forming liquid.

On the other hand, Davies and Jones (Davies & Jones, 1953) pointed out that fictive pressure (P_f) could also be an internal parameter. Gupta (Gupta, 1988) introduced the P_f to his structural relaxation model as an internal parameter together with T_f. The rates of change in fictive temperature T_f and fictive pressure P_f are as following

$$-\frac{dT_f}{dt}=(L_{TT}\frac{\Delta C}{T}-L_{TP}V\Delta\alpha)(T_f-T)+(-L_{TT}V\Delta\alpha+L_{TP}V\Delta J)(P_f-P) \quad (1.9)$$

$$-\frac{dP_f}{dt}=(L_{TP}\frac{\Delta C}{T}-L_{PP}V\Delta\alpha)(T_f-T)+(-L_{PT}V\Delta\alpha+L_{PP}V\Delta J)(P_f-P) \quad (1.10)$$

where $\Delta C = C_{liq} - C_{froz}$ is the specific heat capacity of the liquid (equilibrium) state C_{liq} and the frozen (glassy) state C_{froz}. Similarly, $\Delta\alpha = \alpha_{liq} - \alpha_{froz}$ is the difference in thermal expansion coefficient between the liquid and frozen glass, $\Delta J = J_{liq} - J_{froz}$ is the difference in compressibility between liquid glass and frozen glass with $J = 1/K$ (K is the bulk modulus). L_{TT}, L_{TP}, L_{PT} and L_{PP} are kinetic coefficients(Gupta, 1988) which relate to the partial relaxation times τ_{TT}, τ_{TP}, τ_{PT} and $\tau_{PP}$and also depend on T, P, T_f and P_f.

And the specific volume relaxation model proposed by Gupta (Gupta, 1988) is

$$V_g = V_e - V_e\Delta J\left(P_f - P\right) + V_e\Delta\alpha\left(T_f - T\right) \quad (1.11)$$

where, V_g is in the glassy state depends on T, T_f, P, P_f, V_e is the specific volume in the equilibrium state.

1.2.4 Maxwell model

The most common basic model for viscoelasticity of glass is the Maxwell model, which has an elastic body governed by Hooke's law and a viscous body governed by Newton's law (Wilantewicz & Varner, 2008). For the elastic body, the stress is linearly related to the strain ($\sigma = G\varepsilon$, G is the shear modulus), which can be represented by a spring. And for the viscous body, the shear stress is equal to viscosity times strain rate ($\sigma = \eta\dot{\varepsilon}$), which can be represented by a dashpot.

The single Maxwell viscoelastic model (1-Maxwell) is defined by (Kaus & Becker, 2007; Scherer & Rekhson, 1982)

$$\dot{\varepsilon} = \dot{\varepsilon}_{ela} + \dot{\varepsilon}_{vis} = \frac{1}{G}\frac{d\sigma}{dt} + \frac{\sigma}{\eta} \quad (1.12)$$

$$\frac{d\sigma}{dt} = G\dot{\varepsilon} - \frac{G\sigma}{\eta} \quad (1.13)$$

where $\dot{\varepsilon}$ is the total strain rate, $\dot{\varepsilon}_{ela}$ is the strain rate, $\dot{\varepsilon}_{vis}$ is the strain rate of viscous deformation, σ is the shear stress, η is the viscosity and G is the elastic shear modulus. Under

a constantly applied strain rate $\dot{\varepsilon}_0$, the stress relaxation can be solved by integrating over time as (Scherer & Rekhson, 1982)

$$\sigma(t) = \eta \left(1 - e^{-\frac{t}{\tau}}\right) \dot{\varepsilon}_0 + \sigma(0) e^{-\frac{t}{\tau}} \qquad (1.14)$$

where τ is the Maxwell relaxation time can be calculated by $\tau = \frac{\eta}{G}$, and $\sigma(0)$ is the initial stress.

The single Maxwell model is used to determine the relaxation times, while it is not sufficient to represent the actual relaxation process of glass forming materials (Shelby, 2005) as a reason of it cannot account for the delayed elastic response. Therefore, the generalized Maxwell model, which combines several Maxwell elements in parallel, is better to explain the relaxation process of glass. The generalized Maxwell model can be represented as (Jain et al., 2006; Scherer & Rekhson, 1982)

$$\sigma(t) = \sum_{i=1}^{n} w_i \, \eta \left(1 - e^{-\frac{t}{\tau_i}}\right) \dot{\varepsilon}_0 + \sum_{i=1}^{n} w_i \, \sigma(0) e^{-\frac{t}{\tau_i}} \qquad (1.15)$$

where w_i is the weighting parameters separate the different relaxation times, τ_i is the relaxation times and n are the number of Maxwell elemens in the Prony series. The number of Maxwell elements is determined by the curve fitting process (n=3-5 is commonly used in the glass industry) as a compromise between measurement uncertainty and computational effect.

1.3 Viscosity

The flow of the liquid is highly dependent on its viscosity, and therefore viscosity is the most important property for glass-forming liquids (Zheng & Mauro, 2017). Fig.1.2 shows a typical viscosity-temperature curve for the industrial glass with several typical reference point. Those reference points are very important for industrial glass production, including the process of melting, forming and annealing. The viscosity of glass at ambient pressure can be measured by several methods for certain viscosity range. And the temperature dependence viscosity model (Adam & Gibbs, 1965; Cohen & Turnbull, 1959; Fulcher, 1925; Greet & Turnbull, 1967; Mauro et al., 2009; Tammann & Hesse, 1926; Turnbull & Cohen, 1970; Vogel, 1921; Waterton, 1932; Williams et al., 1955) developed can fit the experimental data well. However, pressure also changes the properties and the behavior of glass even at room temperature which is not well understood yet (Zheng & Mauro, 2017).

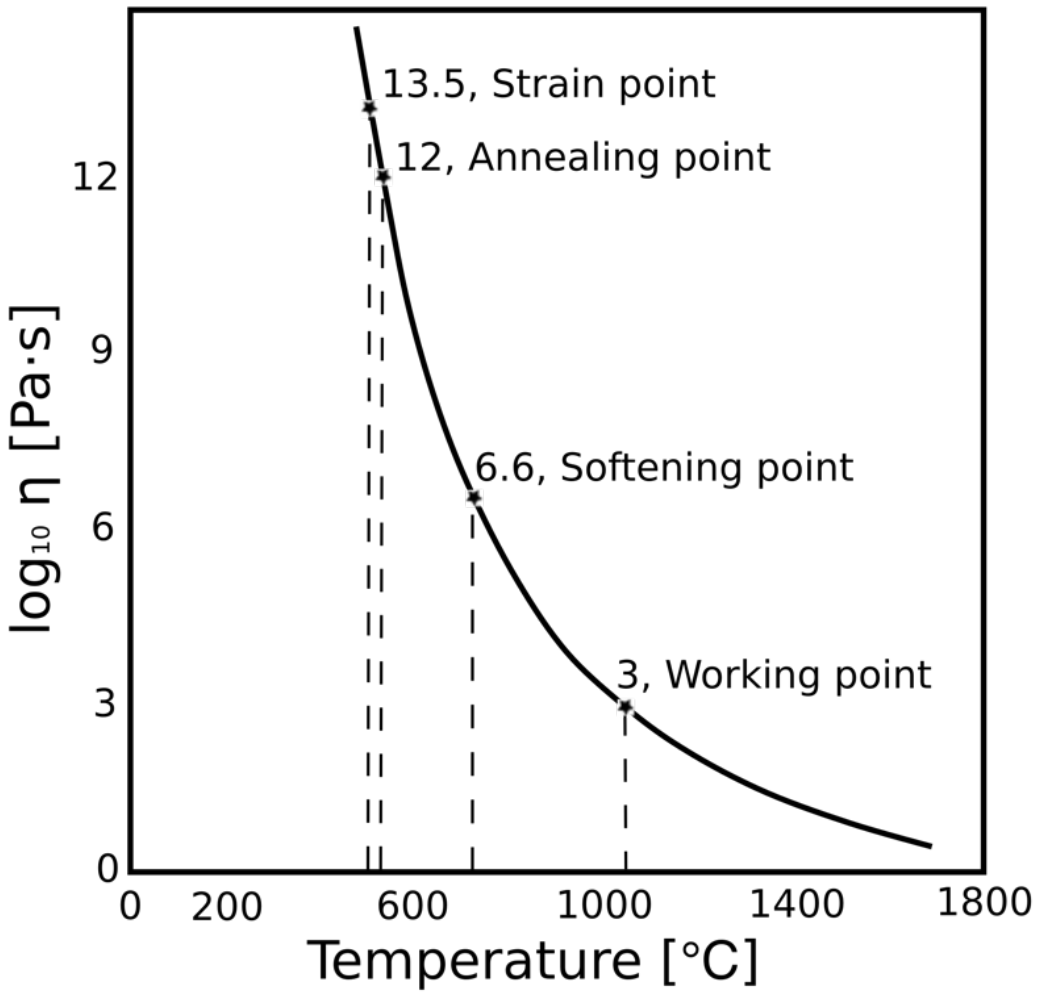

Fig. 1.2 *Typical viscosity-temperature curve for glass. The graph is based on the SCHOTT brochure of technical glasses.*

1.3.1 Viscosity measurement

The viscosity of glass varies a wide range of magnitudes so that there is no single experimental technique can measure the whole viscosity range. A typical viscosity-temperature curve for glass, e.g., Fig.1.2, is obtained by several different viscosity measurements. For example, the beam bending method (ASTM C1350M-96, 2003) could measure the viscosity of glass from approximately 10^8 Pa·s to 10^{13} Pa·s. The parallel plate method (ASTM C1351M-96, 2002) could measure the viscosity of glass from approximately 10^4 Pa·s to 10^8 Pa·s. The rotation viscometer (ISO 7884-2, 1998) could measure the viscosity of glass at high temperatures $<10^6$ Pa·s. The fiber elongation method (ISO 7884-3, 1998) could measure the viscosity of glass from 10^5 Pa·s to $10^{15.5}$ Pa·s.

The viscosity strongly depends on density (Cook et al., 1994) and thus on pressure. Several experimental studies have quantified the pressure dependence of the viscosity of silicate melts,

with a special focus on melts relevant to geological and volcanic systems, such as molten olivine, molten jadeite, dacite and basalt at very high temperatures (> 1700 °C) (Kushiro, 1976; Kushiro, 1978; Mysen et al., 1982; Wang et al., 2014) and pressure up to 8 GPa. Different behaviors were observed with increasing pressure as a function of the degree of polymerization (Scarfe et al., 1987; Wang et al., 2014). The polymerization parameter is best described by the ratio of non-bridging oxygen (NBO) and tetrahedrally coordinated cations (T, e.g., Si^{4+}, Al^{4+}, Ti^{4+}, Fe^{3+}). The ratio of NBO/T can be simply calculated by the ratio of O/T at ambient pressure with satisfying accuracy (Wang et al., 2014). However, under high pressure, highly polymerized silicate melts (NBO/T<1, e.g., obsidian, basalt, dacite) have lower tetrahedral connectivity (fewer oxygen atoms in TO_4 will bond to adjacent tetrahedron and thus forming less 3D networks) than at ambient pressure. These highly polymerized silicate melts (Wang et al., 2014) display a viscosity decrease with an increase of pressure. While the viscosity of depolymerized silicate melts (NBO/T≥2, molten peridotite, molten olivine, Al-poor melt), with higher tetrahedral connectivity, show a viscosity increase with increasing pressure (Wang et al., 2014).

Previous experimental studies on the effect of pressure on viscosity and density of glasses have mostly reported a linear relationship for pressure dependence. For example, the pressure dependence of the viscosity of B_2O_3, studied by Sperry and Makenzie (Sperry & JD, 1968) at 380-465 °C and from 0.1 to 30 MPa, demonstrated a linear increase of viscosity with increasing pressure ($\Delta\eta/\Delta P$ = 0.28 to 0.59 $\log_{10}$(Pa·s)/100 MPa (Sperry & JD, 1968)). A special parallel-plate viscometer was developed by Schulze et al. (Schulze et al., 1999) using an internally heated pressure vessel (IHPV) to deform the standard melt DDG1, Di_{100} (Di=$CaMgSi_2O_6$) and $Ab_{55}Di_{45}$ (Ab=$NaAlSi_3O_8$) silicate melt. And their results also suggest a linear change with increasing pressure up to 350 MPa ($\Delta\eta/\Delta P$ = -0.12 to 0.23 $\log_{10}$(Pa·s)/100 MPa (Schulze et al., 1999)). Deformation of float glass with high water content (Del Gaudio et al., 2007) likewise reported a linear viscosity increase with increasing pressure from 100 MPa to 400 MPa, and a negative correlation with increasing water content (0.03-4.87 wt.%), ($\Delta\eta/\Delta P$ < 0.22 $\log_{10}$(Pa·s)/100 MPa (Del Gaudio et al., 2007)).

1.3.2 Viscosity model

The temperature dependence of the viscosity of glasses at ambient pressure has already been studied experimentally leading to numerous temperature-dependent models of viscosity for glasses. Notably, the Vogel-Fulcher-Tammann (VFT) model (Fulcher, 1925) which is similar to the Williams-Landel-Ferry (WLF) model (Williams et al., 1955), the free-volume model

(Cohen & Turnbull, 1959; Greet & Turnbull, 1967; Turnbull & Cohen, 1970), the Adam-Gibbs (AG) model (Adam & Gibbs, 1965).

Most of the temperature dependence viscosity model for glass is based on the Arrhenius equation

$$\eta = \eta_0 e^{\frac{E_a}{RT}} \qquad (1.16)$$

Where η_0 is a constant viscosity that represents the high temperature limit for $\eta(T)$, E_a is the activation energy for glass flow, R is the ideal gas constant and T is the temperature. The Arrhenius equation with 2 free parameters can fit the viscosity of glass over a narrow range of temperature.

The Vogel- Fulcher-Tammann (VFT) model (Fulcher, 1925; Vogel, 1921; Tammann & Hesse, 1926) is an empirical model with 3 free parameters that can well present the viscosity of the glass-forming liquids.

$$\eta = \eta_0 e^{\frac{A}{T-T_0}} \qquad (1.17)$$

Where η_0, A and T_0 are constants, and T is the temperature. The VFT model can convert to the Arrhenius model when $T_0=0$. While the VFT model is an accurate model fits a very wide range of viscosity data for many glass-forming liquids.

The free volume model proposed by Cohen and Turnbull (Cohen & Turnbull, 1959; Turnbull & Cohen, 1970) supposes that the flow behavior takes place when the movement of molecules produces large enough adjoining vacancies. The model can be express as

$$\eta = \eta_0 e^{\frac{\gamma v_c}{v_f}} \approx \eta_0 e^{\frac{\alpha_l - \alpha_c}{T-T_v}} \qquad (1.18)$$

Where η_0 and γ are constants, v_c is the specific volume of the crystal, and $v_f$ist he free volume roughly corresponding to the volume difference between the liquid and crystal. α_l ist the thermal expansion coeffcient of the liquid which is much greater than the thermal expansion coefficient of the crystal α_c, and T_v is the temperature where the free volume disappears. Therefore, at a finite temperature range, the free volume model can transform to the VFT model by $T_0 = T_v$.

The configuration entropy S_c is included in the Adam-Gibbs (AG) viscosity model as

$$\eta = \eta_0 e^{\frac{C}{TS_c}} \approx \eta_0 e^{\frac{CT_k}{D(T-T_k)}} \qquad (1.19)$$

Where η_0, C and D are constants, T_k is the temperature just below the experimental glass transition temperature and entropy close to zero (Kauzmann, 1948). The primary idea of the AG model is that the decrease of entropy yields a decrease of the rearrangement of molecules,

which leads to the viscosity increasing. The AG model can also transform to VFT model when $T_0 = T_k$.

All in all, the free volume model and the AG model related the glass flow behavior to the molecules movements, and both of those two models can transform to VFT model which is originally the Arrhenius type.

The Arrhenius equation can be extended to Eq. (1.19) by introducing activation volume as has been reported in many studies (Jin et al., 2003; Katayama & Karato, 2008; Poirier, 1985) to account for the pressure effect.

$$\eta = \eta_0 e^{\frac{E_a + PV_a}{RT}} \qquad (1.20)$$

where η_0 ia constant viscosity, E_a is the activation energy, and V_a is the activation volume. The extended Arrhenius model is widely used in geoscience to determine the flow law to analyze the rheological data (Katayama & Karato, 2008).

Besides, some studies directly express the effect of pressure on the viscosity model. For example, the model proposed by Avramov (Avramov, 2000) describes the pressure dependence of viscosity by relating the viscosity to the entropy of the glass forming melts, using a master equation ϕ. The free-volume model indicates that viscosity increases with increasing pressure (Scherer, George W, 1986; Sharma et al., 1979). The equation derived by Gupta (Gupta, 1987), which follows the AG model (Adam & Gibbs, 1965), predicting a negative pressure dependence of viscosity.

1.4 Elasticity and plasticity

1.4.1 Elasticity and glass flow

The elasticity affects the fragility and thermodynamics of glass (Yan et al., 2013). The shoving model proposed by Dyre et al. (Dyre et al., 1996) applied the elastic energy to the non-Arrhenius glass flow (Angell et al., 2000; Bains et al., 2000; Bielowka et al., 2001). They proposed that the flow event takes place by shoving the surrounding liquid aside to increase the volume available for the molecules rearranging. The primary idea is similar as the free volume model.

The temperature-dependent activation energy $E(T)$ in the shoving model is

$$E(T) = V_c G_\infty(T) \qquad (1.21)$$

where V_c is the characteristic volume and also the constant of proportionality to the infinite shear modulus $G_\infty(T)$ change. The V_c is assumed to be temperature independent. The model assumes the elastic shear energy is the main activation energy which dominates the movement of the molecules.

To connect the flow behavior, the shoving model can be transformed to

$$\eta = \eta_0 e^{\frac{V_c G_\infty(T)}{k_B T}} \qquad (1.22)$$

Where η_0 is the constant viscosity and k_B is the Boltzmann's constant. The glass flow process (relaxation) is very slow at the low temperature so that it is hard to relate the flow event with the elasticity in a short timescale. Nevertheless, the flow event does occur instantaneously during the molecular rearrangement, so that the liquid properties could also link to the elastic energy even on a short timescale. However, Potuzak et al. (Potuzak et al., 2013) tested the shoving model with the conclusion that the nonequilibrium viscosity of glass is not solely governed by the instantaneous elasticity.

1.4.2 Plastic yielding

The plastic yield deformation is widely reported in many deformation experiments on polymers (Nanzai, 1993), alloys (Raghavan et al., 2015), metallic glass (Donovan, 1989; Vaidyanathan et al., 2001), steel (Hutchinson et al., 2018), etc. The atomistic origin for the plastic yield criterion on metallic glass under pressure is discussed by Schuh & Lund (Schuh & Lund, 2003), which supports the plastic yield behavior in amorphous materials.

The amorphous materials, including glass, potentially has much higher yield stress in a plastic yield deformation, e.g., up to 3 GPa for oxide glass (Demetriou et al., 2011) and ~0.5 GPa (Xi et al., 2005) to 5 GPa (Inoue et al., 2003) for metallic glass. However, the industrial oxide glass typically has a low fracture toughness in the order of 1 MPa·m$^{0.5}$, and consequently, the brittle fracture occurs much earlier than the plastic yielding.

Plastic yielding is a deep topic in materials science and engineering which is in debating for decades (Barnes, 1999; Moller et al., 2009). The link between yield stress and viscosity remains an open question, since there is no model exist to describe the yield stress and viscosity data over a limited shear strain rate in the same deformation experiments (Barnes, 1999).

1.5 References

Adam, G. & Gibbs, J. H. (1965). On the Temperature Dependence of Cooperative Relaxation Properties in Glass-Forming Liquids. *The Journal of Chemical Physics*, 43 (1): 139-146.

Alkorta, J., Martinez-Esnaola, J. M. & Sevillano, J. G. (2005). Absence of one-to-one correspondence between elastoplastic properties and sharp-indentation load-penetration data. *Journal of Materials Research*, 20 (5): 1369-1369.

Anderson, O. L. (1956). Effect of Pressure on Glass Structure. *Journal of Applied Physics*, 27 (8): 943-949.

Angell, C. A., Ngai, K. L., McKenna, G. B., McMillan, P. F. & Martin, S. W. (2000). Relaxation in glassforming liquids and amorphous solids. *Journal of Applied Physics*, 88 (6): 3113-3157.

Avramov, I. (2000). Pressure dependence of viscosity of glassforming melts. *Journal of Non-Crystalline Solids*, 262 (1-3): 258-263.

Bains, A. S., Gordon, C. A., Granato, A. V. & Schwarz, R. B. (2000). The shear modulus of bulk amorphous Pd40Ni40P20 and its relation to viscosity and specific heat. *Journal of Alloys and Compounds*, 310: 20-23.

Barde, R. V., Nemade, K. R. & Waghuley, S. A. (2015). AC conductivity and dielectric relaxation in V_2O_5-P_2O_5-B_2O_3 glasses. *Journal of Asian Ceramic Societies*, 3 (1): 116-122.

Barnes, H. A. (1999). The yield stress - a review or 'pi alpha nu tau alpha rho epsilon iota' - everything flows? *Journal of Non-Newtonian Fluid Mechanics*, 81 (1-2): 133-178.

Barros, D. A., Ferraz, A. M., Messaddeq, Y. & Aegerter, M. A. (1997). Uniaxial stress relaxation measurement in fluoroindate glasses. *Journal of Non-Crystalline Solids*, 213: 336-340.

Bielowka, S. H., Psurek, T., Ziolo, J. & Paluch, M. (2001). Test of the fractional Debye-Stokes-Einstein equation in low-molecular-weight glass-forming liquids under condition of high compression. *Physical Review E*, 63 (6).

Boyd, F. R. & England, J. L. (1960). Apparatus for Phase-Equilibrium Measurements at Pressures up to 50-Kilobars and Temperatures up to 1750-Degrees-C. *Journal of Geophysical Research*, 65 (2): 741-748.

Bridgman, P. W. & Simon, I. (1953). Effects of Very High Pressures on Glass. *Journal of Applied Physics*, 24 (4): 405-413.

Christiansen, J. d. & Drozdov, A. D. (2002). Rheology of silicate glasses. *Rheol. Bull.* (2): 5.

Cohen, M. H. & Turnbull, D. (1959). Molecular Transport in Liquids and Glasses. *Journal of Chemical Physics*, 31 (5): 1164-1169.

Cook, R. L., King, H. E., Herbst, C. A. & Herschbach, D. R. (1994). Pressure and temperature dependent viscosity of two glass forming liquids: Glycerol and dibutyl phthalate. *The Journal of Chemical Physics*, 100 (7): 5178.

Davies, R. O. & Jones, G. O. (1953). Thermodynamic and Kinetic Properties of Glasses. *Advances in Physics*, 2 (7): 370-410.

Debenedetti, P. G. & Stillinger, F. H. (2001). Supercooled liquids and the glass transition. *Nature*, 410 (6825): 259-267.

Del Gaudio, P., Behrens, H. & Deubener, J. (2007). Viscosity and glass transition temperature of hydrous float glass. *Journal of Non-Crystalline Solids*, 353 (3): 223-236.

Demetriou, M. D., Launey, M. E., Garrett, G., Schramm, J. P., Hofmann, D. C., Johnson, W. L. & Ritchie, R. O. (2011). A damage-tolerant glass. *Nature Materials*, 10 (2): 123-128.

Donovan, P. E. (1989). A Yield Criterion for $Pd_{40}Ni_{40}P_{20}$ Metallic-Glass. *Acta Metallurgica*, 37 (2): 445-456.

Dyre, J. C., Olsen, N. B. & Christensen, T. (1996). Local elastic expansion model for viscous-flow activation energies of glass-forming molecular liquids. *Physical Review B*, 53 (5): 2171-2174.

Fukao, K. & Miyamoto, Y. (2000). Glass transitions and dynamics in thin polymer films: Dielectric relaxation of thin films of polystyrene. *Physical Review E*, 61 (2): 1743-1754.

Fulcher, G. S. (1925). Analysis of recent measurements of the viscosity of glasses. *Journal of the American Ceramic Society*, 8 (6): 339-355.

Grassia, L. & Simon, S. L. (2012). Modeling volume relaxation of amorphous polymers: Modification of the equation for the relaxation time in the KAHR model. *Polymer*, 53 (16): 3613-3620.

Greet, R. J. & Turnbull, D. (1967). Test of Adam-Gibbs Liquid Viscosity Model with O-Terphenyl Specific-Heat Data. *Journal of Chemical Physics*, 47 (6): 2185-2190.

Gupta, P. K. (1987). Negative-Pressure Dependence of Viscosity. *Journal of the American Ceramic Society*, 70 (7): C152-C153.

Gupta, P. K. (1988). Fictive Pressure Effects in Structural Relaxation. *Journal of Non-Crystalline Solids*, 102 (1-3): 231-239.

Haruyama, O., Nakayama, Y., Wada, R., Tokunaga, H., Okada, J., Ishikawa, T. & Yokoyama, Y. (2010). Volume and enthalpy relaxation in $Zr_{55}Cu_{30}Ni_5Al_{10}$ bulk metallic glass. *Acta Materialia*, 58 (5): 1829-1836.

Hodge, I. M. (1994). Enthalpy Relaxation and Recovery in Amorphous Materials. *Journal of Non-Crystalline Solids*, 169 (3): 211-266.

Hutchinson, B., Bate, P., Lindell, D., Malik, A., Barnett, M. & Lynch, P. (2018). Plastic Yielding in lath martensites–an alternative viewpoint. *Acta Materialia*, 152: 239-247.

Inoue, A., Shen, B. L., Koshiba, H., Kato, H. & Yavari, A. R. (2003). Cobalt-based bulk glassy alloy with ultrahigh strength and soft magnetic properties. *Nature Materials*, 2 (10): 661-663.

Jain, A., Yi, A. Y., Xie, X. P. & Sooryakumar, R. (2006). Finite element modelling of stress relaxation in glass lens moulding using measured, temperature-dependent elastic modulus and viscosity data of glass. *Modelling and Simulation in Materials Science and*

Engineering, 14 (3): 465-477.

Jayaraman, A. (1983). Diamond Anvil Cell and High-Pressure Physical Investigations. *Reviews of Modern Physics*, 55 (1): 65-108.

Jin, H. J., Gu, X. J., Wen, P., Wang, L. B. & Lu, K. (2003). Pressure effect on the structural relaxation and glass transition in metallic glasses. *Acta Materialia*, 51 (20): 6219-6231.

Katayama, I. & Karato, S. I. (2008). Effects of water and iron content on the rheological contrast between garnet and olivine. *Physics of the Earth and Planetary Interiors*, 166 (1-2): 57-66.

Kaus, B. J. P. & Becker, T. W. (2007). Effects of elasticity on the Rayleigh-Taylor instability: implications for large-scale geodynamics. *Geophysical Journal International*, 168 (2): 843-862.

Kauzmann, W. (1948). The Nature of the Glassy State and the Behavior of Liquids at Low Temperatures. *Chemical Reviews*, 43 (2): 219-256.

Kushiro, I. (1976). Changes in Viscosity and Structure of Melt of Naalsi2o6 Composition at High-Pressures. *Journal of Geophysical Research*, 81 (35): 6347-6350.

Kushiro, I. (1978). Viscosity and Structural-Changes of Albite (Naalsi3o8) Melt at High-Pressures. *Earth and Planetary Science Letters*, 41 (1): 87-90.

Lee, E. H. & Radok, J. R. M. (1960). The Contact Problem for Viscoelastic Bodies. *Journal of Applied Mechanics*, 27 (3): 438-444.

Li, B. S., Jackson, I., Gasparik, T. & Liebermann, R. C. (1996). Elastic wave velocity measurement in multi-anvil apparatus to 10 GPa using ultrasonic interferometry. *Physics of the Earth and Planetary Interiors*, 98 (1-2): 79-91.

Mauro, J. C., Yue, Y. Z., Ellison, A. J., Gupta, P. K. & Allan, D. C. (2009). Viscosity of glass-forming liquids. *Proceedings of the National Academy of Sciences of the United States of America*, 106 (47): 19780-19784.

Moller, P. C. F., Fall, A. & Bonn, D. (2009). Origin of apparent viscosity in yield stress fluids below yielding. *Epl*, 87 (3):133-178.

Moynihan, C. T., Easteal, A. J., Wilder, J. & Tucker, J. (1974). Dependence of the glass transition temperature on heating and cooling rate. *The journal of physical chemistry*, 78 (26): 2673-2677.

Moynihan, C. T., Macedo, P. B., Montrose, C. J., Gupta, P. K., Debolt, M. A., Dill, J. F., Dom, B. E., Drake, P. W., Easteal, A. J., Elterman, P. B., et al. (1976). Structural Relaxation in Vitreous Materials. *Annals of the New York Academy of Sciences*, 279 (Oct15): 15-35.

Mysen, B. O., Virgo, D. & Seifert, F. A. (1982). The structure of silicate melts: implications for chemical and physical properties of natural magma. *Reviews of Geophysics*, 20 (3): 353-383.

Nanzai, Y. (1993). Molecular Kinetics of Yield Deformation and Ductile Fracture in Polymer Glasses. *Progress in Polymer Science*, 18 (3): 437-479.

Narayanaswamy, O. S. (1971). A Model of Structural Relaxation in Glass. *Journal of the American Ceramic Society*, 54 (10): 491-498.

Paterson, M. S. (1970). A High-Pressure, High-Temperature Apparatus for Rock Deformation. *International Journal of Rock Mechanics and Mining Sciences*, 7 (5): 517-526.

Poirier, J.-P. (1985). *Creep of crystals: high-temperature deformation processes in metals, ceramics and minerals*: Cambridge University Press.

Potuzak, M., Guo, X., Smedskjaer, M. M. & Mauro, J. C. (2013). Are the dynamics of a glass embedded in its elastic properties? *The Journal of chemical physics*, 138 (12): 12A501.

Raghavan, R., Harzer, T. P., Chawla, V., Djaziri, S., Phillipi, B., Wehrs, J., Wheeler, J. M., Miehler, J. & Dehm, G. (2015). Comparing small scale plasticity of copper-chromium nanolayered and alloyed thin films at elevated temperatures. *Acta Materialia*, 93: 175-186.

Ritland, H. N. (1954). Density phenomena in the transformation range of a borosilicate crown glass. *Journal of the American Ceramic Society*, 37 (8): 370-377.

Rouxel, T., Soraru, G. D. & Vicens, J. (2001). Creep viscosity and stress relaxation of gel-derived silicon oxycarbide glasses. *Journal of the American Ceramic Society*, 84 (5): 1052-1058.

Rouxel, T., Ji, H., Hammouda, T. & Moreac, A. (2008). Poisson's ratio and the densification of glass under high pressure. *Physical Review Letters*, 100 (22).

Scarfe, C. M., Mysen, B. O. & Virgo, D. (1987). Pressure dependence of the viscosity of silicate melts. *Magmatic processes: Physicochemical principles*, 1: 59-67.

Scherer, G. W. & Rekhson, S. M. (1982). Viscoelastic- Elastic Composites: I, General Theory. *Journal of the American Ceramic Society*, 65 (7): 352-360.

Scherer, G. W. (1984). Use of the Adam-Gibbs Equation in the Analysis of Structural Relaxation. *Journal of the American Ceramic Society*, 67 (7): 504-511.

Scherer, G. W. (1986). Relaxation in glass and composites. *Wiley, New York*.

Scherer, G. W. (1986). Volume Relaxation Far from Equilibrium. *Journal of the American Ceramic Society*, 69 (5): 374-381.

Scherer, G. W. (1990). Theories of Relaxation. *Journal of Non-Crystalline Solids*, 123 (1-3):

75-89.

Schuh, C. A. & Lund, A. C. (2003). Atomistic basis for the plastic yield criterion of metallic glass. *Nature Materials*, 2 (7): 449-452.

Schulze, F., Behrens, H. & Hurkuck, W. (1999). Determination of the influence of pressure and dissolved water on the viscosity of highly viscous melts: Application of a new parallel-plate viscometer. *American Mineralogist*, 84 (10): 1512-1520.

Schümmer, P. (1979). Mechanics of Non- Newtonian Fluids. Von W. R. Schowalter. Pergamon Press, Oxford–Frankfurt 1978. 1. Aufl., IX, 300 S., zahlr. Abb. u. Tab., geb., $ 35.00. *Chemie Ingenieur Technik*, 51 (7): 766-766.

Shang, H. X. & Rouxel, T. (2005). Creep behavior of soda-lime glass in the 100-500 K temperature range by indentation creep test. *Journal of the American Ceramic Society*, 88 (9): 2625-2628.

Sharma, S. K., Virgo, D. & Kushiro, I. (1979). Relationship between Density, Viscosity and Structure of Geo2 Melts at Low and High-Pressures. *Journal of Non-Crystalline Solids*, 33 (2): 235-248.

Shelby, J. E. (2005). *Introduction to glass science and technology*: Royal Society of Chemistry.

Shen, J. W., Green, D. J., Tressler, R. E. & Shelleman, D. L. (2003). Stress relaxation of a soda lime silicate glass below the glass transition temperature. *Journal of Non-Crystalline Solids*, 324 (3): 277-288.

Simon, S. L., Park, J. Y. & McKenna, G. B. (2002). Enthalpy recovery of a glass-forming liquid constrained in a nanoporous matrix: Negative pressure effects. *European Physical Journal E*, 8 (2): 209-216.

Sperry, L. & JD, M. (1968). Pressure dependence of viscosity of B_2O_3. *Physics and Chemistry of Glasses*, 9 (3): 91-95.

Stickel, F., Fischer, E. W. & Richert, R. (1995). Dynamics of glass- forming liquids. I. Temperature- derivative analysis of dielectric relaxation data. *The Journal of chemical physics*, 102 (15): 6251-6257.

Tammann, G. & Hesse, W. (1926). The dependence of viscosity upon the temperature of supercooled liquids. *Z. Anorg. Allg. Chem*, 156: 245-257.

Taylor, E. W. (1949). Plastic Deformation of Optical Glass. *Nature*, 163 (4139): 323-323.

Tool, A. Q. (1946). Relation between Inelastic Deformability and Thermal Expansion of Glass in Its Annealing Range. *Journal of the American Ceramic Society*, 29 (9): 240-253.

Tribone, J. J., Oreilly, J. M. & Greener, J. (1989). Pressure-Jump Volume-Relaxation Studies of Polystyrene in the Glass-Transition Region. *Journal of Polymer Science Part B-*

Polymer Physics, 27 (4): 837-857.

Turnbull, D. & Cohen, M. H. (1970). On the Free-Volume Model of the Liquid- Glass Transition. *The journal of chemical physics*, 52 (6): 3038-3041.

Vaidyanathan, R., Dao, M., Ravichandran, G. & Suresh, S. (2001). Study of mechanical deformation in bulk metallic glass through instrumented indentation. *Acta Materialia*, 49 (18): 3781-3789.

Varshneya, A. K. (2013). *Fundamentals of inorganic glasses*: Elsevier.

Vogel, H. (1921). The temperature dependence law of the viscosity of fluids. *Phys. Z*, 22: 645-646.

Wang, Y., Sakamaki, T., Skinner, L. B., Jing, Z., Yu, T., Kono, Y., Park, C., Shen, G., Rivers, M. L. & Sutton, S. R. (2014). Atomistic insight into viscosity and density of silicate melts under pressure. *Nature communications*, 5: 3241.

Waterton, S. (1932). The viscosity-temperature relationship and some inferences on the nature of molten and of plastic glass. *J. Soc. Glass Technol*, 16: 244-247.

Welch, R. C., Smith, J. R., Potuzak, M., Guo, X., Bowden, B. F., Kiczenski, T. J., Allan, D. C., King, E. A., Ellison, A. J. & Mauro, J. C. (2013). Dynamics of glass relaxation at room temperature. *Phys Rev Lett*, 110 (26): 265901.

Wilantewicz, T. E. & Varner, J. R. (2008). Vickers indentation behavior of several commercial glasses at high temperatures. *Journal of Materials Science*, 43 (1): 281-298.

Williams, G. & Watts, D. C. (1970). Non-Symmetrical Dielectric Relaxation Behaviour Arising from a Simple Empirical Decay Function. *Transactions of the Faraday Society*, 66 (565p): 80-85.

Williams, M. L., Landel, R. F. & Ferry, J. D. (1955). The Temperature Dependence of Relaxation Mechanisms in Amorphous Polymers and Other Glass-Forming Liquids. *Journal of the American Chemical Society*, 77 (14): 3701-3707.

Xi, X. K., Zhao, D. Q., Pan, M. X., Wang, W. H., Wu, Y. & Lewandowski, J. J. (2005). Fracture of brittle metallic glasses: Brittleness or plasticity. *Physical Review Letters*, 94 (12).

Yan, L., During, G. & Wyart, M. (2013). Why glass elasticity affects the thermodynamics and fragility of supercooled liquids. *Proceedings of the National Academy of Sciences of the United States of America*, 110 (16): 6307-6312.

Zheng, Q. J. & Mauro, J. C. (2017). Viscosity of glass-forming systems. *Journal of the American Ceramic Society*, 100 (1): 6-25.

Chapter 2

2. Experimental methods

2.1 Introduction

The experimental part is the core content throughout the whole thesis. In this chapter, I will briefly review all the experimental materials and machines we applied, and then highlight the calibration works we did in this project. During our previous experimental experience, the real temperature of the sample during experiments is rather difficult to measure. Therefore, a systematic calibration of the machines, especially for temperature, is crucial to get experimental data under control and within uncertainty.

2.2 Sample description

We used two types of optical glass produced by SCHOTT in this project. The borosilicate glass SCHOTT N-BK7® (chemical composition: 70.0 % SiO_2, 11.5 % B_2O_3, 9.5 % Na_2O, 7.5 % K_2O and 1.5 % BaO) is an optical glass (Dyer et al., 2003; Koontz et al., 2012; Mosaddegh & Ziegert, 2011) widely used for lenses and prisms, due to its high homogeneity and high light yield. The density of SCHOTT N-BK7® at room temperature and ambient pressure is 2.508 ± 0.001 g/cm^3. The glass transition temperature T_g = 561 °C is defined as the temperature at which the viscosity is 12 $\log_{10}$(Pa·s).

The alkali-lead-silicate glass SCHOTT SF6® (chemical composition (Heiman et al., 1979): 27.3 % SiO_2, 1.5 % K_2O, 71 % PbO) is an optical glass widely used as photonic crystal fiber (Efimov & Taylor, 2008; Fu et al., 2010; Hundertmark et al., 2009) for efficient spectral broadening at high repetition rates (several GHz). The density of SCHOTT N-BK7® at room temperature and ambient pressure is 5.180 ± 0.001 g/cm^3. The glass transition temperature T_g = 417 °C is defined as the temperature at which the viscosity is 12 $\log_{10}$(Pa·s). The choice of SCHOTT SF6® glass for the experiments mainly due to its glass transition temperature. The temperature limit for the present HPT setup is ~540 °C due to the softening of the anvil steel Boehler S390 MC around that temperature in combination with the loads applied.

2.3 Piston-cylinder apparatus

Piston-cylinder apparatus as used in our study generate pressures ranging from 0.3 to 4 GPa and temperatures of up to ~1800 °C and are widely utilized in geological studies, especially for the investigation of the lower crust and uppermost mantle of the Earth. (Boyd & England, 1960; Hinrichs & Jornada, 1997; Tsuchiya et al., 2016; Ziaja et al., 2014) A custom-build piston-cylinder apparatus (Ziaja et al., 2014), as shown in Fig.2.1(c), with an improved design based on the principle of Boyd and England (Boyd & England, 1960) was applied for the static high-pressure treatment in this project.

The sample was contained in a one-inch pressure vessel, which consisted of a tungsten carbide pressure core surrounded by a pre-stressed steel ring. An internal graphite furnace and B-type thermocouple were used to control the heat-up of the sample. The pressure vessel is supported by a 6500 kN hydraulic press, whereas the sample pressure is generated by a one-inch tungsten carbide piston driven by a second 1500 kN hydraulic cylinder.

The assembly used for this project is shown in Fig. 2.1(a). The sample has been ground to fit the inner dimensions of a Pt capsule which was welded shut. A hydrostatic pressure is achieved by the use of the pressure medium NaCl, which exhibits extraordinary low shear strength, and which effectively converts the uniaxial pressure from the piston into a hydrostatic pressure. A thin inner insulator of alumina ceramic acts as an electric insulator against the furnace. The borosilicate glass sleeve stabilizes the furnace and separates it from the outer NaCl pressure medium. The temperature was measured by a B-type thermocouple which was positioned 0.5 mm above the capsule and is kept stable to ± 1 °C by a temperature control unit. The cooling system with pre-cooled water effectively cools the stress ring of the pressure vessel.

The diameter of the assembly is approximately 0.02 mm smaller than the cavity of the bore in the pressure vessel to ensure the assembly can smoothly sliding into the cavity. Before the high-pressure is applied, the end-load is raised to 60 bar oil pressure to ensure

the proper alignment of the assembly. The oil pressure of the second circuit is then slowly raised. The sample pressure will then increase proportionally with the end load pressure above 60 bars at a rate of 0.5 kbar/min. A Siemens SPS system is used to keep the pressure constant during the experiment. Both of the heating and cooling of the sample proceeds under high pressure. The release of pressure is performed at a slow rate (-0.05-0.2 GPa/h) to allow the pressure medium to flow and release shear stress.

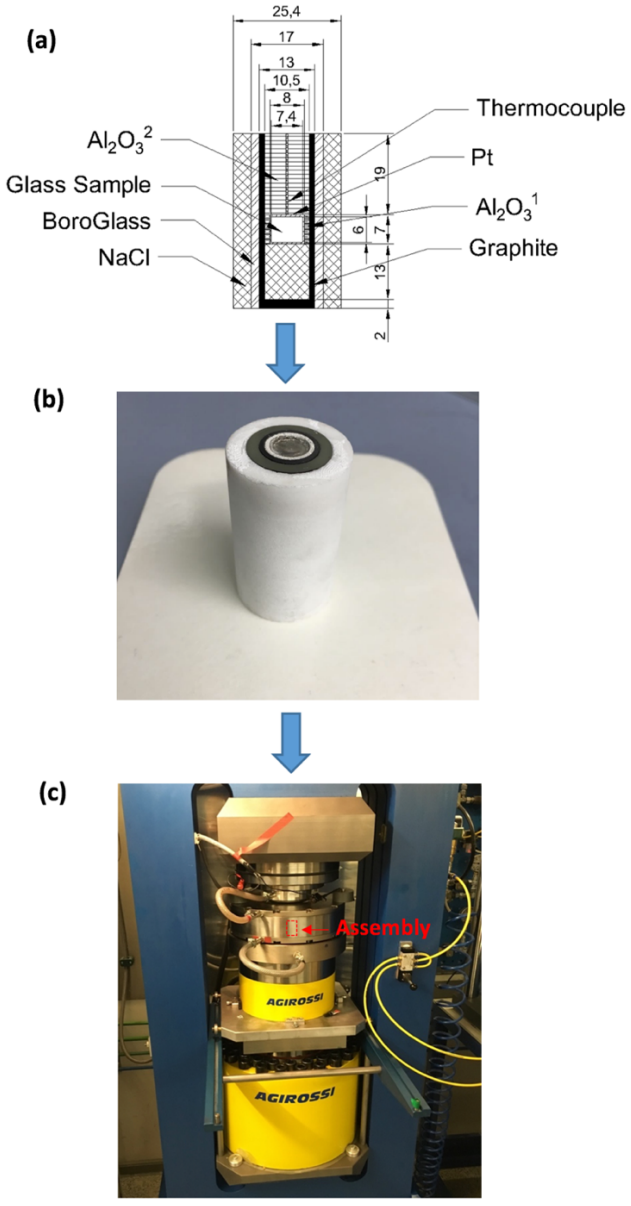

Fig. 2.1 *(a) Design of the assembly; (b) Assembly before being pushed into the position; (c) The Piston-cylinder apparatus used for this study.*

2.3.1 Calibration

The pressure acting on the sample is determined via the measurement of the oil pressure in the hydraulic cylinders. The calibration corrects for the friction in the pressure vessel and the assembly but is almost indistinguishable from the theoretical value (force/piston cross-section).

Whereas temperature can be measured directly at the capsule top, pressure has to be determined indirectly. Therefore, the phase equilibrium Albite ⇔ Jadeite + Quartz was used for the calibration. The boundary between these phases has been determined by (Holland, 1980) and others and can be described as:

$$P = 0.35 + 0.0265T(℃) \pm 0.50\ kbar \qquad (2.1)$$

To put in relation sample pressure with oil pressure a series of experiments with all three phases present was performed along a P, T-grid above and below this boundary. Pressure could be bracketed and corrected in this way.

2.4 Paterson Press

The Paterson Press (Paterson, 1990) is a gas medium high-pressure hot press, widely applied to geological experiments. The simplified schematic graph of the Paterson Press in Geoscience Montpellier is shown in Fig. 2.2 (a). The hot press mainly consists of an argon gas confining medium, and internal force load cell, an internal 3-zone furnace, and a fine displacement sensor.

The apparatus is used with a routine confining pressure of 300 ± 1 MPa, but the confining pressure can range from 50 to 350 MPa. Using argon gas as pressure-medium produces perfectly hydrostatic confining pressure and prevent chemical reactions with the samples even at high temperature. The force is measured using an internal load cell (2 kN to 75 kN), resulting in an uncertainty in net axial stress (σ_{load}) of less than 20 MPa. The internal furnace is designed by using Molybdenum (99.95%, diameter of 0.5 mm) as heating materials, and the heating is consisting of 3 zones with 13 turns on the top, 27

turns in the center and 22 turns at the bottom, to ensure a long thermal equilibrium temperature zone around the sample. The temperature was kept constant using a proportional–integral–derivative (PID) controller during the mechanical experiment as a small variation in temperature could result in significant variations of viscosity. The fine displacement sensor measures the accurate displacement of the sample during deformation with a measurement error of less than 1 μm, which is the most important data record to determine the strain rate.

For the deformation experiment, the glass samples were encapsulated with zirconia and alumina pistons and alumina spacers inside a copper jacket as shown in Fig. 2.2 (b), following well-established experimental protocols (Demouchy et al., 2009; Demouchy et al., 2013; Karato et al., 1986; Mei & Kohlstedt, 2000a; Mei & Kohlstedt, 2000b).

To determine the viscosity, firstly, the displacement is corrected concerning the elastic distortion of the machine.

$$DisF_{corr} = DisF - Dist = DisF - 1/82.5F_{corr} \qquad (2.2)$$

Where $DisF_{corr}$ is the corrected displacements, $DisF$ is the displacement measured by the machine, $Dist$ is the distortion of the machine (approximately 1/82.5 mm/kN). The length of the sample then change by the deformation can be calculated by

$$L = L_0 - DisF_{corr} \qquad (2.3)$$

Therefore, the uniaxial strain ε is

$$\varepsilon = 1 - L/L_0 \qquad (2.4)$$

To calculate the net uniaxial stress σ we use

$$\sigma = F_{corr}/S \qquad (2.5)$$

where F_{corr} is the net uniaxial force on the sample, and S is the instantaneous surface area of the sample during deformation. The F_{corr} is corrected by excluding the force on the copper jacket F_{Cu} by following (Frost & Ashby, 1982)

$$F_{corr} = F - F_{Cu} \qquad (2.6)$$

where F is the internal force measured by the internal load cell. And the deformation area is changing by

$$S = S_0(L_0/L) \qquad (2.7)$$

Finally, we calculate the viscosity η in the uniaxial deformation by using

$$\eta = \sigma/(3\dot{\varepsilon}) \qquad (2.8)$$

where the strain rate $\dot{\varepsilon}$ is calculated by

$$\dot{\varepsilon} = \frac{dDisF_{corr}}{dt}\frac{1}{L_0} \qquad (2.9)$$

we applied a mathematical approximation (not unique) to the displacement and time curve to obtain smooth derivative results.

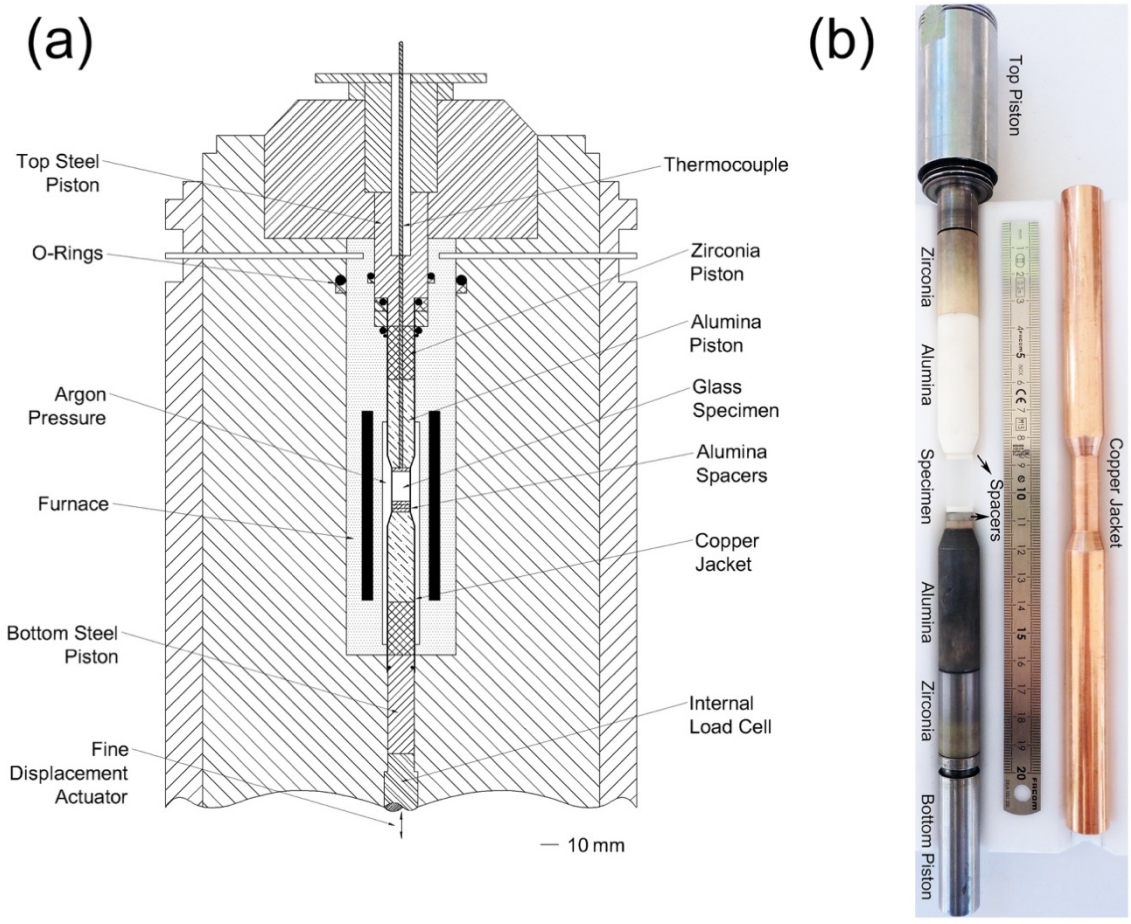

Fig. 2.2 *(a) Simplified schematic graph of the Paterson press used in this project; (b) Photograph of the high-pressure assembly for the deformation experiment.*

2.4.1 Calibration

The temperature calibration experiments were performed at the pressure of 300 MPa and temperature close to the glass transition temperature of the SCHOTT N-BK7® glass (561℃). The results are shown in Fig. 2.3 and have excellent reproducibility. However, the calibration assembly used a hollow alumina cylinder instead of the SCHOTT N-BK7® glass cylinder, which may have affected the temperature distribution. We have tried to calibrate the furnace using a specifically designed hollow SCHOTT N-BK7® glass cylinder, but at high temperature and pressure the hole for the thermocouple (which is at room pressure) shrunk as a result of viscous flow under high confining pressure, preventing any successful temperature calibration with a glass specimen. The different thermal conductivity between the SCHOTT N-BK7® glass hollow cylinder and the alumina hollow cylinder could have caused a slight change in temperature distribution.

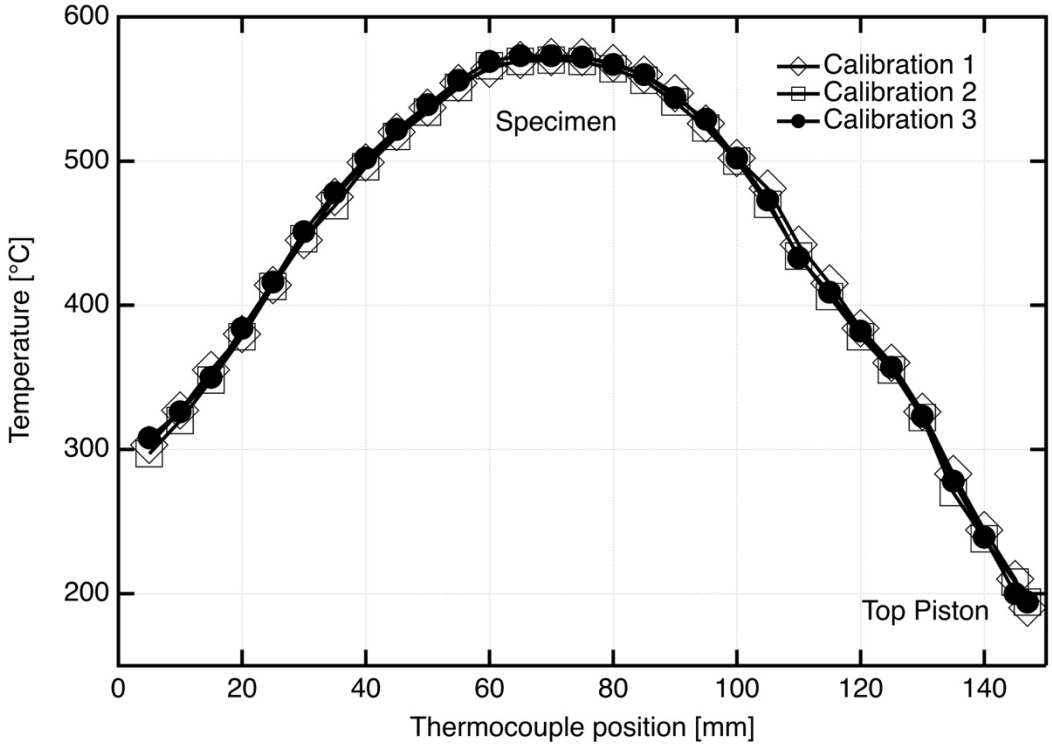

Fig. 2.3 *Results of temperature calibration experiments in Paterson Press*

2.5 High-pressure torsion apparatus

High-pressure torsion (HPT) is a well-known method of severe plastic deformation [31-33]. It allows for the controlled generation of high pressures and large strains at a number of exterior physical parameters such as strain rate and temperature. Thus, HPT is a good choice for highly reproducible experiments under extreme conditions (i.e., high pressure and high temperature). The high-pressure torsion (HPT) apparatus used in these experiments is a Klement HTP pre-series machine, with the same basic design as described in Vorhauer, et al. [32] and Wetscher, et al. [34], a sketch of the principle of operation of HPT in University of Vienna is shown in Fig. 2.4.

In the HPT machine, the shear strain γ is related to the number of turns n, the deformation radius r, and thickness of sample H, according to

$$\gamma = \frac{2\pi n r}{H} \qquad (2.10)$$

Two anvils are pressed against each other with the (glass) sample in between thus applying hydrostatic pressure. The contact surfaces between sample and anvil can be both flat (unconstrained HPT), both with identical cavities or with asymmetric cavities (quasi-constrained HPT). The unconstrained HPT configuration is most similar for a classical rheometer whereas the symmetric cavities are most common and correspond closest to a true hydrostatic loading of the sample, as during the initial uniaxial compression, a burr forms in the gap between the anvils on the rim of the cavity providing a sealing of the sample as well as preventing the anvils from touching which results in the measurement of the friction of the anvils instead of the load on the samples. In the present case for a proper formation of the burr, the total depth of both cavities was determined to be approximately 20% smaller than the thickness of the glass sample. With this experimentally determined value, only a small amount of the material freely flows into the burr during the initial part of the experiment.

The heating was performed using a Hüttinger induction heater, symmetrically heating the anvils. The temperature control and monitoring were done by using a Sensortherm pyrometer with a control unit capable of detecting temperatures above 75 °C. The control window of the setup is below 0.5 °C. A temperature increase during deformation was detected by (Edalati et al., 2011) on the experiments of Al, Cu, Fe, etc. Depends on the anvil materials, the loading pressure can go up to ~7 GPa, the temperature is maximum ~540 ℃, and the lowest torsion speed is ~0.01 rounds per minute (RPM).

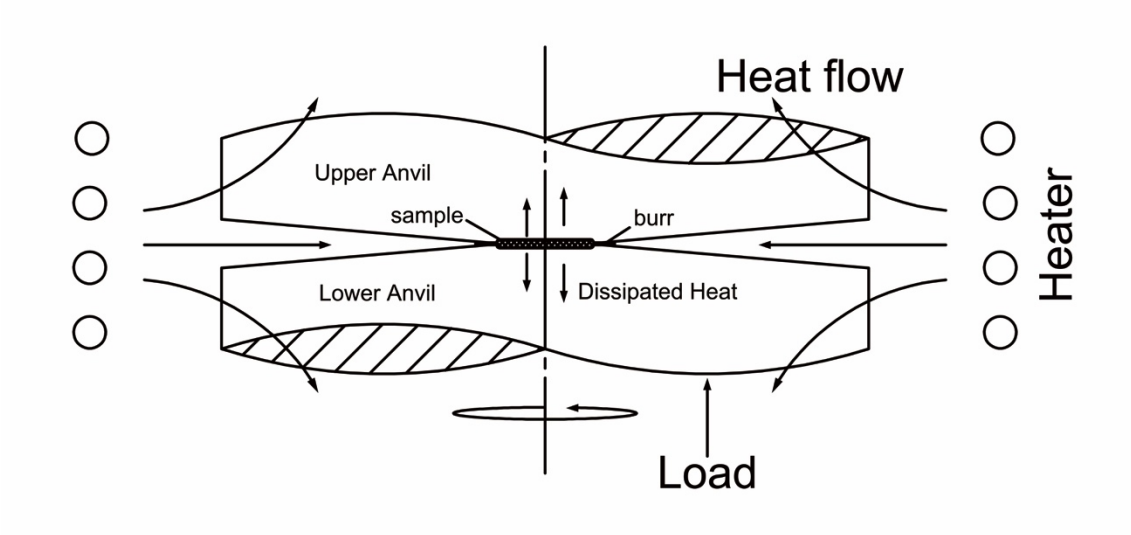

Fig. 2.4 *Schematic graph of the high-pressure torsion apparatus in this project.*

2.5.1 Calibration

The temperature calibration is done by performing a reference measurement using a thermocouple in a copper disc in place of the sample showed that the sample lags at most two minutes behind the Pyrometer data (large deviation at low temperatures). The total uncertainty of the temperature is about ±5 °C.

Before each set of the deformation experiments, the raw physical value (mV/V) of the strain-gauge signal was calibrated using a standard Gedore torque-wrench at 100 Nm, with a limiting precision of 2% without any pressure applied. The calibration was also

monitored randomly between experiments. The schematic graph of torque calibration experiment is shown in Fig. 2.5 (a), and one of the calibration result is shown in Fig. 2.5 (b). The calibration device is firstly fixed on the torque sensor, and then we push the force tool forward or backward many times to get the calibration data. For example, the calibration experiment in Fig. 2.5 (b) indicates that approximately 0.22 mV/V is equal to 100 N·m. The zero point of the torque calibration was also checked to ensure the accuracy of the torque calibration.

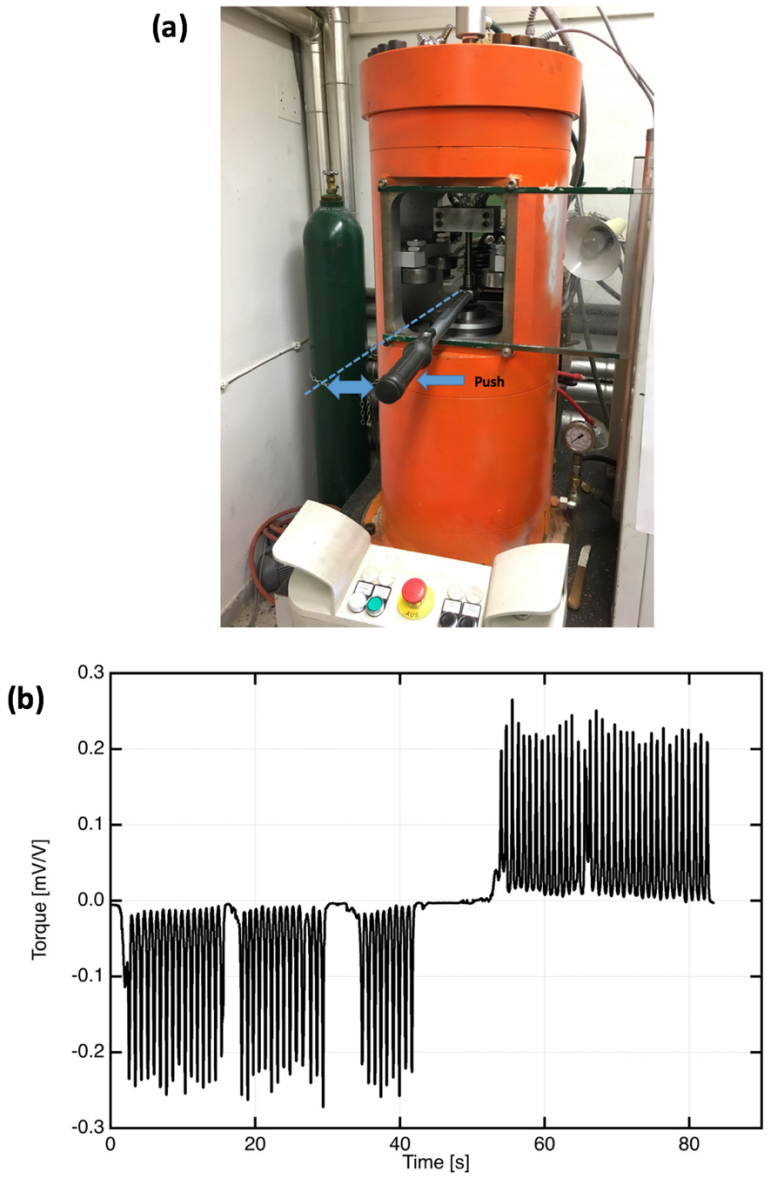

Fig. 2.5 *(a) The schematic graph of torque calibration experiment; (b) Result of one torque calibration experiment.*

2.6 Dilatometer

The DIL 806 (Bähr) optical dilatometer (Li et al., 2015; Li et al., 2013), which can measure length change entirely without contact, is widely used in linear thermal expansion measurement for glass.

Normally, the result of a temperature measurement can be obtained from a simple calibration, $T_{sample}=T_{measure}+\Delta T$, ΔT is the difference of α-β transformation temperature of standard quartz between data measured from the dilatometer and records in references (573±0.5 °C) (Kelley, 1960; Majumdar et al., 1964; Van Groos & Heege, 1973).

However, based on the results of previous measurements, the temperature inside the DIL 806 is not homogenous enough for accurate linear thermal expansion coefficient measurements, as the furnace is designed for large heating and cooling rate experiments. Therefore, a system calibration must be done on the DIL 806 to get data with high credibility.

2.6.1 Calibration

The standard square quartz specimen with dimensions of 10mm×5mm×3mm was used for the calibration measurements. The dilatometer (DIL806, Bähr) was heating from room temperature to 520 °C by a rate of 20 K/min, then applied a 5K/min to 600 °C.

The standard quartz specimen was moved away from the border of the furnace (laser sender side) in setup 1 (Fig. 2.6 (a)), with a distance of 26.50±0.20 mm (1Q2650), 29.00±0.20 mm, 31.50±0.20 mm and 34.00±0.20 mm, respectively. It can be seen in Fig. 2.6 (b) that the measured α-β transformation temperature of the standard quartz specimen was changed by the changing of measure position. The measured starting α-β transformation temperatures are 564.1±0.1 °C, 560.1±0.1 °C, 557.3±0.1 °C, 553.8±0.0 °C with each distance increasing of 2.5 mm. The consequence α-β transformation temperature change from 1.1 °C/mm to 1.9 °C/mm by the movement of the specimen in setup 1. Besides, there are 2-3 peaks around the α-βtransformation temperatures in each

linear thermal expansion coefficient calculation (α_{diff}). The multiple peaks are probably analytical results from smoothing within the software or the heating control algorithm.

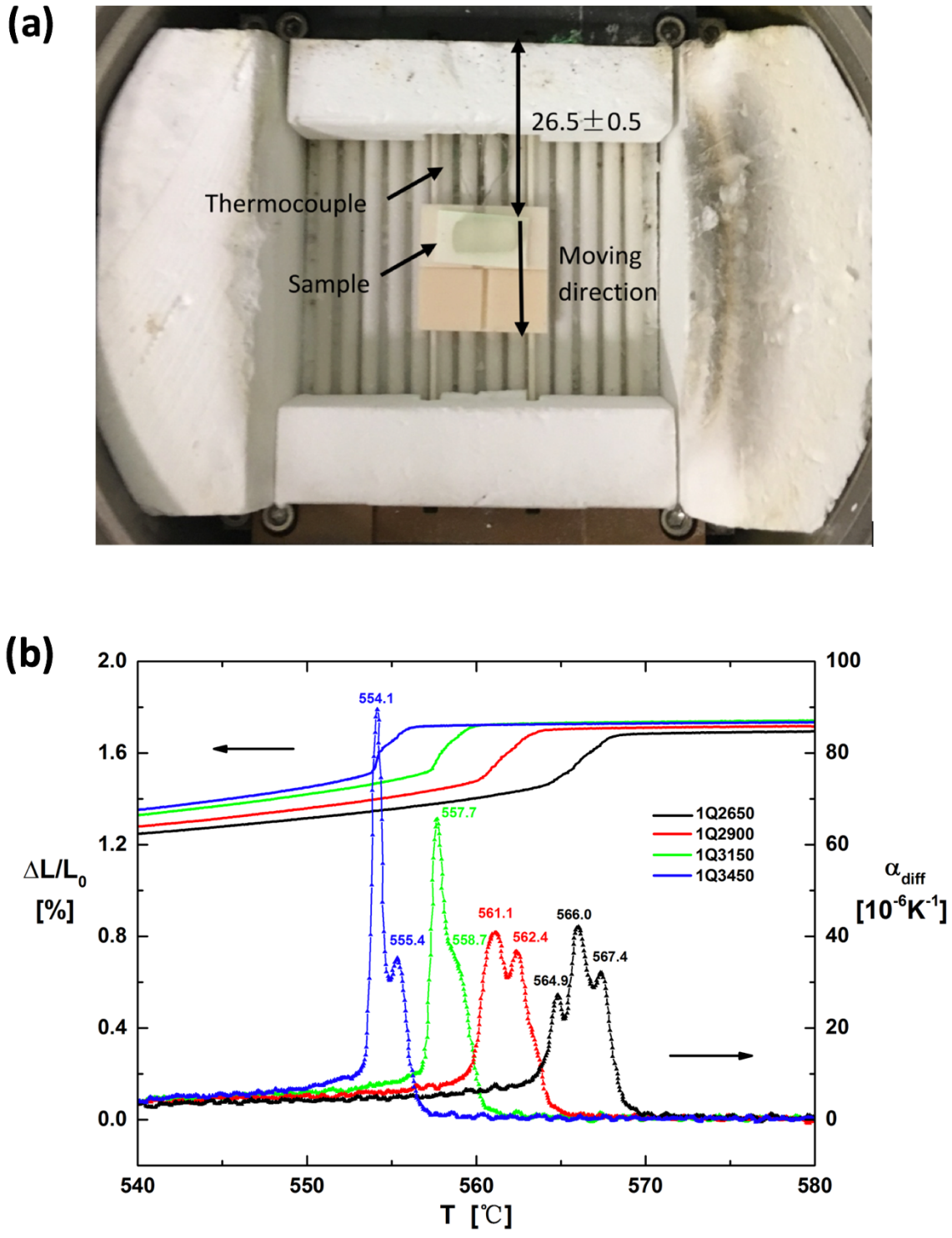

Fig. 2.6 *(a) Setup 1; (b) The relative of position change and it's calculated linear thermal expansion coefficient as a function of temperature.*

To account for the effect of the shape, the thermocouple in DIL 806 was changed to another two different shapes to build 2 new setups, namely setup 2 and setup 3. Results show in Fig. 2.7 that the shape of the thermocouple could greatly influence the temperature measurement. The measured starting α-β transformation temperature in setup 2 is 552.3±0.0°C at the position of 24.00±0.20 mm (2Q2400) and 550.5±0.2 °C at the position of 26.50±0.20 mm (2Q2650), which are very different from setup 1. The two thermocouple wires were clearly separated to avoid the early touching in setup 3 (3Q2650) (one above the alumina support and the other down). The measured α-β transformation temperature is increased to 574.6±0.0 °C, which is approximately 24 °C higher than the setup 2.

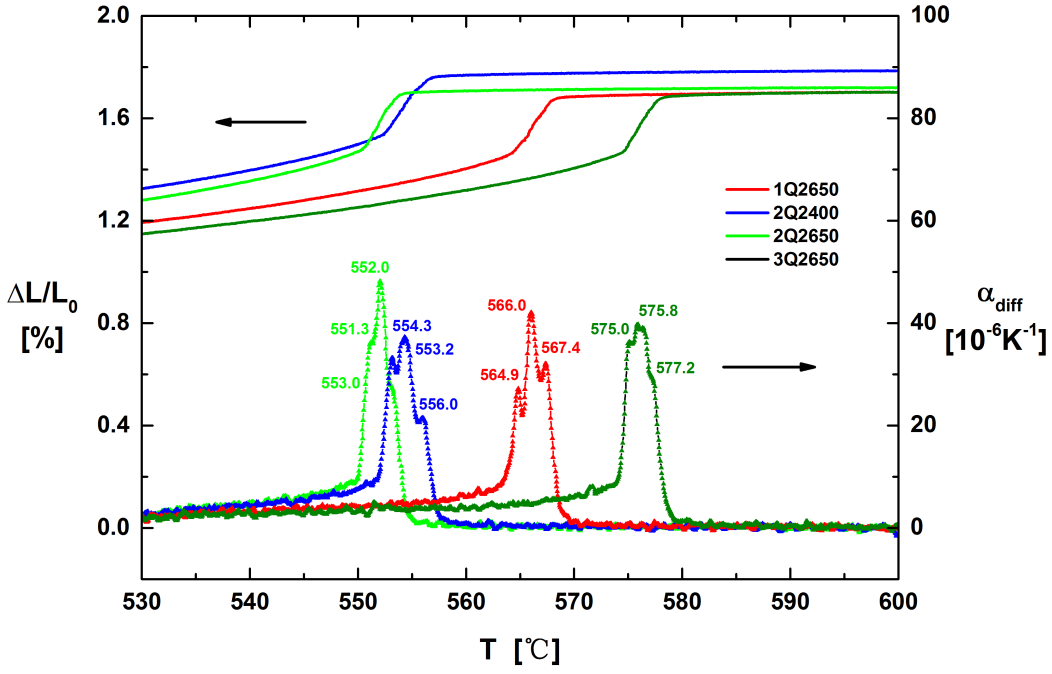

Fig. 2.7 *The relative of measured position change and it's calculated differential thermal expansion coefficient as a function of temperature in setups 1-3.*

To avoid the thermocouple shape change, the alumina support was machined with grooves perfectly separates the thermocouple wires. The new setup 4 can measure a wide

range of positions starting from a distance of 16.20±0.20 mm (4Q1620). The position of standard quartz specimen was moved from 16.20±0.20 mm to 32.20±0.20 mm by a constant distance of 2 mm further to the laser sender side. As shown in Fig. 2.8, the α-β transformations were not finished by the temperature of 600 °C at the positions of 16.20±0.20 mm and 18.20±0.20 mm, which indicates that the real temperatures in these two positions were below the real α-βtransformation temperature of quartz (573 °C). The following α-β transformation temperatures with a change from 1.55 °C/mm to 5.54 °C/mm at different positions.

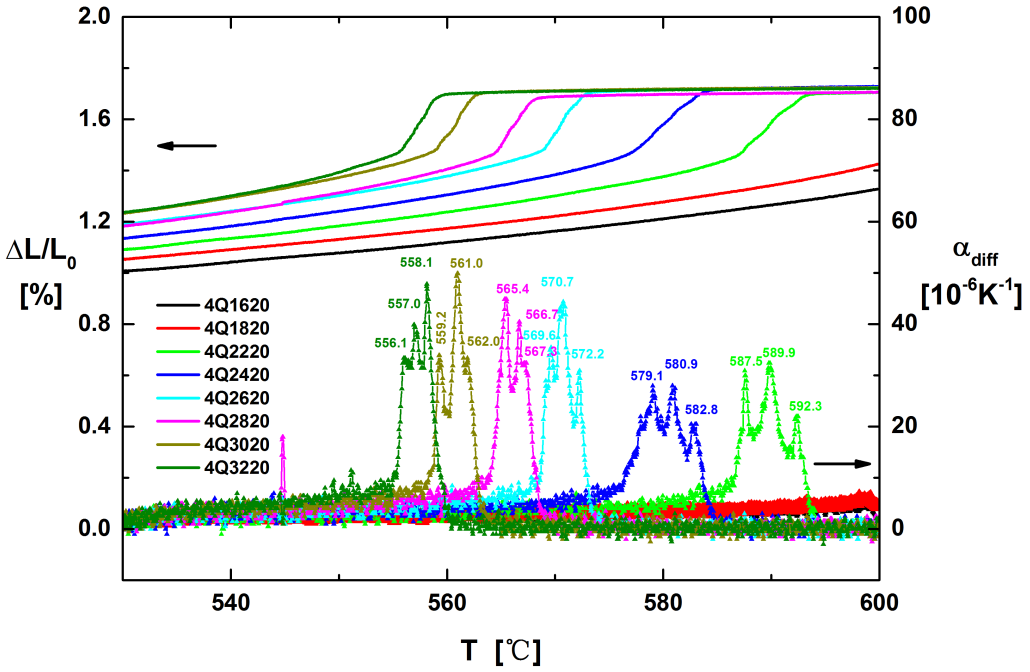

Fig. 2.8 *The relative of measured position change and it's calculated differential thermal expansion coefficient as a function of temperature in setup 4.*

Finally, as the thermocouple in the DIL 806 was seriously aged, the new setup 5 (shown in Fig. 2.9 (a)) was built by replacing a new thermocouple. Based on the results mentioned above, the specimen should place in a settled position without changing the shape of the thermocouple for the measurements. The last series of calibration

experiments were performed at a distance of 26.50±0.20 mm. As shown in Fig. 2.9 (b), the measured α-β transformation temperatures of the standard quartz specimen are very stable at 568.7±0.3°C. The peaks of the linear thermal expansion coefficient temperatures (α_{diff}) are very similar close to the α-β transformation temperatures, which indicates a reasonable repeatability.

In summary, the setup 5 with reasonable repeatability is used to perform the volume recovery measurements to study the volumetric flow of glass.

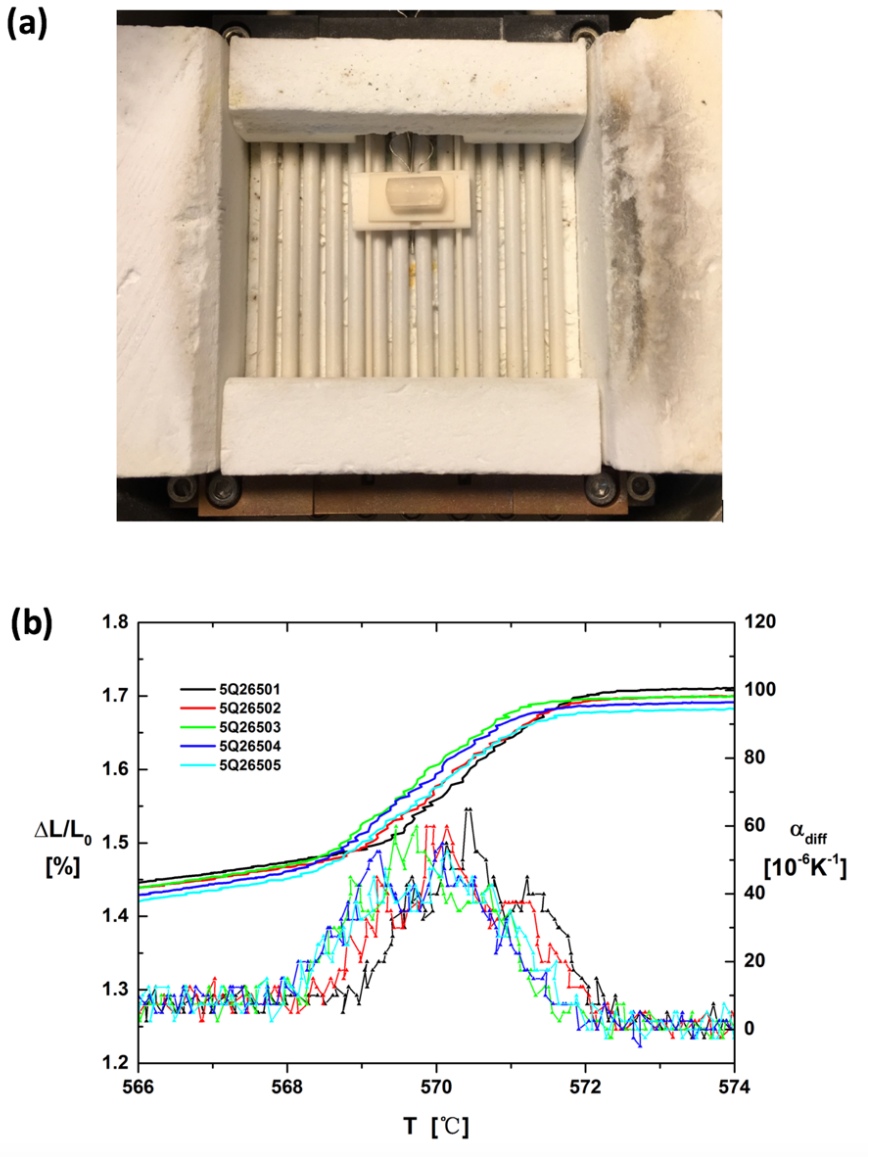

Fig. 2.9 *(a) Setup 5; (b) The relative of measured position change and it's calculated differential thermal expansion coefficient as a function of temperature.*

2.7 Density balance

The Mettler Toledo-XP205 analytical balance produced by Archimedes principle was used for the density experiments. The density of the sample is calculated with Eq. 2.11

$$\rho = \frac{G_a * \rho_l - G_l * \rho_a}{G_a - G_l} \qquad (2.11)$$

where is the density of the sample, g/cm^3, G_a is the mass in air, g, ρ_l is the density of the liquid, g/cm^3, G_l is the mass of sample in liquid, g, and ρ_a is the density of air, g/cm^3.

The uncertainty of density was then calculated by Eq. 2.12

$$\Delta\rho_t = \sqrt{\left(\frac{\rho_l}{G_a - G_l}\right)^2 * \Delta G_a^{\,2} + \left(\frac{G_l * \rho_a - G_a * \rho_l}{(G_a - G_l)^2}\right)^2 * \Delta G_a^{\,2} + \left(\frac{G_a}{G_a - G_l}\right)^2 * \Delta\rho_l^{\,2} + \left(\frac{G_a * \rho_l - G_l * \rho_a}{(G_a - G_l)^2}\right)^2 * \Delta G_l^{\,2} + \left(\frac{\rho_a}{G_a - G_l}\right)^2 * \Delta G_l^{\,2} + \left(\frac{G_l}{G_a - G_l}\right)^2 * \Delta\rho_a^{\,2}}$$

(2.12)

where $\Delta\rho_t$ is the theoretical uncertainty for the density measurement equipment calculated by Eq. 2.12, in which ΔG_a=±0.000022 g, ΔG_l=±0.000022 g, $\Delta\rho_l$=±0.000021 g/cm^3, $\Delta\rho_a$=±0.000001 g/cm^3. The statistical uncertainty $\Delta\rho_s$ was from the 95% confidence interval of the student's t-test and the standard deviation. The uncertainty of density is calculated by Eq. 2.13

$$\Delta\rho = \sqrt{\Delta\rho_t^{\,2} + \Delta\rho_s^{\,2}} \qquad (2.13)$$

All the samples were measured for five times and the results were the average value rounded to four decimals.

2.7.1 Calibration

The calibration of the density machine is done by the technician in SCHOTT physics laboratory in Mainz. To secure the measurement accuracy, the calibration work is conducting by the following four steps:

(1) Every day before starting the measurement, the balance with a single standard weight is checked. Moreover, the balance itself has an internal adjustment-function that runs automatically at least once.

(2) Every week, a check measurement with control samples is performed.

(3) Every month, the liquid for the measurement is changed and meanwhile the balance with 3 different weights is checked.

(4) Every year, an external service for checking the balance is performed.

2.8 References

Boyd, F. R. & England, J. L. (1960). Apparatus for Phase-Equilibrium Measurements at Pressures up to 50-Kilobars and Temperatures up to 1750-Degrees-C. *Journal of Geophysical Research*, 65 (2): 741-748.

Demouchy, S., Schneider, S. E., Mackwell, S. J., Zimmerman, M. E. & Kohlstedt, D. L. (2009). Experimental deformation of olivine single crystals at lithospheric temperatures. *Geophysical Research Letters*, 36: L04304.

Demouchy, S., Tommasi, A., Ballaran, T. B. & Cordier, P. (2013). Low strength of Earth's uppermost mantle inferred from tri-axial deformation experiments on dry olivine crystals. *Physics of the Earth and Planetary Interiors*, 220: 37-49.

Dyer, P. E., Maswadi, S. M., Walton, C. D., Ersoz, M., Fletcher, P. D. I. & Paunov, V. N. (2003). 157-nm laser micromachining of N-BK7 glass and replication for microcontact printing. *Applied Physics a-Materials Science & Processing*, 77 (3-4): 391-394.

Edalati, K., Miresmaeili, R., Horita, Z., Kanayama, H. & Pippan, R. (2011). Significance of temperature increase in processing by high-pressure torsion. *Materials Science and Engineering a-Structural Materials Properties Microstructure and Processing*, 528 (24): 7301-7305.

Efimov, A. & Taylor, A. J. (2008). Supercontinuum generation and soliton timing jitter in SF6 soft glass photonic crystal fibers. *Optics Express*, 16 (8): 5942-5953.

Frost, H. J. & Ashby, M. F. (1982). *Deformation mechanism maps: the plasticity and creep of metals and ceramics*: Pergamon press.

Fu, B., Li, S. G., Yao, Y. Y., Zhang, L. & Zhang, M. Y. (2010). Supercontinuum

Generation with High Birefringence SF6 Soft Glass Photonic Crystal Fibers. *Chinese Physics Letters*, 27 (7).

Heiman, D., Hamilton, D. S. & Hellwarth, R. W. (1979). Brillouin-Scattering Measurements on Optical-Glasses. *Physical Review B*, 19 (12): 6583-6592.

Hinrichs, R. & Jornada, J. A. H. (1997). Piston-cylinder apparatus for high pressure impedance spectroscopy. *Review of Scientific Instruments*, 68 (1): 193-196.

Holland, T. (1980). The reaction albite= jadeite+ quartz determined experimentally in the range 600-1200 degrees C. *American Mineralogist*, 65 (1-2): 129-134.

Hundertmark, H., Rammler, S., Wilken, T., Holzwarth, R., Hansch, T. W. & Russell, P. S. (2009). Octave-spanning supercontinuum generated in SF6-glass PCF by a 1060 nm mode-locked fibre laser delivering 20 pJ per pulse. *Optics Express*, 17 (3): 1919-1924.

Karato, S. I., Paterson, M. S. & Fitz Gerald, J. D. (1986). Rheology of Synthetic Olivine Aggregates - Influence of Grain-Size and Water. *Journal of Geophysical Research-Solid Earth and Planets*, 91 (B8): 8151-8176.

Kelley, K. K. (1960). Contributions to the data on theoretical metallurgy, XIII. High-temperature heat-content, heat-capacity, and entropy data for the elements and inorganic compounds. *Bulletin 584 Bureau of Mines*.

Koontz, E., Blouin, V., Wachtel, P., Musgraves, J. D. & Richardson, K. (2012). Prony Series Spectra of Structural Relaxation in N-BK7 for Finite Element Modeling. *Journal of Physical Chemistry A*, 116 (50): 12198-12205.

Li, F., Wan, W. J., Lai, J. C., Liu, F., Qi, H. X., Li, X. S. & You, X. Z. (2015). Investigations on the polyimides derived from unfunctionalized symmetric cyclopentyl-containing alicyclic cardo-type dianhydride. *Journal of Applied Polymer Science*, 132 (42).

Li, J., Zhang, H. S., Liu, F., Lai, J. C., Qi, H. X. & You, X. Z. (2013). A new series of fluorinated alicyclic-functionalized polyimides derivated from natural-(D)-

camphor: Synthesis, structure-properties relationships and dynamic dielectric analyses. *Polymer*, 54 (21): 5673-5683.

Majumdar, A., McKinstry, M. & Roy, R. (1964). Thermodynamic parameters for the α-β quartz and α-β cristobalite transitions. *Journal of Physics and Chemistry of Solids*, 25 (12): 1487-1489.

Mei, S. & Kohlstedt, D. L. (2000a). Influence of water on plastic deformation of olivine aggregates 1. Diffusion creep regime. *Journal of Geophysical Research-Solid Earth*, 105 (B9): 21457-21469.

Mei, S. & Kohlstedt, D. L. (2000b). Influence of water on plastic deformation of olivine aggregates 2. Dislocation creep regime. *Journal of Geophysical Research-Solid Earth*, 105 (B9): 21471-21481.

Mosaddegh, P. & Ziegert, J. C. (2011). Friction measurement in precision glass molding: An experimental study. *Journal of Non-Crystalline Solids*, 357 (16-17): 3221-3225.

Paterson, M. (1990). Rock deformation experimentation. *Geophysical monograph*: 187-194.

Tsuchiya, S., Kino, Y., Nakagawa, K., Nakagawa, D., Yamada, J. & Toda, Y. (2016). Development of an optical time-resolved measurement system under high-pressure and low-temperature with a piston-cylinder pressure cell. *Review of Scientific Instruments*, 87 (4).

Van Groos, A. K. & Heege, J. T. (1973). The high-low quartz transition up to 10 kilobars pressure. *The Journal of Geology*, 81 (6): 717-724.

Ziaja, K., Foley, S. F., White, R. W. & Buhre, S. (2014). Metamorphism and melting of picritic crust in the early Earth. *Lithos*, 189: 173-184.

Chapter 3

3. Volumetric flow of glass under high pressure

Published in *Journal of the American Ceramic Society*

Ding L, Buhre S, Kunisch C, Kaus B. Pressure dependence of density and structural relaxation of glass near the glass transition region. *J Am Ceram Soc*. 2018;101:1149–1158.

3.1 Summary

A simplified and effective pressure cell together with an experimental procedure has been developed and applied to compress samples of SCHOTT N-BK7® glass under static high pressures in a piston-cylinder apparatus. Results from the density and volume recovery measurements show that, the glass samples were effectively densified in piston-cylinder apparatus with the density at room temperature increasing linearly with frozen-in pressure. To explain the experimental data, we developed a mathematical model based on a suggestion by Gupta (1988) with two internal parameters, named fictive temperature (T_f) and fictive pressure (P_f), which fits the experimental data well.

3.2 Introduction

It is well known that the properties of glass at room temperature are influenced by temperature, particularly around the glass transition region (Ritland, 1956). Glass is not in equilibrium, but instead, the structure and properties of glass are time-dependent while it aims to reach equilibrium (Scherer, 1986; Welch et al., 2013). The temperature and time-dependence of properties as well as the structural relaxation of glass in the glass transition region have been well-characterized experimentally and can be explained with several mathematical models (Mauro et al., 2009; Narayanaswamy, 1971; Ritland, 1956; Scherer, 1986; Tool, 1946). Yet, those studies were all performed for 1 bar, and did not consider the effect of increases in pressure.

However, pressure also changes the properties and the behavior of glass even at room temperature. Experimental examples are hardness measurement (Shang & Rouxel, 2005; Taylor, 1949) and scribing of glass. In the glass transition range, the viscosity strongly depends on density (Cook et al., 1994) and thus on pressure. For example, Bridgman and Simon (Bridgman & Simon, 1953) compressed thin samples of oxide glasses (SiO_2 and B_2O_3) and several mixed silicate glasses samples between two flat dies

(uniaxial) made of carboloy at room temperature, and demonstrated that the vitreous SiO_2 had a density increase of almost 7.5% at 20 GPa, whereas the vitreous B_2O_3 has an asymptotic increase of density near 6% at pressures close to 20 GPa. An experimental study on a borosilicate glass with pressure of up to 0.66 GPa and temperatures up to 300°C, showed that the density change was very small with only 0.05% at 0.66 GPa, 200°C and 24 hours (Anderson, 1956). A compilation of experimental data shows that there are significant differences in the manner in which different glass-types react to increases in pressure (Rouxel et al., 2008). Jin et al. (Jin et al., 2003) reported a 6 K/GPa change in T_g of a metallic glass by DSC measurements, and activation volume was suggested to describe the pressure dependence of glass relaxation in a free volume model.

Several phenomenological models (Grassia & Simon, 2012; Hodge, 1994; Simon et al., 2002; Tribone et al., 1989) describe the time dependent frozen-in state and departure from equilibrium (δ) (Williams & Watts, 1970) of glass forming materials depending on temperature history (Moynihan et al., 1976; Narayanaswamy, 1971; Tool, 1946) and also pressure history (Grassia & Simon, 2012; Hodge, 1994; Simon et al., 2002; Tribone et al., 1989). Those models are based on the Tool-Narayanaswamy-Moynihan (Moynihan et al., 1976; Narayanaswamy, 1971; Tool, 1946) model and use one internal parameter named fictive temperature (T_f). On the other hand, Davies and Jones (Davies & Jones, 1953) pointed out that fictive pressure (P_f) could also be an internal parameter. Gupta (Gupta, 1988) introduced the P_f to his structural relaxation model as an internal parameter together with T_f, but has not compared his two-internal-parameter model to experimental data.

Here, we present new experimental data to study the density and structural relaxation of glass under elevated pressure of up to 1.5 GPa and elevated temperature, which were obtained using a piston-cylinder apparatus. We describe the new experimental procedure developed for this as well as a two-internal-parameter model that can overall fit the data.

3.3 Experimental procedure

3.3.1 Samples

The SCHOTT N-BK7® glass samples had been originally cooled at a rate of -0.4 K/h at ambient pressure and machined to cylinders with diameters of 7.40±0.02 mm and heights of 6.00±0.02 mm for the experiments. The density of those slow-cooled samples at room temperature is 2.5082±0.0006 g/cm^3. The glass transition temperature T_g=561 °C is taken as the temperature at which the viscosity is 10^{12} Pa·s. Specially, the sample relatively fast-cooled at a rate of -120 K/h at ambient pressure in the lab was used for comparison to the samples after high pressure treatment, as all the samples in high pressure treatment were cooled at a rate of -120 K/h. The density of this fast-cooled sample at room temperature is 2.4957±0.0007 g/cm^3.

3.3.2 High pressure treatment

Test equipment: A self-assembled piston-cylinder apparatus (Ziaja et al., 2014) with an improved design based on the principle of Boyd and England (Boyd & England, 1960) with uniaxial pressure up to 3 GPa was applied for the high pressure treatment. The uncertainty of pressure in the piston-cylinder apparatus was ±0.05 GPa.

Pressure cell development: A special pressure cell needed to be developed, to obtain glass samples with no cracks at the end of the experiments such that we obtain sufficient material for further measurements. If not, during subsequent measurements, the cracks in the sample may open and increase the apparent macroscopic volume of the sample, which erroneously would be interpreted as a decrease in density.

Experimental process: The experimental processes of high pressure treatment are shown in Fig. 3.1 (a). Glass samples are first subjected to high pressures and then heated up to 700 °C at 600 K/h. The temperature is chosen for the glass to be viscous enough for a hydrostatic pressure state to build up and to avoid crystallization. After keeping the temperature fixed for 24 hours (2 hours for the 1 GPa sample at the first experiment), the

samples are relatively fast-cooled at -120 K/h to room temperature. Pressure release is done at a rate of -0.2 GPa/h to 0.5 GPa and further at a lower rate of -0.05 GPa/h to 0.1 MPa (-1.5 GPa/h to 0.1 MPa for 1.25 GPa sample due to the programming error, purple line with open stars in Fig. 3.1 (a)). Glass samples reach stage ① after this process.

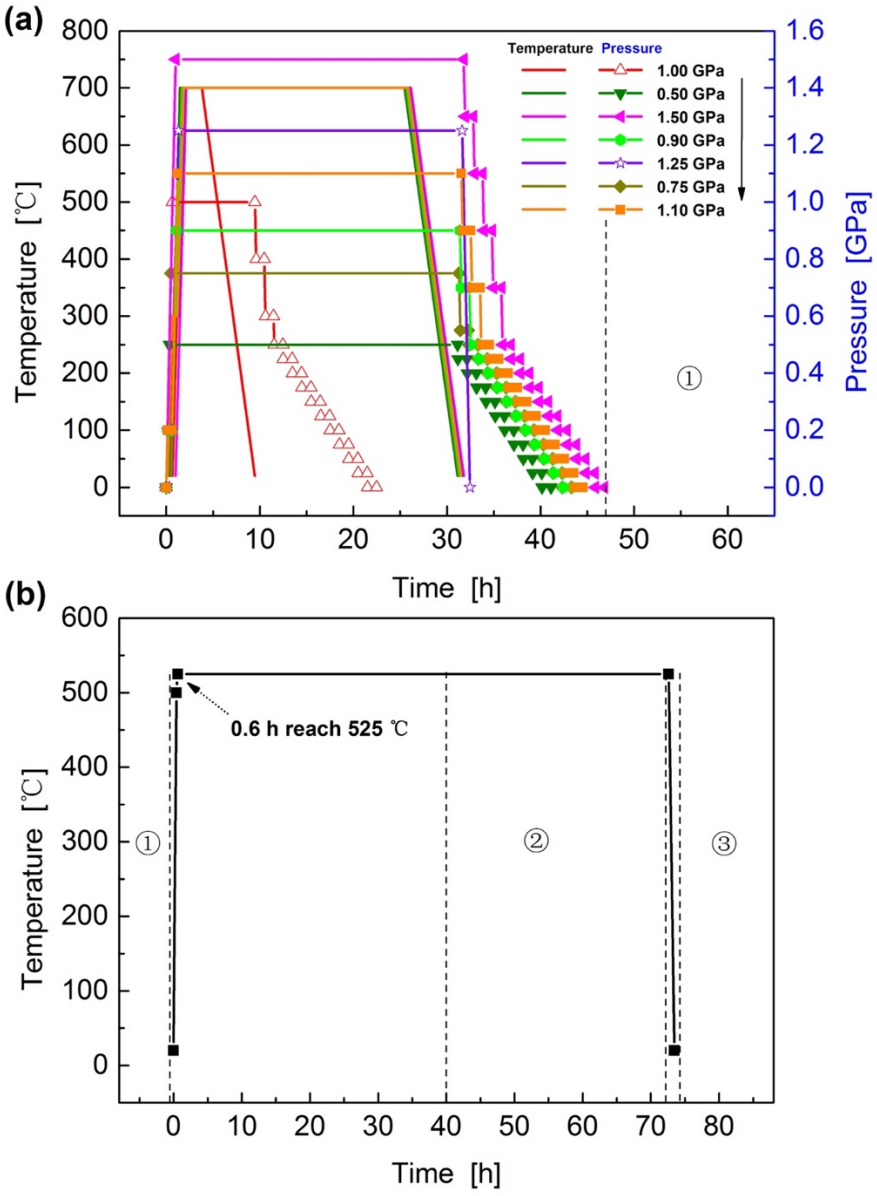

Fig. 3.1 *(a) Process of high pressure treatment in piston-cylinder apparatus; (b) process of volume recovery measurements in dilatometer for all the samples. Arrow in (a) shows the time sequence of high pressure treatment. Stage ①: samples compressed by high pressure and before volume recovery measurement; Stage ②: samples reach equilibrium in dilatometer at 525 °C; Stage ③: samples cooled down from 525 °C and moved out from the dilatometer.*

Stress condition: The stress state in the glass sample in the piston-cylinder apparatus is influenced by gaps in the pressure cell that develop during assembling, especially the gap from sample to the other parts, the stiffness and Poisson's ratio of the insulator (Rouxel et al., 2008) and by the thermal expansion coefficients of the materials used for the pressure cell. To make the glass sample more deformable than the surrounding materials, it is heated up to a temperature of 700 °C at which it behaves mainly viscous such that the glass sample obtains a hydrostatic stress state. During cooling, the glass changes from mainly viscous to frozen-in, during which the hydrostatic stress state may change into a uniaxial stress state. Therefore, the frozen-in stress state is not known precisely. For the calculations, we assume a hydrostatic stress state always. Compared to this uncertainty in the overall stress state, the stress introduced to the sample by the frozen-in temperature gradient during cooling is small.

3.3.3 Density measurement

Test equipment: The Mettler Toledo-XP205 was used for the density measurement using the Archimedes principle. The density uncertainty was calculated by the statistical uncertainty from the 95% confidence interval of the student's t-test and the standard deviation.

Experimental process: Firstly, the mass of the samples was measured in air, then the mass of samples in the liquid was measured and the temperature of the liquid was recorded at the same time. Each sample was measured 5 times and the results reported are the average values rounded to four decimals.

3.3.4 Volume recovery measurement

Test equipment: The Bähr DIL 806 optical dilatometer is used to measure the length change of the sample diameter without mechanical contact. The temperature of the dilatometer has been calibrated by a pure quartz crystal with a repeatability of α-β transformation temperature of ±0.39 °C in the same position.

Experimental process: The change in diameter was measured by applying the temperature history shown in Fig. 3.1 (b). The dilatometer was heated from room temperature to 500 °C at a rate of +1200 K/h, then at +120 K/h to 525 °C and holding for 72 hours. At the end of this isothermal hold the sample diameter does not change any more. This equilibrium state is denoted as stage ②. Afterwards, the samples were freely cooling down to the room temperature, at which they reached stage ③.

3.4 Results

3.4.1 High pressure treatment

The standard pressure cell (1#) for rock experiment resulted in a glass sample broken to many pieces. Thus, we designed and prepared the other four pressure cells seeking for a suitable pressure cell for the high pressure experiments to obtain glass samples with no crack and no blackening. The designed pressure cells and accordingly images of glass samples after high pressure treatment are shown in Fig. 3.2.

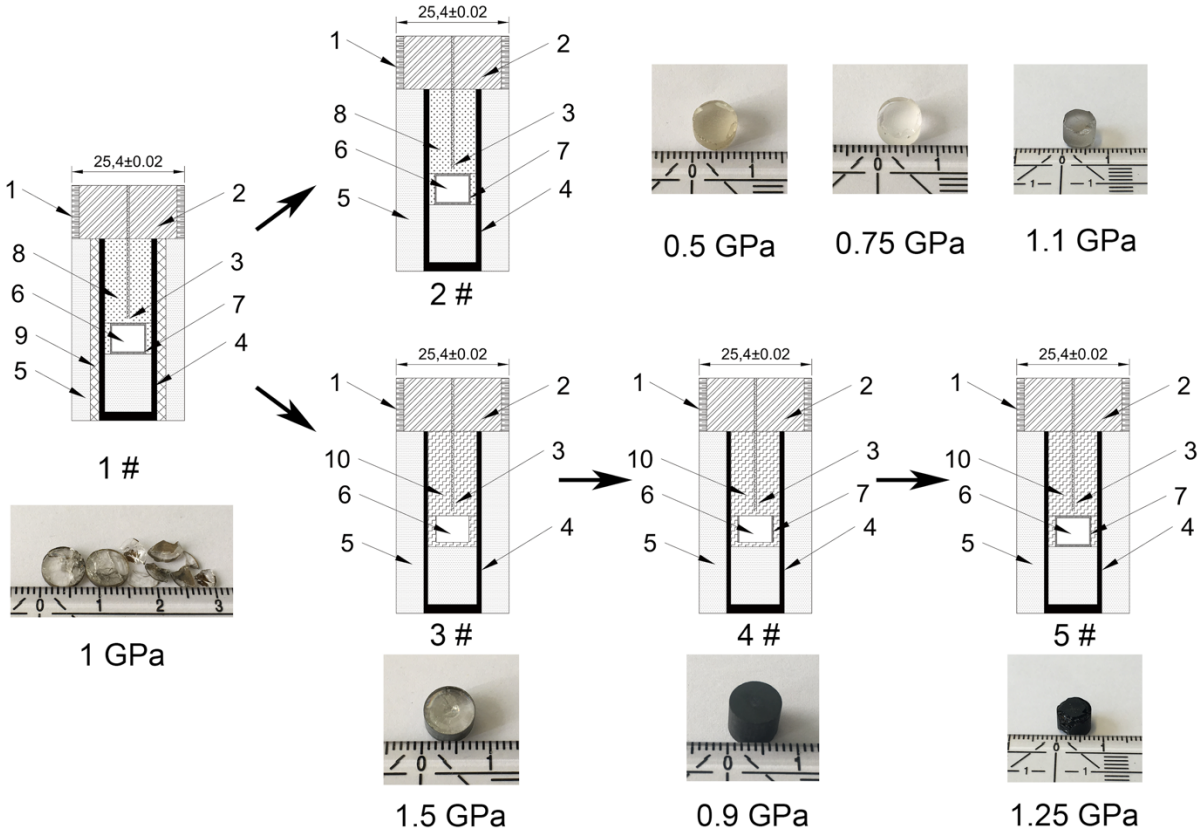

Fig. 3.2 *Pressure cells development and images of glass samples after high pressure treatment for different pressure cells. 1-Pyrophyllite; 2-Steel plug; 3-Thermocouple; 4-Graphite; 5-NaCl; 6-Sample; 7-Pt; 8-Al_2O_3; 9-Borosilicate glass; 10-h-BN.*

Pressure cell 1#: The sample was in a welded Pt capsule. The inner insulator of alumina ceramic acts as the pressure transmitting medium. The borosilicate glass separates it from the pure NaCl powder which acts as the outer insulator. The 1 GPa treatment resulted in a glass sample that was broken into many pieces, which indicates that this pressure cell is not suitable for very high pressures.

Pressure cell 2#: The borosilicate glass was removed, because it is not ductile at low temperature and it broke with a load noise during the pressurization which made the pressure cell less isostatic. The NaCl was used as the outermost sleeve and low spacer for the Pt capsule because it behaves like a liquid even at low temperature, and thereby

transmits more isostatic pressure to the furnace and the sample. The 0.5 GPa treatment resulted in a sample with only few cracks on the surface.

Pressure cell 3#: Compared to 2#, the Al_2O_3 ceramic and Pt capsule were replaced by insulating hexagonal boron nitride (h-BN). The h-BN has a graphite structure, which makes it behaves like a lubricant and leading to a more isostatic compression. The 1.5 GPa treatment resulted in a sample with a thin black layer outside and large amounts of cracks inside.

Pressure cell 4#: Based on 3#, the h-BN was kept, and a Pt sleeve was added to separate the sample from the h-BN sleeve. The 0.9 GPa treatment resulted in an optically black sample with an approximately 0.4 mm thick crystal layer outside. This crystal layer was ground off before further measurements to obtain a sample with cylindrical shape without any cracks.

Pressure cell 5#: To avoid blackening of the sample, a sealed Pt capsule replaced the Pt sleeve. However, the 1.25 GPa treatment resulted in a sample with considerable blackening and lots of fractures inside, which indicates that sealing with Pt cannot solve the blackening problem.

For further measurements, we used the pressure cell 2#, because 2# was the only pressure cell which obtained glass sample without cracks and blackening. The further compression treatment at 0.75 GPa and 1.1 GPa resulted in only small amounts of cracks at the surface and no blackening inside (similar to the 0.5 GPa sample). Moreover, the slight black film on the 1.1 GPa sample disappeared during the volume recovery measurement. Therefore, the pressure cell 2# is suitable for compressing glass.

3.4.2 Density after high pressure treatment

In the high pressure treatment, the glass samples were cooled at the fast cooling rate of -120 K/h to room temperature (Fig. 3.3, stage ①). Compared to the fast-cooled uncompressed sample with density of 2.4957±0.0007 g/cm^3, their density increases approximately linearly with pressure, which can be fitted with:

$$\rho = 0.0723P + 2.4958 \qquad (3.1)$$

where ρ is the density of the sample at room temperature in g/cm^3, P is the applied pressure in GPa. Specifically, the density increased by 4.49% after the 1.5 GPa treatment. The sample compressed at 1 GPa (red square in Fig. 3.3) broke into several parts which led to a very high uncertainty.

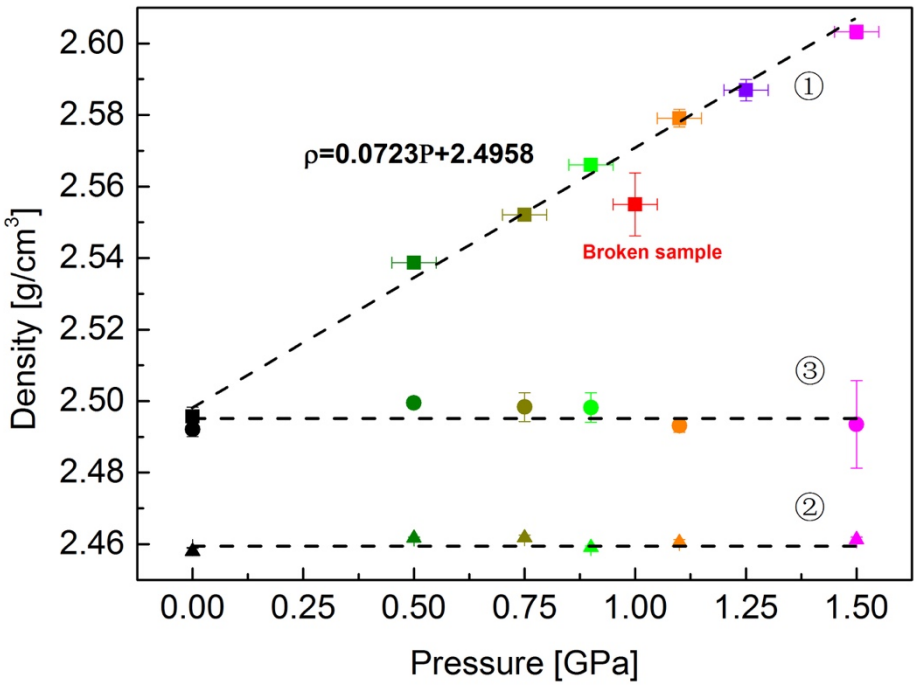

Fig. 3.3 *Density of glass samples at three different stages: Stage ① = at room temperature after high pressure treatment; Stage ② = at 525 °C, at the end of the volume recovery measurement (= equilibrium density); Stage ③ = at room temperature after free cooling from Stage ②.*

Moreover, from the density in stage ① and the measured relative length change (Fig. 3.4) during heating up and isothermal hold (Fig. 3.1 (b)) for volume recovery, the time dependent specific volume at 525 °C was calculated. At the end of the isothermal hold (stage ②), all the samples reached similar equilibrium densities of around 2.4602±0.0011 g/cm^3 at 525 °C. After free cooling to room temperature (stage ③), the density of all

samples increased to approximately 2.4958±0.0056 g/cm^3, with most measurements having a higher uncertainty than before.

The 1 GPa and 1.25 GPa samples that were treated with different experimental procedures are not used for further volume recovery measurements.

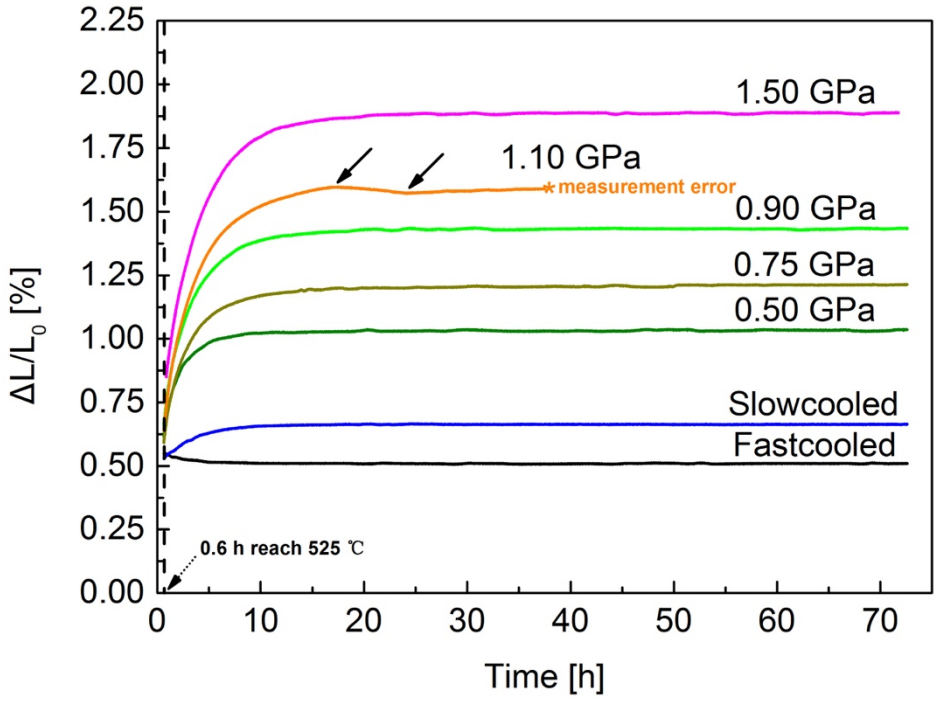

Fig. 3.4 *Relative length change of samples versus time at volume recovery temperature of 525 °C.*

3.4.3 Volume recovery

The measured relative length changes in diameter during volume recovery of the uncompressed samples were smaller in magnitude than those of the compressed samples (Fig. 3.4), which go from an increase in diameter of 1.03 % after 0.5 GPa compression to 1.89 % after 1.5 GPa compression. Particularly, the two arrows in Fig. 3.4 indicate that the 1.1 GPa curve shows fluctuations after reaching equilibrium and lost data points after approximately 37 h (the sample was broken up which caused measurement error). The

difference between these two arrows in relative length change is only approximately 0.02%, which leads to an uncertainty in specific volume of ±0.0003 cm^3/g. This sample does not reach 72 h, therefore does not contribute to the average specific volume. During the volume recovery, the more the samples have been compressed in the high pressure treatment, the more the measured change in relative length increases.

3.4.4 Mathematical Model

To describe the measured volume recovery, we firstly applied the exponential decay model (Koontz et al., 2012; Phillips, 1996; Welch et al., 2013; Williams & Watts, 1970), which fits the data well but reached different relaxation times in the new equilibrium state at 525 °C and 1 bar. A new mathematical model is developed following the suggestion by Gupta (Gupta, 1988), in which the volume relaxation depends on two internal parameters, named fictive temperature (T_f) (Tool, 1946) and fictive pressure (P_f) (Gupta, 1988), to account for the thermal history and the pressure history.

The mathematical model assumes a true hydrostatic stress during the whole high pressure treatment. The specific volume depends on T, T_f, P, P_f according to

$$V = V_{ref}\exp\left[J_{froz}\left(P_{ref} - P\right) + \Delta J\left(P_{ref} - P_f\right) + 3\alpha_{froz}\left(T - T_{ref}\right) + 3\,\Delta\,\alpha\left(T_f - T_{ref}\right)\right] \quad (3.2)$$

with T_{ref} =525 °C, P_{ref}=0.0001 GPa, and V_{ref}=0.4065 cm^3/g. The rates of change in fictive temperature T_f and fictive pressure P_f

$$-\frac{dT_f}{dt} = \left(L_{TT}\frac{\Delta C}{T} - L_{TP}V\Delta\,\alpha\right)(T_f - T) + \left(-L_{TT}V\,\Delta\,\alpha + L_{TP}V\,\Delta J\right)(P_f - P) \quad (3.3)$$

$$-\frac{dP_f}{dt} = \left(L_{TP}\frac{\Delta C}{T} - L_{PP}V\Delta\,\alpha\right)(T_f - T) + \left(-L_{PT}V\,\Delta\,\alpha + L_{PP}V\,\Delta J\right)(P_f - P) \quad (3.4)$$

are taken from Gupta (Gupta, 1988). Here, $\Delta\, C = C_{liq} - C_{froz}$ is the specific heat capacity of the liquid (equilibrium) state C_{liq} and the frozen (glassy) state C_{froz}. Similarly, $\Delta\,\alpha = \alpha_{liq} - \alpha_{froz}$ is the difference in thermal expansion coefficient between liquid and frozen glass, $\Delta J = J_{liq} - J_{froz}$ is the difference in compressibility between liquid glass

and frozen glass with $J = 1/K$ (K is the bulk modulus). L_{TT}, L_{TP}, L_{PT} and L_{PP} are kinetic coefficients (Gupta, 1988) which depend on T, P, T_f and P_f. For the model in this report, the assumptions $L_{TT} = \frac{T}{\Delta C \tau_c}$, $L_{TP} = L_{PT} = \frac{1}{V \Delta \alpha \tau_\alpha}$ and $L_{PP} = \frac{1}{V \Delta J \tau_J}$ are used. This introduces three time constants: τ_c for changes in specific heat, τ_J for changes in compressibility, and τ_α for changes in thermal expansion coefficient. Those three different time constants

$$\tau_c = f_c \tau_G \tag{3.5}$$

$$\tau_\alpha = f_\alpha \tau_G \tag{3.6}$$

$$\tau_J = f_J \tau_G \tag{3.7}$$

differ from the characteristic time τ_G for changes in the shear modulus by constant factors f_c, f_α, f_J only.

Following the idea of Markovsky and Soules (Markovsky & Soules, 1984), the T_{f_new} and P_{f_new} at the end of a time step Δt are calculated from the T_{f_old} and P_{f_old} at the beginning of the same time step Δt.

$$T_{f\_new} = \frac{T_{f\_old}\tau_\alpha\tau_c + (\tau_\alpha - \tau_c)T\Delta t + (-TV\Delta\alpha\tau_\alpha/\Delta C + \Delta J\tau_\alpha/\Delta\alpha)(P - P_{f\_old})\Delta t}{\tau_\alpha\tau_c + (\tau_\alpha - \tau_c)\Delta t} \tag{3.8}$$

$$P_{f\_new} = \frac{P_{f\_old}\tau_\alpha\tau_J + (\tau_\alpha - \tau_J)P\Delta t + (\Delta C\Delta J/(V\Delta\alpha T) - \Delta\alpha\tau_\alpha/\Delta J)(T - T_{f\_old})\Delta t}{\tau_\alpha\tau_J + (\tau_\alpha - \tau_J)\Delta t} \tag{3.9}$$

In the model of this report, the characteristic time constant for changes of the shear modulus

$$\tau_G = \tau_{ref} exp\left\{\frac{x}{T}\left[\frac{\Delta H}{R} + f_p\frac{\Delta V_a}{R}\left(P - P_{ref}\right)\right] + \frac{1-x}{T_f}\left[\frac{\Delta H}{R} + f_p\frac{\Delta V_a}{R}\left(P_f - P_{ref}\right)\right] - \frac{\Delta H}{RT_{ref}}\right\} \tag{3.10}$$

depends on real pressure and fictive pressure via an apparent activation volume(Jin et al., 2003; Karato, 2012) ΔV_a ($\Delta V_a = M_{mol}V_{ref}$) with a percentage factor of f_p ($0 \le f_p \le 1$) and $\tau_{ref} = 0.45\ h$. In case of $P_f = P = P_{ref}$, the characteristic time $\tau_G(T, T_f, P, P_f)$ reduces to the characteristic time τ in the Tool-Narayanaswamy (Narayanaswamy, 1971; Tool, 1946) model

$$\frac{dT_f}{dt} = \frac{T - T_f}{\tau} \tag{3.11}$$

$$\tau = \tau_{ref} exp\left[\frac{x\Delta H}{RT} + \frac{(1-x)\Delta H}{RT_f} - \frac{\Delta H}{RT_{ref}}\right] \qquad (3.12)$$

where T_f is the fictive temperature and x is a fixed factor.

This mathematical model captures the influence of the pressure pre-history on the volume recovery measurements at 525 °C with a single set of parameters (see figure caption for employed constants in Fig. 3.5 (a)). The calculation for each sample comprises the initial cooling at fast or slow cooling rate, the high pressure treatment (if any), the heating-up stage and, finally, the isothermal volume recovery measurement.

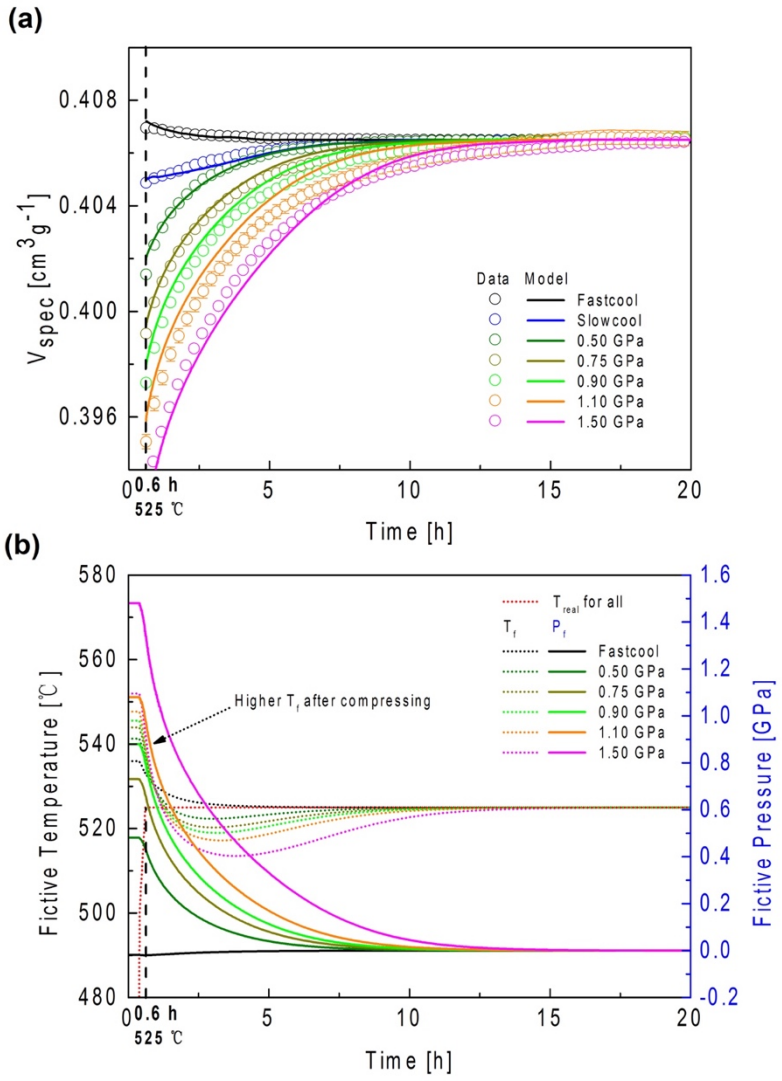

Fig. 3.5 *(a) Measured volume recovery data fitted by the new model with ΔH/R=74000 K, x=0.6, f_c=2, f_J=3, f_α=20, K_{liq}=20 GPa, f_p=1. (b) Change of T_f and P_f of fast-cooled samples versus time in our mathematic model.*

The calculated temporal change of T_f and P_f is given in Fig. 3.5 (b). P_f starts close to the real pressure of the compression treatment at the beginning of the isothermal stage, and then gradually decreases to ambient pressures. Particularly, the model gives a negative value (close to 0) of P_f for the uncompressed fast-cooled sample until approximately 10 hours. On the other hand, T_f is also strongly influenced by fictive pressure and goes down to lower than 525 °C before gradually back to 525 °C. This is similar to the crossover phenomenon which has been reported in studies (Macedo & Napolitano, 1967; Ritland, 1956) on refractive index of glass. In our model, the T_f and P_f are coupled. The coupling is at different time constants which leads to the crossover during approaching to the equilibrium value. The compression treatment increases the calculated T_f at the beginning of the volume recovery as a function of

$$T_{f\_begin} = 7.04P_{f\_begin} + T_{f\_begin\_0} \qquad (3.13)$$

where $T_{f\_begin\_0} = 533.15$ °C is the fictive temperature of the uncompressed fast-cooled sample when it firstly reaches the volume recovery temperature of 525 °C. At the zero time in Fig. 3.5, the glass sample is still frozen-in. The glass sample is gradually wake-up and reaches the volume recovery temperature at approximately 0.6 hour. After a recovery time long enough, all samples reach the same calculated $T_f = 525$ °C, $P_f = 0.0001\ GPa$.

At the beginning of the isothermal volume recovery, the time constant τ_{G_begin} increases approximately linear with fictive pressure (Fig. 3.6)

$$\tau_{G\_begin} = 3.50P_{f\_begin} + \tau_{G\_begin\_0} \qquad (3.14)$$

where $\tau_{G\_begin\_0} = 0.30\ h$ is the characteristic time when the uncompressed fast-cooled sample first reaches 525 °C. Based on the Maxwell relationship(Webb, 1997) on shear modulus relaxation time

$$\tau_G = \eta_s / G_\infty \qquad (3.15)$$

where η_s is the shear viscosity and G_∞ is the unrelaxed shear modulus (34 GPa of SCHOTT N-BK7® glass), the viscosity of glass increases with pressure as does the characteristic time τ_G.

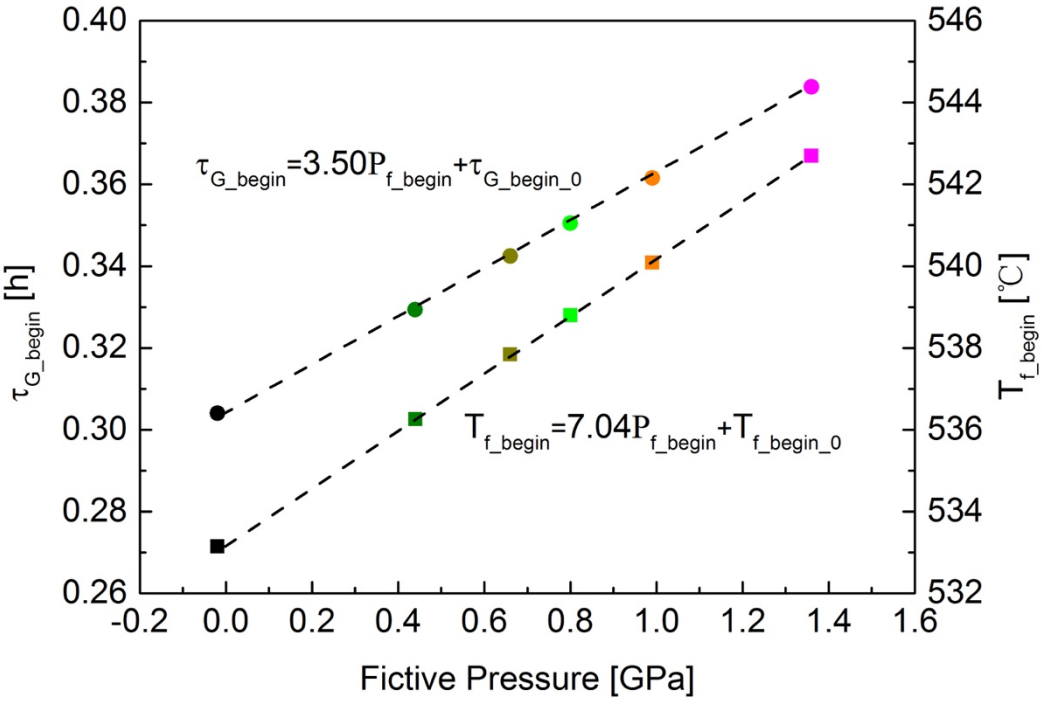

Fig. 3.6 *τ_G and T_f of fast-cooled samples at the beginning of the isothermal volume recovery at 525 °C as a function of fictive pressure in our mathematic model.*

3.5 Discussion

In our experiments, sample blackening occurred during pressurization of silicate glasses in all pressure cells using h-BN as pressure transmitting medium. The mechanism of blackening is not clear. Brooker et al. (Brooker et al., 1998) reported that it may be caused by carbon infiltration (Brooker et al., 1998) from the graphite furnace. The blackening of 0.9 GPa sample was not reversible at 525 °C and showed no absorption bands measured in the transmission spectrum. On the other hand, the sample from the 1.1 GPa experiment

(no h-BN) became visibly clear after heating up again in air to 525 °C during the volume recovery, which may thus be due to the reduction of oxygen (Ratso et al., 2014) in the glass and different from the nonreversible blackening.

We note that the shapes of length change curves in Fig. 3.4 are not exactly the same although the overall change is quite regular. This is attributed to the measurement accuracy of the optical dilatometer. The volume recovery shows that, at sufficiently high temperature and holding time, the densification of glass under high pressure is reversible (Anderson, 1956). The isothermal hold of 72 h at 525 °C is sufficient for SCHOTT N-BK7® to reach the equilibrium state in our experiments. During the 72 h isothermal hold, the cracks in the sample might have changed (especially cracks might have opened), therefore, at stage ③, the uncertainty of density could become larger.

The solution for the mathematical model used in this work is not unique. The bulk modulus of the solid glass is K_{froz} =46.5 GPa, from which one can estimate K_{liq}=K_{froz}/3=15.5 GPa following a rule of thumb. The change of density with applied pressure (Fig. 3.3) gives a bulk modulus of approximately K_{liq} =20.1 GPa. Our mathematical model (Fig. 3.5 (a)) uses K_{liq}=20±2 GPa to describe the experimental data. The K_{liq} has a strong influence on the specific volume at the beginning of the isothermal volume recovery in this model. To improve the model, one could also introduce weight factors to discriminate silicate from the other compositions like Narayanaswamy (Narayanaswamy, 1971), at the cost of requiring more free parameters.

The new model developed in this work can also be used to predict the volume recovery of SCHOTT N-BK7® under various pressure and temperature histories. For example, in Fig. 3.7, we model the volume recovery experiments at a heating rate of 600 K/h to 700 °C for 4 samples with different temperature and pressure histories, fast-cooled (-120 K/h) at 1 bar, slow-cooled (-0.4 K/h) at 1 bar, fast-cooled at 1 GPa, and slow-cooled at 1 GPa, respectively. The peak temperature (T_{peak}) is taken from the peak value of the $\alpha_v = \frac{1}{V}\frac{dV}{dT}$ in Fig. 3.7 (a). The T_{peak} of samples (values are shown in Fig. 3.7 (a)) after 1

GPa high pressure treatment (with higher P_f at the beginning) are increased only by approximately 5 °C. The α_v starts to change early at around 540 °C and finish rather abruptly at around 600 °C. The high overshot of the slow-cooled samples at -0.4 K/h is due to the 3 orders magnitude difference in cooling rate.

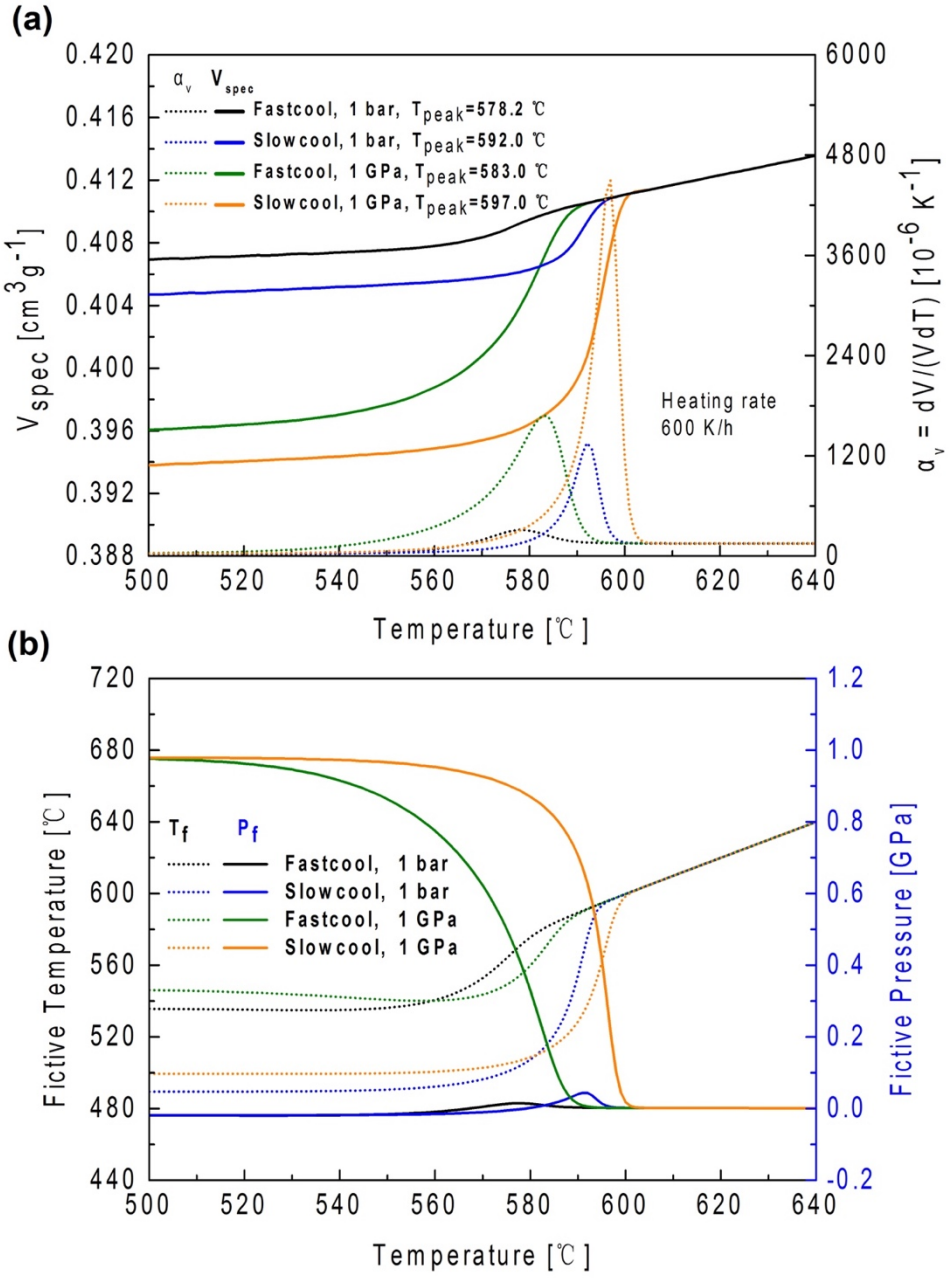

Fig. 3.7 *(a) Prediction of the volume recovery at a constant heating rate after various temperature and pressure treatments from our mathematic model. (b) Corresponding change of T_f and P_f in our mathematic model.*

3.6 Conclusions

The effects of high pressure on density and volume recovery of SCHOTT N-BK7® glass near the glass transition region has been measured and quantitatively described in this work.

(1) A simplified and effective pressure cell (2#) together with an experimental process is developed to compress glass at high pressures around the transition region using a piston-cylinder apparatus.

(2) Glass samples can be effectively densified in the piston cylinder apparatus with an approximately linear increase in density at increasing pressure.

(3) A mathematical model with two internal parameters is developed that describes the volume recovery of all samples with a single set of parameters.

3.7 Acknowledgments

This project has received funding from the European Union's Horizon 2020 research and innovation programme under the Marie Sklodowska-Curie grant agreement No 642029 - ITN CREEP. The authors appreciate the constructive comments from two anonymous reviewers. The authors thank Ms. Silvia Weitzel for the help on the volume recovery measurements, Ms. Andrea Baltes on the density measurements, and Mr. Harald Schmück on the high pressure treatment.

3.8 References

Anderson, O. L. (1956). Effect of Pressure on Glass Structure. *Journal of Applied Physics*, 27 (8): 943-949.

Boyd, F. R. & England, J. L. (1960). Apparatus for Phase-Equilibrium Measurements at Pressures up to 50-Kilobars and Temperatures up to 1750-Degrees-C. *Journal of Geophysical Research*, 65 (2): 741-748.

Bridgman, P. W. & Simon, I. (1953). Effects of Very High Pressures on Glass. *Journal of Applied Physics*, 24 (4): 405-413.

Brooker, R., Holloway, J. R. & Hervig, R. (1998). Reduction in piston-cylinder experiments: The detection of carbon infiltration into platinum capsules. *American Mineralogist*, 83 (9-10): 985-994.

Cook, R. L., King, H. E., Herbst, C. A. & Herschbach, D. R. (1994). Pressure and temperature dependent viscosity of two glass forming liquids: Glycerol and dibutyl phthalate. *The Journal of Chemical Physics*, 100 (7): 5178.

Davies, R. O. & Jones, G. O. (1953). Thermodynamic and Kinetic Properties of Glasses. *Advances in Physics*, 2 (7): 370-410.

Grassia, L. & Simon, S. L. (2012). Modeling volume relaxation of amorphous polymers: Modification of the equation for the relaxation time in the KAHR model. *Polymer*, 53 (16): 3613-3620.

Gupta, P. K. (1988). Fictive Pressure Effects in Structural Relaxation. *Journal of Non-Crystalline Solids*, 102 (1-3): 231-239.

Hodge, I. M. (1994). Enthalpy Relaxation and Recovery in Amorphous Materials. *Journal of Non-Crystalline Solids*, 169 (3): 211-266.

Jin, H. J., Gu, X. J., Wen, P., Wang, L. B. & Lu, K. (2003). Pressure effect on the structural relaxation and glass transition in metallic glasses. *Acta Materialia*, 51 (20): 6219-6231.

Karato, S.-i. (2012). *Deformation of earth materials: an introduction to the rheology of solid earth*: Cambridge University Press.

Koontz, E., Blouin, V., Wachtel, P., Musgraves, J. D. & Richardson, K. (2012). Prony Series Spectra of Structural Relaxation in N-BK7 for Finite Element Modeling. *Journal of Physical Chemistry A*, 116 (50): 12198-12205.

Macedo, P. & Napolitano, A. (1967). Effects of a distribution of volume relaxation times in the annealing of BSC glass. *J Res Natl Bur Stand*, 71: 231-238.

Markovsky, A. & Soules, T. F. (1984). An Efficient and Stable Algorithm for Calculating Fictive Temperatures. *Journal of the American Ceramic Society*, 67 (4): C56-C57.

Mauro, J. C., Allan, D. C. & Potuzak, M. (2009). Nonequilibrium viscosity of glass. *Physical Review B*, 80 (9).

Moynihan, C. T., Macedo, P. B., Montrose, C. J., Gupta, P. K., Debolt, M. A., Dill, J. F., Dom, B. E., Drake, P. W., Easteal, A. J., Elterman, P. B., et al. (1976). Structural Relaxation in Vitreous Materials. *Annals of the New York Academy of Sciences*, 279 (Oct15): 15-35.

Narayanaswamy, O. S. (1971). A Model of Structural Relaxation in Glass. *Journal of the American Ceramic Society*, 54 (10): 491-498.

Phillips, J. C. (1996). Stretched exponential relaxation in molecular and electronic glasses. *Reports on Progress in Physics*, 59 (9): 1133-1207.

Ratso, S., Kruusenberg, I., Vikkisk, M., Joost, U., Shulga, E., Kink, I., Kallio, T. & Tammeveski, K. (2014). Highly active nitrogen-doped few-layer graphene/carbon nanotube composite electrocatalyst for oxygen reduction reaction in alkaline media. *Carbon*, 73: 361-370.

Ritland, H. N. (1956). Limitations of the Fictive Temperature Concept. *Journal of the American Ceramic Society*, 39 (12): 403-406.

Rouxel, T., Ji, H., Hammouda, T. & Moreac, A. (2008). Poisson's ratio and the densification of glass under high pressure. *Physical Review Letters*, 100 (22).

Scherer, G. W. (1986). Volume Relaxation Far from Equilibrium. *Journal of the American Ceramic Society*, 69 (5): 374-381.

Shang, H. X. & Rouxel, T. (2005). Creep behavior of soda-lime glass in the 100-500 K temperature range by indentation creep test. *Journal of the American Ceramic Society*, 88 (9): 2625-2628.

Simon, S. L., Park, J. Y. & McKenna, G. B. (2002). Enthalpy recovery of a glass-forming liquid constrained in a nanoporous matrix: Negative pressure effects. *European*

Physical Journal E, 8 (2): 209-216.

Taylor, E. W. (1949). Plastic Deformation of Optical Glass. *Nature*, 163 (4139): 323-323.

Tool, A. Q. (1946). Relation between Inelastic Deformability and Thermal Expansion of Glass in Its Annealing Range. *Journal of the American Ceramic Society*, 29 (9): 240-253.

Tribone, J. J., Oreilly, J. M. & Greener, J. (1989). Pressure-Jump Volume-Relaxation Studies of Polystyrene in the Glass-Transition Region. *Journal of Polymer Science Part B-Polymer Physics*, 27 (4): 837-857.

Webb, S. (1997). Silicate melts: Relaxation, rheology, and the glass transition. *Reviews of Geophysics*, 35 (2): 191-218.

Welch, R. C., Smith, J. R., Potuzak, M., Guo, X., Bowden, B. F., Kiczenski, T. J., Allan, D. C., King, E. A., Ellison, A. J. & Mauro, J. C. (2013). Dynamics of glass relaxation at room temperature. *Phys Rev Lett*, 110 (26): 265901.

Williams, G. & Watts, D. C. (1970). Non-Symmetrical Dielectric Relaxation Behaviour Arising from a Simple Empirical Decay Function. *Transactions of the Faraday Society*, 66 (565p): 80-+.

Ziaja, K., Foley, S. F., White, R. W. & Buhre, S. (2014). Metamorphism and melting of picritic crust in the early Earth. *Lithos*, 189: 173-184.

Chapter 4

4. Deviatoric flow of glass under high pressure

Published in *Journal of the American Ceramic Society*

Ding L, Thieme M, Demouchy S, Kunisch C, Kaus B. Effect of pressure and temperature on viscosity of a borosilicate glass. *J Am Ceram Soc.* 2018;00:1–11.

4.1 Summary

During industrial glass production processes, the actual distribution of stress components in the glass during scribing remains, to date, poorly quantified, and thus continues to be challenging to model numerically. In this work, we experimentally quantified the effect of pressure and temperature on the viscosity of SCHOTT N-BK7® glass, by performing *in situ* deformation experiments at temperatures between 550 and 595 °C and confining pressures between 100 MPa and 300 MPa. Experiments were performed at constant displacement rates to produce almost constant strain rates between 9.70×10^{-6} s^{-1} and 4.98×10^{-5} s^{-1}. The resulting net axial stresses range from 81 MPa to 802 MPa, and the finite strains range from 1.4 % to 8.9 %. The mechanical results show that the SCHOTT N-BK7® glass is viscoelastic near the glass transition temperature at 300 MPa of confining pressure. To elucidate the data, we incorporated both 1-element and 2-element generalized Maxwell viscoelastic models in an inversion approach, for which we provide MATLAB scrips. Results show that the 2-element Maxwell model fits the experimental data well. The stress decreases with increasing temperature at 300 MPa and the temperature dependence yields a similar activation energy (601±10 kJ·mol^{-1} or $\Delta H/R = 7.2\times10^4$ K) to a previously reported value at 1-atm (615 kJ·mol^{-1} or $\Delta H/R = 7.4\times10^4$ K). The SCHOTT N-BK7® glass shows a limited linear increase of viscosity with increasing pressure of ~0.1 $\log_{10}$(Pa·s)/100 MPa, which is in agreement with the most recent two-internal-parameter relaxation model (based on experiments).

4.2 Introduction

Hardness measurements (Peter, 1970; Shang & Rouxel, 2005) have reported that glass flows viscously at room temperature as well as at high temperature (e.g., up to 630 °C for soda-lime-silica float glass (Wilantewicz & Varner, 2008)). Nevertheless, during

industrial production processes, scribing with defined tools and breaking are used to separate glass sheets. If scribing velocity or scribing force is not well adjusted, it can lead to poor edge quality with non-desirable cracks at the edges or cracks are not deep enough (or sufficiently well developed) for further breaking (An et al., 2015; Dick, 1970; Peter, 1970). The propagation of these cracks, desired or not, depends on the stress state underneath the indenter during scribing (Hagan & Swain, 1978; Lawn et al., 1983). The actual distribution of stress components in the glass during scribing remains, to date, poorly quantified, and thus continues to be challenging to model numerically (Alkorta et al., 2005; Lee & Radok, 1960). To better quantify the viscous contribution to the deformation (Rouxel & Sangleboeuf, 2000) underneath an indenter or scribing tool, the effect of pressure on the viscosity of an industrial optical glass, needs to be quantified experimentally by *in situ* measurements.

The temperature dependence of the viscosity of glasses at ambient pressure has already been studied experimentally leading to numerous temperature-dependent models of viscosity for glasses. Notably, the Vogel-Fulcher-Tammann (VFT) model (Fulcher, 1925) which is similar to the Williams-Landel-Ferry (WLF) model (Williams et al., 1955), the free-volume model (Cohen & Turnbull, 1959; Greet & Turnbull, 1967; Turnbull & Cohen, 1970), the Adam-Gibbs (AG) model (Adam & Gibbs, 1965) and the Mauro-Yue-Ellison-Gupta-Allan(MYEGA) model. (Mauro et al., 2009) The VFT model can accurately fit the temperature dependence of viscosity of SCHOTT N-BK7® glass in the range from 1 to 13 $\log_{10}$(Pa·s).

Several experimental studies have quantified the pressure dependence of the viscosity of silicate melts, with a special focus on melts relevant to geological and volcanic systems, such as molten olivine, molten jadeite, dacite and basalt at very high temperatures (> 1700 °C) (Kushiro, 1976; Kushiro, 1978; Mysen et al., 1982; Wang et al., 2014) and pressure up to 8 GPa. Different behaviors were observed with increasing pressure as a function of the degree of polymerization (Scarfe et al., 1987; Wang et al.,

2014). The polymerization parameter is best described by the ratio of non-bridging oxygen (NBO) and tetrahedrally coordinated cations (T, e.g., Si^{4+}, Al^{4+}, Ti^{4+}, Fe^{3+}). The ratio of NBO/T can be simply calculated by the ratio of O/T at ambient pressure with satisfying accuracy (Wang et al., 2014). However, under high pressure, highly polymerized silicate melts (NBO/T<1, e.g., obsidian, basalt, dacite) have a lower tetrahedral connectivity (less oxygen atoms in TO_4 will bond to adjacent tetrahedron and thus forming less 3D networks) than at ambient pressure. These highly polymerized silicate melts (Wang et al., 2014) display a viscosity decrease with an increase of pressure. While the viscosity of depolymerized silicate melts (NBO/T≥2, molten peridotite, molten olivine, Al-poor melt), with higher tetrahedral connectivity, show a viscosity increase with increasing pressure (Wang et al., 2014). For borosilicate glasses, in addition to the NBO/T ratio, the structure is greatly influenced by the BO_3/BO_4 ratio (Limbach et al., 2015). Indeed, the viscosity model presented by Jantzen (Jantzen, 2017) showed an irregular behavior of viscosity versus NBO in radio-active borosilicate glasses, making the prediction of the pressure effect on borosilicate problematic.

Previous experimental studies on the effect of pressure on viscosity and density of glasses have mostly reported a linear relationship for pressure dependence. For example, the pressure dependence of the viscosity of B_2O_3, studied by Sperry and Makenzie (Sperry & JD, 1968) at 380-465 °C and from 0.1 to 30 MPa, demonstrated a linear increase of viscosity with increasing pressure ($\Delta\eta/\Delta P$ = 0.28 to 0.59 $\log_{10}$(Pa·s)/100 MPa (Sperry & JD, 1968)). A special parallel-plate viscometer was developed by Schulze et al. (Schulze et al., 1999) using an internally heated pressure vessel (IHPV) to deform the standard melt DDG1, Di_{100} (Di=$CaMgSi_2O_6$) and $Ab_{55}Di_{45}$ (Ab=$NaAlSi_3O_8$) silicate melt. And their results also suggest a linear change with increasing pressure up to 350 MPa ($\Delta\eta/\Delta P$ = -0.12 to 0.23 $\log_{10}$(Pa·s)/100 MPa (Schulze et al., 1999)). Deformation of float glass with high water content (Del Gaudio et al., 2007) likewise reported a linear viscosity increase with increasing pressure from 100 MPa to 400 MPa, and a negative correlation

with increasing water content (0.03-4.87 wt.%), ($\Delta\eta/\Delta P < 0.22$ $\log_{10}$(Pa·s)/100 MPa (Del Gaudio et al., 2007)). To date, the latest high-pressure dataset available for SCHOTT N-BK7® is based on relatively fast-cooled glass under high pressure (0.5 GPa to 1.5 GPa using a piston cylinder). Combined with the post-mortem density and volume recovery measurements (Ding et al., 2018), which also indicate a linear viscosity increase with increasing pressure ($\Delta\eta/\Delta P$ =0.05 $\log_{10}$(Pa·s)/100 MPa (Ding et al., 2018)).

Several phenomenological models (Grassia & Simon, 2012; Hodge, 1994; Simon et al., 2002; Tribone et al., 1989) describe the time dependence of glass relaxation as a function of both temperature and pressure history. A recent relaxation model was developed by Ding et al.,(Ding et al., 2018) following the approach of Gupta (Gupta, 1988) to use two internal parameters, named fictive temperature (Tool, 1946) (T_f) and fictive pressure (Gupta, 1988) (P_f). This type of phenomenological models can predict the pressure dependence of the viscosity of glass forming materials through the Maxwell relation:

$$\eta = G\tau \qquad (4.1)$$

where η is viscosity, τ is the Maxwell relaxation time, and G is the unrelaxed elastic shear modulus (Dingwell & Webb, 1989). For instance, the two-internal-parameter relaxation model presented by Ding et al. (Ding et al., 2018). predicts a positive linear dependence of pressure on viscosity for pressures up to 1.5 GPa based on the density and volume recovery measurements. On the other hand, some studies directly express the effect of pressure on the viscosity model. For example, the model proposed by Avramov (Avramov, 2000) describes the pressure dependence of viscosity by relating the viscosity to the entropy of the glass forming melts, using a master equation ϕ. The equation derived by Gupta (Gupta, 1987), which follows the Adam-Gibbs model (Adam & Gibbs, 1965), predicting a negative pressure dependence of viscosity.

SCHOTT N-BK7® is available in large formats with high homogeneity. Internally at SCHOTT, it is used as a reference material. It was already used in several studies (Dyer

et al., 2003; Koontz et al., 2012; Mosaddegh & Ziegert, 2011), (An et al., 2015) but the rheological properties were never quantified experimentally *in situ* at pressures above 1-atm. To quantify the viscosity of SCHOTT N-BK7® glass, compared to (Ding et al., 2018) we use a totally different experiment set up by performing *in situ* deformation experiments in a gas-medium pressure vessel.

4.3 Experimental method

4.3.1 Sample description and preparation

The borosilicate glass SCHOTT N-BK7® (chemical composition: 70.0 % SiO_2, 11.5 % B_2O_3, 9.5 % Na_2O, 7.5 % K_2O and 1.5 % BaO) is an optical glass widely used for lenses and prisms, due to its high homogeneity and high light yield. The density of SCHOTT N-BK7® at room temperature and ambient pressure is 2.508 ± 0.001 g/cm^3. The glass transition temperature T_g = 561 °C is defined as the temperature at which the viscosity is 12 $\log_{10}$(Pa·s). Cylinders of SCHOTT N-BK7® with a diameter of 9.95 ± 0.05 mm and a length of 17.00 ± 0.10 mm were drilled from large glass blocks, which had been slowly cooled at a rate of -0.4 °C/h. Both ends of the glass cylinder were mirror polished, and parallelism of both extremities was ensured.

4.3.2 Deformation experiments

Uniaxial deformation experiments were performed with a high temperature and high pressure *in situ* deformation gas-medium apparatus also called a Paterson Press (Paterson, 1990). The apparatus is used with a routine confining pressure of 300 ± 1 MPa, but the confining pressure can range from 50 to 350 MPa. Using Argon as pressure-medium prevents chemical reactions with the samples. Diffusion experiments at high pressure and high temperature have reported an Argon diffusivity of about -3.3 × 10^{-20} cm^2 s^{-1} at 600 °C in silicate glasses (Carroll & Stolper, 1991). Thus, for the short duration of our experiments (1h), the incorporation of Argon is considered negligible. The force is

measured using an internal load cell (2 kN to 75 kN), resulting in an uncertainty in net axial stress (σ_{load}) of less than 20 MPa. In this study, uniaxial compressive deformation experiments on SCHOTT N-BK7® were performed at constant displacement rates (~1 × 10^{-5} to ~5 × 10^{-5} mm/s) resulting in almost constant strain rates.

For the deformation experiment, the glass samples were encapsulated with zirconia and alumina pistons and alumina spacers inside a copper jacket as shown in Fig. 4.1, following well-established experimental protocols (Demouchy et al., 2009; Demouchy et al., 2013; Karato et al., 1986; Mei & Kohlstedt, 2000a; Mei & Kohlstedt, 2000b).

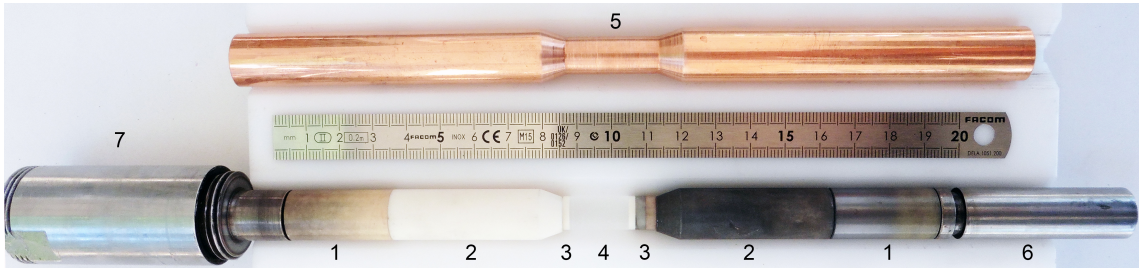

Fig. 4.1 *(a) Photograph of the high-pressure assembly for a deformation experiment; 1-Zirconia piston; 2-Alumina piston; 3-Alumina spacers; 4-SCHOTT N-BK7® glass cylinder; 5-Fitted copper jacket; 6-Bottom steel piston; 7-Top steel piston.*

A self-made internal furnace is used to anneal the sample at high temperature, with a low thermal gradient (±5 °C) along the sample zone. The thermal gradient is established from separate calibration experiments before deformation experiments. The temperature was increased at a rate of ~15 °C/min to the target temperature and maintained stable for 20 to 30 minutes to insure sufficient relaxation of the glass structure before applying an axial load to the sample. The temperature was kept constant using a proportional–integral–derivative (PID) controller during the mechanical experiment as a small variation in temperature could result in significant variations of viscosity. A data point is recorded each 1 or 2 s. After the end of the deformation, the piston was maintained in position, and the temperature was decreased at a rate of 70 °C/min by decreasing power. Afterward, the pressure was slowly released at a rate of ~10 MPa/min to ambient pressure.

4.3.3 Data treatment

The mechanical data must be corrected to account for several experimental approximations adequately. Firstly, the displacement has to be corrected for the elastic distortion (Paterson, 1970) of the apparatus (stiffness = 82.5 kN/mm). Secondly, to determine the contribution of the copper jacket to the measured force, the power flow law for copper from (Frost & Ashby, 1982) is used. Thirdly, values of stresses and strain rates were corrected for instantaneous changes in the cross-sectional area of the copper jacket and the glass cylinder during deformation assuming that samples maintained a cylindrical shape (i.e., negligible barreling) and constant volume. These corrections of the mechanical data are identical to corrections used in numerous published experimental studies (Demouchy et al., 2009; Demouchy et al., 2013; Demouchy et al., 2014; Karato et al., 1986; Mei & Kohlstedt, 2000a; Mei & Kohlstedt, 2000b) on polycrystalline silicates using the same gas-medium deformation apparatus, guaranteeing that this source of uncertainty was properly corrected.

The mean stress (total pressure) on the glass sample during deformation is defined as:

$$\sigma_{mean} = (\sigma_{load} + 2\sigma_{Ar}) / 3 \qquad (4.2)$$

where σ_{load} is the net uniaxial stress(Paterson & Wong, 2005) measured by an internal load cell and σ_{Ar} is the confining pressure of Argon.

4.4 Results

Experimental conditions and measured mechanical data obtained from the *in situ* deformation experiments are reported in Table 4-1. Repeating the experiments permits to check the reproducibility of the mechanical results and the number of the repeated experiments at identical experimental conditions are reported in Table 1 and shown in Figure S1 (supplementary material). A few samples showed a variation in diameter along the deformed cylinder post-deformation (*i.e.*, classic barreling), which could indicate that

the temperature distribution on the sample is not perfectly homogenous. Or more likely that, the viscous flow continued to occur post-data acquisition and during quenching, when the temperature distribution has become heterogeneous (*i.e.*, the bottom cylinder being hotter than top).

Table 4-1 *Experimental conditions for deformation experiments and mechanical results*

Samples	Length [mm]	Diameter [mm]	Confining Pressure [MPa]	Temperature [°C]	Displacement Rate [mm/s]	Strain Rate [s^{-1}]	Finite Strain [%]	Axial Stress [MPa]	Mean Stress [MPa]	Viscosity* Log_{10}[Pa·s]	Repeat times
Constant pressure and strain rate, variable temperature											
LD6	17.10	9.95	300	550 ± 5	5×10^{-5}	1.50×10^{-5}	1.4	802 ± 6	467 ± 7	-	2
LD9	17.07	9.95	303	565 ± 5	5×10^{-5}	3.89×10^{-5}	3.9	792 ± 6	466 ± 7	-	1
LD15	17.05	9.95	302	575 ± 5	5×10^{-5}	4.82×10^{-5}	6.5	560 ± 6	388 ± 7	12.6 ± 0.2	3
LD17	17.10	9.95	303	585 ± 5	5×10^{-5}	4.77×10^{-5}	8.7	219 ± 6	275 ± 7	12.2 ± 0.2	1
LD18	17.10	9.95	300	595 ± 5	5×10^{-5}	4.98×10^{-5}	8.4	81 ± 6	227 ± 7	11.7 ± 0.2	2
Constant temperature and strain rate, variable pressure											
LD13	17.05	9.95	105	575 ± 5	5×10^{-5}	4.67×10^{-5}	5.7	340 ± 6	183 ± 7	12.4 ± 0.2	2
LD16	17.05	9.95	203	575 ± 5	5×10^{-5}	4.86×10^{-5}	6.5	430 ± 6	279 ± 7	12.5 ± 0.2	3
LD15	17.05	9.95	302	575 ± 5	5×10^{-5}	4.82×10^{-5}	6.5	560 ± 6	388 ± 7	12.6 ± 0.2	3
Constant temperature and pressure, variable strain rate											
LD20	17.00	9.95	301	575 ± 5	1×10^{-5}	9.70×10^{-6}	7.6	144 ± 6	249 ± 7	12.7 ± 0.2	1
LD19	17.02	9.95	302	575 ± 5	3×10^{-5}	2.88×10^{-5}	8.9	235 ± 6	280 ± 7	12.4 ± 0.2	1
LD15	17.05	9.95	302	575 ± 5	5×10^{-5}	4.82×10^{-5}	6.5	560 ± 6	388 ± 7	12.6 ± 0.2	3

* Viscosity is calculated according to Eq. 4.17

4.4.1 Mechanical data

The stress-strain curves for all deformation experiments are shown in Fig. 4.2. The deformation experiments at constant displacement rates yield strain rates ranging from 9.70×10^{-6} s^{-1} to 4.98×10^{-5} s^{-1} and finite strains ranging from 1.4 % to 8.9 %. To find the proper temperature and strain rate to study the pressure dependence of the viscosity of our samples, we ran experiments at different temperatures. The temperature dependence is shown in Fig. 4.2a for experiments performed at a confining pressure of 300 MPa, at a constant displacement rate of $\sim 5 \times 10^{-5}$ s^{-1} and for temperatures from 550 °C up to 595 °C. The glass sample showed an approximately constant stress increase at 550 °C, with the stress-strain curve displaying an almost pure elastic behavior. Between 565 and 575 °C, the samples behave viscoelastic. Steady state (viscous) flow is finally achieved at 595 °C. The stress at 595 °C (81 MPa, sample LD18) is rather low with an applied force of approximately 7 kN.

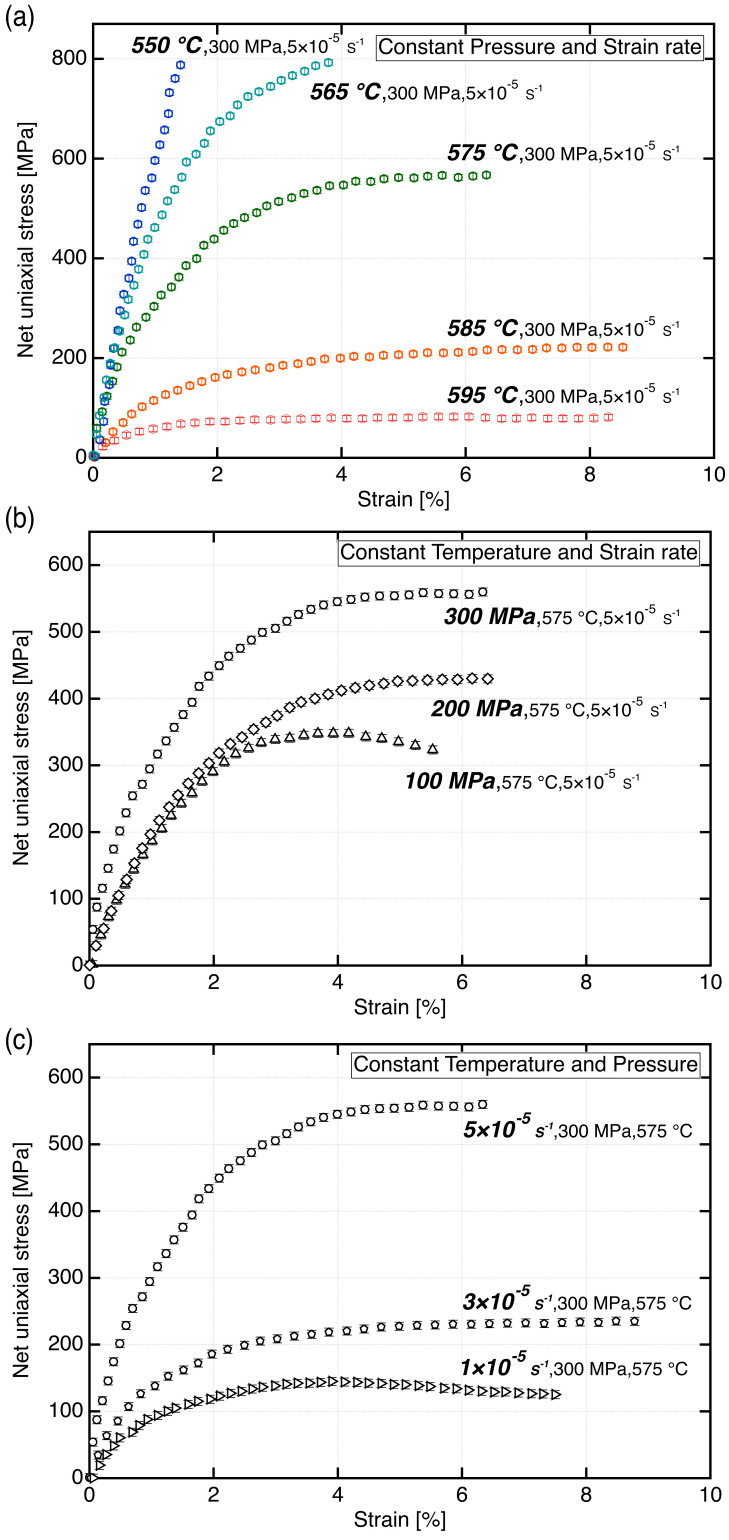

Fig. 4.2 *Net uniaxial stress versus strain (a) at a constant confining pressure and constant strain rate for increasing temperatures; (b) at a constant temperature and constant strain rate for increasing confining pressures; (c) at a constant temperature and constant confining pressure for increasing strain rates. For all curves, 1 data point out of every 50 points is shown for clarity.*

To determine the pressure dependence, we conducted experiments at a constant temperature of 575 °C, at a constant strain rate of ~5 × 10^{-5} s^{-1} and confining pressures ranging from 100 MPa to 300 MPa as shown in Fig. 4.2b. The σ_{load} increases with increasing pressure from 340, to 430, and to 560 MPa for a confining pressure of 100, 200 and 300 MPa, respectively (see Table 1). The sample at 100 MPa confining pressure reached steady-state deformation after approximately 4% of strain, which is significantly earlier than for the experiments at 200 MPa and 300 MPa. The stress of the experiment at 100 MPa slightly decreases after reaching steady state, indicating some limited weakening.

To quantify the effect of strain rate, experiments at a constant temperature of 575 °C, a constant pressure of 300 MPa and axial deformation at different strain rates ranging from 9.7 × 10^{-6} s^{-1} to 4.82 × 10^{-5} s^{-1}, as shown in Fig. 4.2c. The maximal stress increases with increasing strain rate. Indeed, the σ_{load} increases by ~91 MPa from ~1 × 10^{-5} s^{-1} to ~3 × 10^{-5} s^{-1}, while the σ_{load} increases by ~325 MPa from ~3 × 10^{-5} s^{-1} to ~5 × 10^{-5} s^{-1} (Fig. 4.2c).

4.4.2 Maxwell model

We use both a single Maxwell and a two-Maxwell viscoelastic model to fit the experimental data combined with an optimization algorithm (MATLAB scripts are provided as supplementary materials).

The single Maxwell viscoelastic model (1-Maxwell) is defined by (Kaus & Becker, 2007)

$$\dot{\varepsilon} = \dot{\varepsilon}_{ela} + \dot{\varepsilon}_{vis} = \frac{1}{G}\frac{d\sigma}{dt} + \frac{\sigma}{\eta} \qquad (4.3)$$

$$\frac{d\sigma}{dt} = G\dot{\varepsilon} - \frac{G\sigma}{\eta} \qquad (4.4)$$

where $\dot{\varepsilon}$ is the total strain rate, $\dot{\varepsilon}_{ela}$ is the strain rate of elastic deformation, $\dot{\varepsilon}_{vis}$ is the strain rate of viscous deformation, σ is the shear stress converted from the net uniaxial stress by assuming a constant Poisson's ratio of 0.206 for SCHOTT N-BK7®, η is the viscosity and G is the elastic shear modulus. To keep the model simple, we neglect the

contributions from the volumetric bulk deformation strain. Under a constantly applied strain rate $\dot{\varepsilon}_0$, the stress can be solved by integrating over time as:

$$\sigma(t) = \eta \left(1 - e^{-\frac{t}{\tau}}\right) \dot{\varepsilon}_0 + \sigma(0) e^{-\frac{t}{\tau}} \qquad (4.5)$$

where τ is the Maxwell relaxation time can be calculated by Eq. 4.1, and $\sigma(0)$ is the initial stress (in the model, we assume $\sigma(0) = 0$). For the elastic shear modulus, we assume *G* as a free parameter, determined during the inversion process. In the limited temperature range of the present study, the dependence of viscosity on temperature can be described by an Arrhenius law. To account for the influence of pressure on viscosity, the Arrhenius equation is extended to Eq. 4.6 by introducing an activation volume as has been done in several studies (Ding et al., 2018; Jin et al., 2003).

$$\eta = \eta_0 e^{\frac{E+PV_a}{RT}} \qquad (4.6)$$

Combining Eq. 4.6 with the idea from Narayanaswamy (Narayanaswamy, 1971), we assume that the viscosity depends on temperature and pressure as

$$\eta = \eta_0 e^{\frac{\Delta H+PV_a}{RT} - \frac{\Delta H+P_{ref}V_a}{RT_{ref}}} \qquad (4.7)$$

where P_{ref}= 10^5 Pa and T_{ref}=561 °C are reference material parameters, and the initial viscosity η_0, activation energy $\frac{\Delta H}{R}$ and activation volume V_a are free parameters (Ding et al., 2018).

The 1-Maxwell model can fit each experiment separately very well by allowing a change of elastic shear modulus G between the different experiments. However, the elastic shear modulus is known to be nearly constant in both glass science and geoscience applications (Narayanaswamy, 1971; Scherer, 1990; Webb & Dingwell, 1990; Zheng & Mauro, 2017) for small pressure changes (<2 GPa). Therefore, we tested fitting a single set of material parameters to all experimental mechanical data using a 1-Maxwell model. In order to fit the model to the experiments, we employ a multidimensional unconstrained nonlinear minimization optimization algorithm (using the Nelder-Mead Simplex search algorithm as incorporated in the MATLAB function fminsearch (Lagarias et al., 1998)), to find the best-fit parameters for the model. The best-fit model we obtained (after

experimenting with a range of starting values $\eta = 10^{12}$ Pa · s, $G = 34$ GPa, $\Delta H/R$ = 7.4×10^4 K, $V_a = 8.129\times10^{-6}$ m^3/mol (Ding et al., 2018) is shown in Fig. 4.3a (best-fit yields G=24.9 GPa $\Delta H/R = 5.4\times10^4$ K which are different than the reference value of G_{ref}=34 GPa (Ding et al., 2018) and $(\Delta H/R)_{ref} = 7.4\times10^4$ K at 1-atm), which is rather poor.

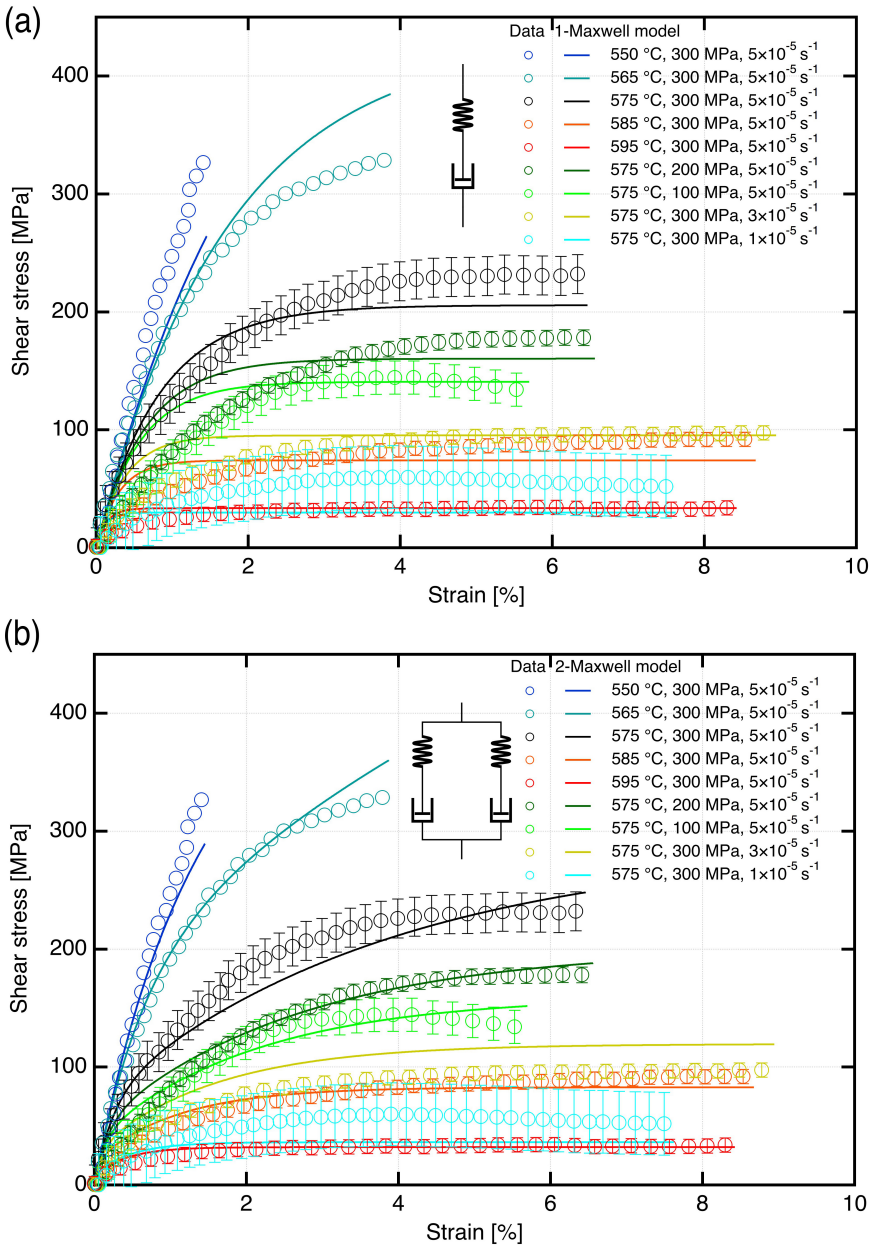

Fig. 4.3 *(a) Best-fit from the 1-Maxwell model with the fitting parameters:* $\eta_0 = 4.9\times10^{12}$ *Pa·s, G=24.9 GPa,* $\frac{\Delta H}{R} = 5.4\times10^4$ *K, and* $V_a = 2.0\times10^{-6}$ *m^3/mol; (b) Best-fit from the 2-Maxwell model with the fitting parameters:* $\eta_0 = 5.4\times10^{12}$ *Pa·s, G=34.2 GPa,* $\frac{\Delta H}{R} = 6.1\times10^4$ *K,* $V_a = 2.9\times10^{-6}$ *m^3/mol, w=0.83, and fac=15.6. The uncertainty of the shear stress is calculated from the standard deviation of steady-state viscosity and strain rate.*

For many glass types, more than one Maxwell element is needed to describe the experimental data (Koontz et al., 2012). To improve the fitting, we applied a generalized Maxwell model with 2 Maxwell elements (Jain et al., 2006) (2-Maxwell model applied, MATLAB script available in supplemental materials), which models the rheology of glass as two parallel Maxwell bodies, which was previously found to approximate the uniaxial stress relaxation of glass successfully (Scherer & Rekhson, 1982). For the stress revolution, we introduce a weighting parameter w for 2-Maxwell model and a free parameter *fac* to separate the viscosities (Narayanaswamy, 1971)

$$\sigma(t) = (1-w)\sigma_1 + w\sigma_2 \tag{4.8}$$

where the stresses are

$$\sigma_1 = \eta_1 \left(1 - e^{-\frac{t}{\tau_1}}\right)\dot{\varepsilon}_0 + \sigma_1(0)e^{-\frac{t}{\tau_1}} \tag{4.9}$$

$$\sigma_2 = \eta_2 \left(1 - e^{-\frac{t}{\tau_2}}\right)\dot{\varepsilon}_0 + \sigma_2(0)e^{-\frac{t}{\tau_2}} \tag{4.10}$$

and the viscosities are

$$\eta_1 = \eta_0/(1-w+w/fac)\, e^{\frac{\Delta H+PV_a}{RT} - \frac{\Delta H+P_{ref}V_a}{RT_{ref}}} \tag{4.11}$$

$$\eta_2 = \eta_1/fac \tag{4.12}$$

$$\tau_1 = \eta_1/G_1 \tag{4.13}$$

$$\tau_2 = \eta_2/G_2 \tag{4.14}$$

$$G = (1-w)G_1 + wG_2 \tag{4.15}$$

$$\eta = (1-w)\,\eta_1 + w\eta_2 \tag{4.16}$$

The best overall fit parameters and curves of the 2-Maxwell model are shown in Fig. 4.3b. We note that the best-fit is not unique, and it is slightly influenced by the initial guess of the free parameters. We have performed a series of tests with different initial parameters and found an initial guess of $\eta = 4.9 \times 10^{12}$ Pa · s (best-fit of 1-Maxwell model), $G = 34$ GPa, ΔH/R = 7.4×10^4 K, V_a= 8.129×10^{-6} m^3/mol (Ding et al., 2018), w=0.7 and fac = 10 to give an overall lowest misfit. The best-fit G=34.2 GPa is fit with the reference value of 34 GPa (Ding et al., 2018), while the best-fit activation energy ΔH/R= 6.1×10^4 K (482 kJ·mol^{-1}) is lower than the value obtained at 1-atm of ΔH/R=

7.4×10^4 K (615 kJ·mol^{-1}) (Ding et al., 2018). The fitting is improved compared to the 1-Maxwell model. Still, the fit is not perfect, especially for the data measured at 1×10^{-5} s^{-1} and 3×10^{-5} s^{-1}. A generalized Maxwell model with 3-Maxwell elements was also tested, but the results show no significant fitting improvement compared to the 2-Maxwell model. Therefore, the outcome of a 3-Maxwell model is not further discussed here.

4.4.3 Viscosity

The glass sample is in a uniaxial stress state during the deformation experiment, and the viscosity is then calculated as follows: (Rouxel et al., 1989)

$$\eta = \sigma/(3\dot{\varepsilon}) \qquad (4.17)$$

where σ is the net uniaxial stress, and $\dot{\varepsilon}$ is the instantaneous strain rate. The uncertainty of the applied force results in a stress uncertainty of ± 6 MPa. Together with a 1 % error of the strain rate, this yields an uncertainty of the viscosity of ± 0.01 $\log_{10}$(Pa·s). The uncertainty of the temperature distribution along the sample (maximal ± 5 °C) would yield more important uncertainties on viscosity, up to ± 0.22 $\log_{10}$(Pa·s), based on the Arrhenius equation at 1-atm. The latter values are reported in Table 1. Our results show that to change the viscosity of SCHOTT N-BK7® glass by 0.1 $\log_{10}$(Pa·s) has to change the temperature by 2.5 °C (at 300 MPa) or the pressure by 100 MPa. As shown in Fig. 4.4a, the viscosity decreases by ~0.4 $\log_{10}$(Pa·s)/10 °C from 575 °C to 595 °C. Furthermore, the viscosity curve at 595 °C furthermore takes less time to achieve steady state than deformation experiments at 575 °C.

The effect of pressure on the viscosity of SCHOTT N-BK7® is rather small. Viscosity-time curves for 100 MPa and 200 MPa of confining pressure, shown in Fig. 4.4b, almost overlap each other for finite strains < 1 %. Increasing the strain rate to ~ 5 × 10^{-5} s^{-1} results in a viscosity offset of ± 0.2 $\log_{10}$(Pa·s) (Fig. 4.4c), which is close to the uncertainty of the machine and also consistent with the results from the 2-Maxwell model. Besides, samples deformed with different strain rates achieve steady state (Fig. 4.4c) at the similar strain of approximately 2 %, indicating that the viscosity of SCHOTT N-BK7® does not significantly depend on strain for this strain level.

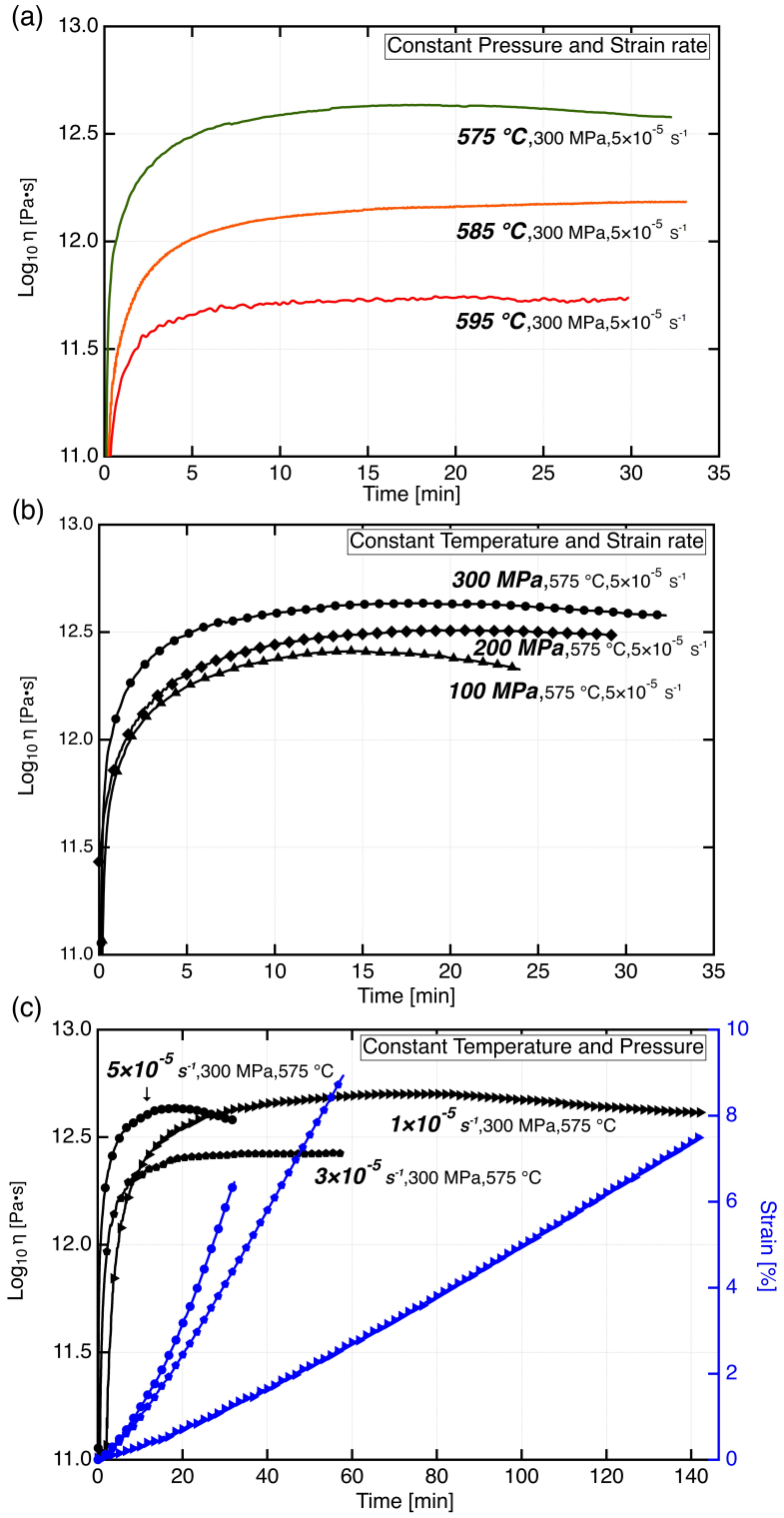

Fig. 4.4 *Time dependence of viscosity (a) at a constant confining pressure and constant strain rate for increasing temperatures; (b) at a constant temperature and constant strain rate for increasing confining pressures; (c) at a constant temperature and constant confining pressure for increasing strain rates. The time dependence of strain is also shown in (c). For all curves, 1 data point out of every 50 points is shown for clarity.*

Using an Arrhenius model to describe the temperature dependence of the steady-state viscosity obtained from the deformation experiments at 300 MPa from this study gives $\Delta H/R = 7.2\times10^4$ K (activation energy: 601 ± 10·kJ mol^{-1}, R^2=0.99) as illustrated in Fig. 4.5. The result is in good agreement with the activation energy of approximately $\Delta H/R = 7.4\times10^4$ K (activation energy:615 kJ·mol^{-1}) obtained experimentally at 1-atm (Ding et al., 2018). However, the viscosities have a significant offset of approximately +1.0 $\log_{10}$(Pa·s) compared to the results from the latest two-internal-parameter relaxation model.

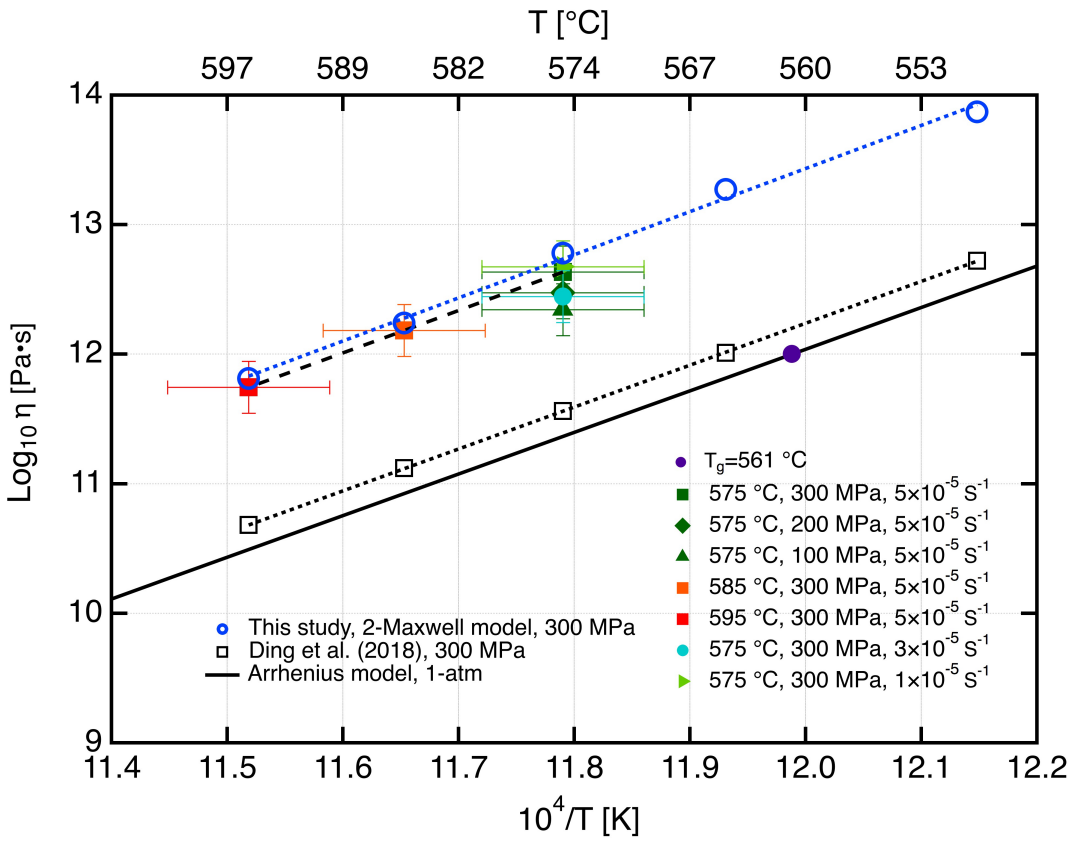

Fig. 4.5 *Temperature dependence of the viscosity of SCHOTT N-BK7® at high pressure compared to an Arrhenius model at 1-atm, a 2-Maxwell model at 300 MPa and the latest two-internal-parameter relaxation model at 300 MPa (Ding et al., 2018).*

The model developed by Ding et al. (Ding et al., 2018) can be transformed into a viscosity model

$$\eta = \eta_{ref} exp\left\{\frac{x}{T}\left[\frac{\Delta H}{R} + f_p \frac{\Delta V_a}{R}\left(P - P_{ref}\right)\right] + \frac{1-x}{T_f}\left[\frac{\Delta H}{R} + f_p \frac{\Delta V_a}{R}\left(P_f - P_{ref}\right)\right] - \frac{\Delta H}{RT_{ref}}\right\} \quad (18)$$

and gives a positive linear dependence of viscosity on the pressure of SCHOTT N-BK7®, with a slope of 0.05 $\log_{10}$(Pa·s)/100 MPa. The pressure dependent viscosity data from this study, together with the viscosity predicted by the 2-Maxwell model and the latest two-internal-parameter relaxation model(Ding et al., 2018) are shown in Fig. 4.6. We recall that the mean stress used in Fig. 4.6 equals to $\sigma_{mean} = (\sigma_{load} + 2\sigma_{Ar}) / 3$ (see Eq. 4.2 (Paterson & Wong, 2005)), and that the viscosity is calculated using Eq. 4.17. The overall viscosity change in this study is approximately 0.1 $\log_{10}$(Pa·s)/100 MPa, which is similar to the prediction from the 2-Maxwell model and the latest two-internal-parameter relaxation model. The absolute viscosities are still different from the most recent two-internal-parameter relaxation model of approximately +1.0 $\log_{10}$(Pa·s) (same as the variable temperature experiments), even though the 2-Maxwell model can fit the data well with a negligible difference.

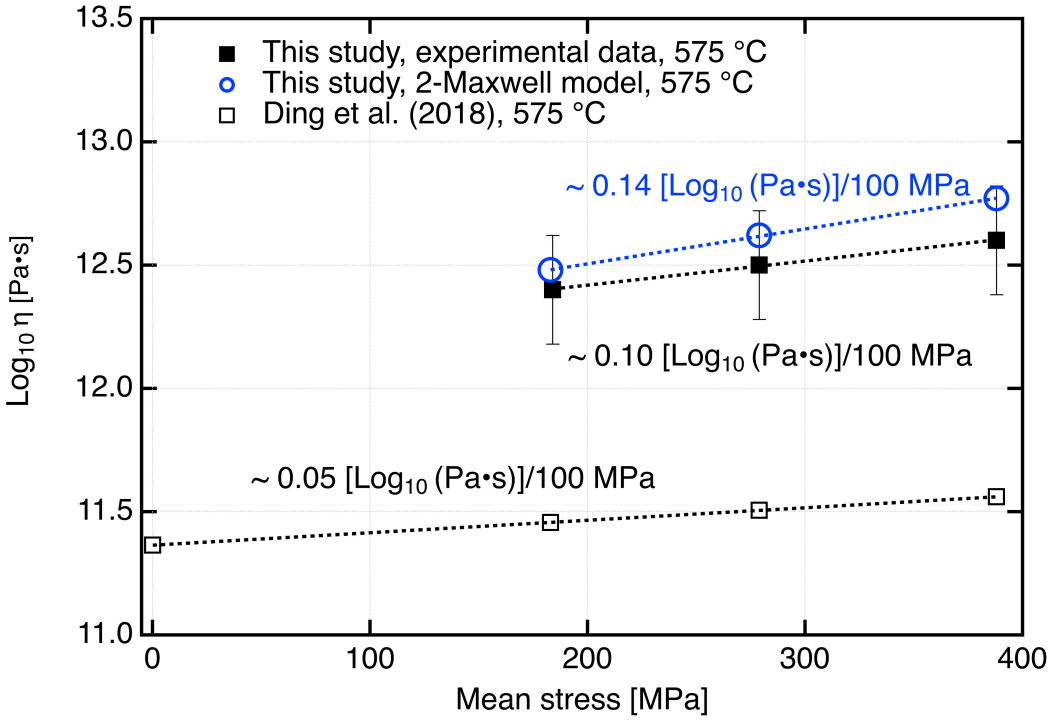

Fig. 4.6 *Viscosity as a function of the mean stress of SCHOTT N-BK7® for the experimental data at 575 °C compared to the values calculated by using a 2-Maxwell model as well as the latest two-internal-parameter relaxation model (Ding et al., 2018).*

4.5 Discussion

Since the viscosity increases with increasing pressure, SCHOTT N-BK7® glass behaves as a depolymerized glass. The pressure yields a positive effect on forming the 3D networks (oxygen atoms in TO_4 connect to adjacent tetrahedron) in SCHOTT N-BK7® glass.

The present *in situ* experiments confirm the previous overall temperature dependence results fitted by an Arrhenius equation. However, the viscosity dependence on pressure is rather small and sensitive to uncertainties in temperature. Indeed, ± 5 °C can yield an uncertainty as high as ± 0.22 $\log_{10}$(Pa·s) on the viscosity at 300 MPa.

Glass (i.e., non-crystalline materials) typically behaves like a Newtonian fluid(Simmons et al., 1982) under applied stress, yet non-Newtonian viscous flow has also been observed in soda-lime silicate glass(Simmons et al., 1982) at strain rates around 10^{-4} s^{-1}. Here, mechanical data as a function of strain rate indicate that the SCHOTT N-BK7® glass at 300 MPa and 575 °C might have a non-Newtonian behavior (Fig. 4.2c), which partly affects the overall fit of the 2-Maxwell model in Fig. 4.3b. During the industrial glass production, the process parameters are chosen to avoid fracture, that is, to be slow enough to remain perfectly Newtonian. Thus, the influence of a large strain rate range on SCHOTT N-BK7® viscosity will need further experiments to properly quantify. On the other hand, the non-linear viscosity change with increasing strain rates might also be due to the uncertainty in temperature, such as a local heterogeneous temperature distribution (e.g., radial gradient or the heat distribution difference between the deformation assembly containing the glass cylinder and the furnace calibration assembly containing an alumina cylinder).

For the large absolute viscosity discrepancy between experimental data and the latest two-internal-parameter relaxation model (based on static high pressure and volume recovery measurement), we do not have an unambiguous explanation. It may be due to the following aspects: (i) the deformation apparatus does not permit experiments at 1-atm

and high temperature and thus the current data set cannot be confirmed by experimental data at 1-atm and 575 °C. (ii) The temperature calibration was done by using a hollow alumina cylinder instead of the SCHOTT N-BK7® glass cylinder, which may have affected the temperature distribution. We have tried to calibrate the furnace using a specially designed hollow SCHOTT N-BK7® glass cylinder, but at high temperature and pressure the hole for the thermocouple (which is at room pressure) shrunk as a result of viscous flow under high confining pressure, preventing any successful temperature calibration with a glass specimen. The different thermal conductivity between the SCHOTT N-BK7® glass hollow cylinder and the alumina hollow cylinder could have caused a slight change in temperature distribution. (iii) the surface tension (Parikh, 1958) and friction (Liu, 1964) between the glass sample and the copper jacket were not taken into account during the stress determination; or (iv) some other fundamental process is missing in the two-internal parameter relaxation model.

4.6 Conclusions

Deformation experiments in uniaxial compression on SCHOTT N-BK7® glass were performed at temperatures near the glass transition temperature (561 °C) and at confining pressures of 100 to 300 MPa. The main results of this study are:

(a) The viscosity of SCHOTT N-BK7® glass increases linearly with increasing pressure at ~0.1 $\log_{10}$(Pa·s)/100 MPa in the range of confining pressure investigated.

(b) The pressure dependence of viscosity measured in this study (~0.1 $\log_{10}$(Pa·s)/100 MPa) is consistent with the latest two-internal-parameter relaxation model.

(c) At the same temperature and the same pressure, the viscosity measured in this study is approximately +1.0 $\log_{10}$(Pa·s) higher than in Ding et al. (2018).(Ding et al., 2018) The reason for this discrepancy has not been identified clearly.

(d) The mechanical data can be overall fitted by a Maxwell viscoelastic model with two parallel elements.

4.7 Acknowledgments

S.D. thanks D. Mainprice and M.A. Bouhifd for informative discussions during this study. The authors thank the technicians and engineers at the SCHOTT machine-shop for the sample preparation. This project has received funding from the European Union's Horizon 2020 research and innovation program under the Marie Sklodowska-Curie grant agreement N° 642029.

4.8 References

Adam, G. & Gibbs, J. H. (1965). On the Temperature Dependence of Cooperative Relaxation Properties in Glass-Forming Liquids. *The Journal of Chemical Physics*, 43 (1): 139-146.

Alkorta, J., Martinez-Esnaola, J. M. & Sevillano, J. G. (2005). Absence of one-to-one correspondence between elastoplastic properties and sharp-indentation load-penetration data (vol 20, pg 432, 2005). *Journal of Materials Research*, 20 (5): 1369-1369.

An, Q. L., Ming, W. W. & Chen, M. (2015). Experimental Investigation on Cutting Characteristics in Nanometric Plunge-Cutting of BK7 and Fused Silica Glasses. *Materials*, 8 (4): 1428-1441.

Avramov, I. (2000). Pressure dependence of viscosity of glassforming melts. *Journal of Non-Crystalline Solids*, 262 (1-3): 258-263.

Carroll, M. R. & Stolper, E. M. (1991). Argon Solubility and Diffusion in Silica Glass - Implications for the Solution Behavior of Molecular Gases. *Geochimica Et Cosmochimica Acta*, 55 (1): 211-225.

Cohen, M. H. & Turnbull, D. (1959). Molecular Transport in Liquids and Glasses. *Journal of Chemical Physics*, 31 (5): 1164-1169.

Del Gaudio, P., Behrens, H. & Deubener, J. (2007). Viscosity and glass transition temperature of hydrous float glass. *Journal of Non-Crystalline Solids*, 353 (3):

223-236.

Demouchy, S., Schneider, S. E., Mackwell, S. J., Zimmerman, M. E. & Kohlstedt, D. L. (2009). Experimental deformation of olivine single crystals at lithospheric temperatures. *Geophysical Research Letters*, 36: L04304.

Demouchy, S., Tommasi, A., Ballaran, T. B. & Cordier, P. (2013). Low strength of Earth's uppermost mantle inferred from tri-axial deformation experiments on dry olivine crystals. *Physics of the Earth and Planetary Interiors*, 220: 37-49.

Demouchy, S., Mussi, A., Barou, F., Tommasi, A. & Cordier, P. (2014). Viscoplasticity of polycrystalline olivine experimentally deformed at high pressure and 900 degrees C. *Tectonophysics*, 623: 123-135.

Dick, E. (1970). New experiments on the microplasticity of glass. *Ger.), Glastech. Ber*, 43 (1): 16-21.

Ding, L., Buhre, S., Kunisch, C. & Kaus, B. (2018). Pressure dependence of density and structural relaxation of glass near the glass transition region. *Journal of the American Ceramic Society*, 101 (3): 1149-1158.

Dingwell, D. B. & Webb, S. L. (1989). Structural Relaxation in Silicate Melts and Non-Newtonian Melt Rheology in Geologic Processes. *Physics and Chemistry of Minerals*, 16 (5): 508-516.

Dyer, P. E., Maswadi, S. M., Walton, C. D., Ersoz, M., Fletcher, P. D. I. & Paunov, V. N. (2003). 157-nm laser micromachining of N-BK7 glass and replication for microcontact printing. *Applied Physics a-Materials Science & Processing*, 77 (3-4): 391-394.

Frost, H. J. & Ashby, M. F. (1982). *Deformation mechanism maps: the plasticity and creep of metals and ceramics*: Pergamon press.

Fulcher, G. S. (1925). Analysis of recent measurements of the viscosity of glasses. *Journal of the American Ceramic Society*, 8 (6): 339-355.

Grassia, L. & Simon, S. L. (2012). Modeling volume relaxation of amorphous polymers: Modification of the equation for the relaxation time in the KAHR model. *Polymer*,

53 (16): 3613-3620.

Greet, R. J. & Turnbull, D. (1967). Test of Adam-Gibbs Liquid Viscosity Model with O-Terphenyl Specific-Heat Data. *Journal of Chemical Physics*, 47 (6): 2185-2190.

Gupta, P. K. (1987). Negative-Pressure Dependence of Viscosity. *Journal of the American Ceramic Society*, 70 (7): C152-C153.

Gupta, P. K. (1988). Fictive Pressure Effects in Structural Relaxation. *Journal of Non-Crystalline Solids*, 102 (1-3): 231-239.

Hagan, J. & Swain, M. V. (1978). The origin of median and lateral cracks around plastic indents in brittle materials. *Journal of Physics D: Applied Physics*, 11 (15): 2091.

Hodge, I. M. (1994). Enthalpy Relaxation and Recovery in Amorphous Materials. *Journal of Non-Crystalline Solids*, 169 (3): 211-266.

Jain, A., Yi, A. Y., Xie, X. P. & Sooryakumar, R. (2006). Finite element modelling of stress relaxation in glass lens moulding using measured, temperature-dependent elastic modulus and viscosity data of glass. *Modelling and Simulation in Materials Science and Engineering*, 14 (3): 465-477.

Jantzen, C. M. (2017). Using Polymerization, Glass Structure, and Quasicrystalline Theory to Produce High Level Radioactive Borosilicate Glass Remotely: A 20+ Year Legacy. *Journal of the South Carolina Academy of Science*, 15 (1): 4.

Jin, H. J., Gu, X. J., Wen, P., Wang, L. B. & Lu, K. (2003). Pressure effect on the structural relaxation and glass transition in metallic glasses. *Acta Materialia*, 51 (20): 6219-6231.

Karato, S. I., Paterson, M. S. & Fitz Gerald, J. D. (1986). Rheology of Synthetic Olivine Aggregates - Influence of Grain-Size and Water. *Journal of Geophysical Research-Solid Earth and Planets*, 91 (B8): 8151-8176.

Kaus, B. J. P. & Becker, T. W. (2007). Effects of elasticity on the Rayleigh-Taylor instability: implications for large-scale geodynamics. *Geophysical Journal International*, 168 (2): 843-862.

Koontz, E., Blouin, V., Wachtel, P., Musgraves, J. D. & Richardson, K. (2012). Prony

Series Spectra of Structural Relaxation in N-BK7 for Finite Element Modeling. *Journal of Physical Chemistry A*, 116 (50): 12198-12205.

Kushiro, I. (1976). Changes in Viscosity and Structure of Melt of Naalsi2o6 Composition at High-Pressures. *Journal of Geophysical Research*, 81 (35): 6347-6350.

Kushiro, I. (1978). Viscosity and Structural-Changes of Albite (Naalsi3o8) Melt at High-Pressures. *Earth and Planetary Science Letters*, 41 (1): 87-90.

Lagarias, J. C., Reeds, J. A., Wright, M. H. & Wright, P. E. (1998). Convergence properties of the Nelder-Mead simplex method in low dimensions. *Siam Journal on Optimization*, 9 (1): 112-147.

Lawn, B. R., Dabbs, T. P. & Fairbanks, C. J. (1983). Kinetics of Shear-Activated Indentation Crack Initiation in Soda-Lime Glass. *Journal of Materials Science*, 18 (9): 2785-2797.

Lee, E. H. & Radok, J. R. M. (1960). The Contact Problem for Viscoelastic Bodies. *Journal of Applied Mechanics*, 27 (3): 438-444.

Limbach, R., Winterstein-Beckmann, A., Dellith, J., Möncke, D. & Wondraczek, L. (2015). Plasticity, crack initiation and defect resistance in alkali-borosilicate glasses: From normal to anomalous behavior. *Journal of Non-Crystalline Solids*, 417: 15-27.

Liu, T. (1964). Sliding friction of copper. *Wear*, 7 (2): 163-174.

Mauro, J. C., Yue, Y. Z., Ellison, A. J., Gupta, P. K. & Allan, D. C. (2009). Viscosity of glass-forming liquids. *Proceedings of the National Academy of Sciences of the United States of America*, 106 (47): 19780-19784.

Mei, S. & Kohlstedt, D. L. (2000a). Influence of water on plastic deformation of olivine aggregates 1. Diffusion creep regime. *Journal of Geophysical Research-Solid Earth*, 105 (B9): 21457-21469.

Mei, S. & Kohlstedt, D. L. (2000b). Influence of water on plastic deformation of olivine aggregates 2. Dislocation creep regime. *Journal of Geophysical Research-Solid Earth*, 105 (B9): 21471-21481.

Mosaddegh, P. & Ziegert, J. C. (2011). Friction measurement in precision glass molding: An experimental study. *Journal of Non-Crystalline Solids*, 357 (16-17): 3221-3225.

Mysen, B. O., Virgo, D. & Seifert, F. A. (1982). The structure of silicate melts: implications for chemical and physical properties of natural magma. *Reviews of Geophysics*, 20 (3): 353-383.

Narayanaswamy, O. S. (1971). A Model of Structural Relaxation in Glass. *Journal of the American Ceramic Society*, 54 (10): 491-498.

Parikh, N. M. (1958). Effect of Atmosphere on Surface Tension of Glass. *Journal of the American Ceramic Society*, 41 (1): 18-22.

Paterson, M. (1990). Rock deformation experimentation. *Geophysical monograph*: 187-194.

Paterson, M. S. (1970). A High-Pressure, High-Temperature Apparatus for Rock Deformation. *International Journal of Rock Mechanics and Mining Sciences*, 7 (5): 517-526.

Paterson, M. S. & Wong, T.-f. (2005). *Experimental rock deformation-the brittle field*: Springer Science & Business Media.

Peter, K. (1970). Densification and flow phenomena of glass in indentation experiments. *Journal of Non-Crystalline Solids*, 5 (2): 103-115.

Rouxel, T., Besson, J.-L., Gault, C., Goursat, P., Leigh, M. & Hampshire, S. (1989). Viscosity and Young's modulus of an oxynitride glass. *Journal of Materials Science Letters*, 8 (10): 1158-1160.

Rouxel, T. & Sangleboeuf, J. C. (2000). The brittle to ductile transition in a soda-lime-silica glass. *Journal of Non-Crystalline Solids*, 271 (3): 224-235.

Scarfe, C. M., Mysen, B. O. & Virgo, D. (1987). Pressure dependence of the viscosity of silicate melts. *Magmatic processes: Physicochemical principles*, 1: 59-67.

Scherer, G. W. & Rekhson, S. M. (1982). Viscoelastic-Elastic Composites: I, General Theory. *Journal of the American Ceramic Society*, 65 (7): 352-360.

Scherer, G. W. (1990). Theories of Relaxation. *Journal of Non-Crystalline Solids*, 123 (1-3): 75-89.

Schulze, F., Behrens, H. & Hurkuck, W. (1999). Determination of the influence of pressure and dissolved water on the viscosity of highly viscous melts: Application of a new parallel-plate viscometer. *American Mineralogist*, 84 (10): 1512-1520.

Shang, H. X. & Rouxel, T. (2005). Creep behavior of soda-lime glass in the 100-500 K temperature range by indentation creep test. *Journal of the American Ceramic Society*, 88 (9): 2625-2628.

Simmons, J. H., Mohr, R. K. & Montrose, C. J. (1982). Non-Newtonian Viscous-Flow in Glass. *Journal of Applied Physics*, 53 (6): 4075-4080.

Simon, S. L., Park, J. Y. & McKenna, G. B. (2002). Enthalpy recovery of a glass-forming liquid constrained in a nanoporous matrix: Negative pressure effects. *European Physical Journal E*, 8 (2): 209-216.

Sperry, L. & JD, M. (1968). Pressure dependence of viscosity of B2O3. *PHYSICS AND CHEMISTRY OF GLASSES*, 9 (3): 91-95.

Tool, A. Q. (1946). Relation between Inelastic Deformability and Thermal Expansion of Glass in Its Annealing Range. *Journal of the American Ceramic Society*, 29 (9): 240-253.

Tribone, J. J., Oreilly, J. M. & Greener, J. (1989). Pressure-Jump Volume-Relaxation Studies of Polystyrene in the Glass-Transition Region. *Journal of Polymer Science Part B-Polymer Physics*, 27 (4): 837-857.

Turnbull, D. & Cohen, M. H. (1970). On the Free-Volume Model of the Liquid-Glass Transition. *The journal of chemical physics*, 52 (6): 3038-3041.

Wang, Y., Sakamaki, T., Skinner, L. B., Jing, Z., Yu, T., Kono, Y., Park, C., Shen, G., Rivers, M. L. & Sutton, S. R. (2014). Atomistic insight into viscosity and density of silicate melts under pressure. *Nature communications*, 5: 3241.

Webb, S. L. & Dingwell, D. B. (1990). Non-Newtonian Rheology of Igneous Melts at High Stresses and Strain Rates - Experimental Results for Rhyolite, Andesite,

Basalt, and Nephelinite. *Journal of Geophysical Research-Solid Earth and Planets*, 95 (B10): 15695-15701.

Wilantewicz, T. E. & Varner, J. R. (2008). Vickers indentation behavior of several commercial glasses at high temperatures. *Journal of Materials Science*, 43 (1): 281-298.

Williams, M. L., Landel, R. F. & Ferry, J. D. (1955). The Temperature Dependence of Relaxation Mechanisms in Amorphous Polymers and Other Glass-Forming Liquids. *Journal of the American Chemical Society*, 77 (14): 3701-3707.

Zheng, Q. J. & Mauro, J. C. (2017). Viscosity of glass-forming systems. *Journal of the American Ceramic Society*, 100 (1): 6-25.

Chapter 5

5. Plastic yielding of glass under high pressure

Submitted to *International Journal of Applied Glass Science*

Ding L, Kerber M, Kunisch C, Kaus B. Plastic yielding of glass in high-pressure torsion apparatus. *International Journal of Applied Glass Science. (Under review)*

5.1 Summary

Hardness measurements performed at room temperature have demonstrated that glass can flow under elevated pressure, whereas the effect of high pressure on glass rheology remains poorly quantified. Here, we applied a high-pressure torsion (HPT) apparatus to deform SCHOTT SF6® glass and attempted to quantify the effect of pressure and temperature on the shear deformation of glass subjected to pressures from 0.3 GPa to 7 GPa and temperatures from 25 ℃ to 496 ℃. Results show that the plastic yield deformation was occurring during the HPT experiments on the SF6 glass at elevated temperature from 350 ℃ to 496 ℃. The yield stress of SF6 glass decreases with increasing temperature and decreasing pressure. An extended Arrhenius model with one set of parameters, namely infinite yield stress Y_0=0.17±0.1 GPa, activation energy E_a=4.8±0.5 kJ/mol and activation volume V_a=1.4±0.2 cm^3/mol, can explain the experimental results well.

5.2 Introduction

The viscosity of glass at different temperature regions under ambient pressure has been well studied (Zheng & Mauro, 2017), and numerous models for the temperature dependence of viscosity have been developed that fit the experimental data well (Adam & Gibbs, 1965; Cohen & Turnbull, 1959; Fulcher, 1925; Greet & Turnbull, 1967; Mauro et al., 2009; Turnbull & Cohen, 1970; Williams et al., 1955). On the other hand, hardness measurements (Peter, 1970; Shang & Rouxel, 2005; To et al., 2018) performed at room temperature have demonstrated that glass can flow at room temperature under elevated pressure. Yet the actual pressure level and its distribution in the glass underneath an indenter and its consequences on the mechanical behavior remain poorly understood (Alkorta et al., 2005; Lee & Radok, 1960).

The importance of understanding both the temperature and the pressure dependence of the viscosity of the glass is connected to the fact that density strongly relates to the

dynamics of the fluid (Cook et al., 1994). Several experimental and modeling studies focused on the effect of pressure on the viscosity of glass (Avramov, 2000; Grassia & Simon, 2012; Hodge, 1994; Schulze et al., 1999; Simon et al., 2002; Sperry & JD, 1968; Tribone et al., 1989). In our previous work (Ding et al., 2018), the effect of pressure on density and volume recovery of SCHOTT N-BK7® glass has been studied, and a two-internal-parameter relaxation model was developed, that predicts a linear increase of viscosity with pressure. Moreover, deviatoric deformation experiments (Ding et al.) on SCHOTT N-BK7® glass have also been performed in a Paterson press (Paterson, 1990), which is an argon gas medium hot press with a compression deformation mechanism, are in general agreement with the prediction of the two-internal-parameter relaxation model (Ding et al., 2018) at the pressure range of 0.1 GPa-0.3 GPa.

On the other hand, viscous flow is not the only deformation mechanism for materials under high pressure. A deformation via plastic yield is widely reported in many deformation experiments on polymers (Nanzai, 1993), alloys (Raghavan et al., 2015), and metallic glass (Donovan, 1989; Vaidyanathan et al., 2001). The atomistic origin for the plastic yield criterion for metallic glass under pressure is discussed by Schuh & Lund (Schuh & Lund, 2003), which generally supports the plastic yield behavior in amorphous materials. Amorphous materials, including glass, lack the microstructural defects which facilitate plastic flow in crystalline materials, and thus potentially have a much higher yield stress in a plastic yield deformation, e.g., up to 3 GPa for oxide glass (Demetriou et al., 2011) and ~0.5 GPa (Xi et al., 2005) to 5 GPa (Inoue et al., 2003) for metallic glass. However, industrial oxide glass typically has a low fracture toughness, on the order of 1 $MPa \cdot m^{0.5}$, and consequently, brittle fractures usually occur much earlier than plastic yielding.

High-pressure torsion (HPT) is a well-known method to induce severe plastic deformation (Bachmaier et al., 2012; Vorhauer & Pippan, 2004; Xu et al., 2013; Zhilyaev et al., 2003). For scientific purposes, it is one of the best methods as it allows for the controlled generation of high pressures and large strains at a number of exterior physical

parameters such as strain rate and temperature. Thus, HPT is ideal for highly reproducible experiments under rather extreme conditions. To the knowledge of the authors, the HPT deformation experiments have not yet been conducted on an optical glass before. In this work, we applied HPT to deform the SCHOTT SF6® optical glass by torsion at very low rotations speeds and at different temperatures to study the flow of glass under high pressure and as a function of temperature.

5.3 Experimental

5.3.1 Samples

The alkali-lead-silicate glass SCHOTT SF6® (chemical composition(Heiman et al., 1979): 27.3 % SiO_2, 1.5 % K_2O, 71 % PbO) is an optical glass widely used as photonic crystal fiber(Efimov & Taylor, 2008; Fu et al., 2010; Hundertmark et al., 2009) for efficient spectral broadening at high repetition rates (several GHz). The density of SCHOTT SF6® glass at room temperature and ambient pressure is 5.180 ± 0.001 g/cm^3. The glass transition temperature T_g of the SCHOTT SF6® glass is 417 °C, which is the temperature at which the viscosity is 12 $\log_{10}$(Pa·s). The SCHOTT SF6® glass specimens with diameters of 6.0±0.02 mm and 10.0±0.02 mm and thickness of 0.54±0.02 and 0.62±0.02 mm were used for the HPT experiments. All glass specimens were ground with a 59 μm sandblast grinding apparatus resulting in uniform surfaces and edges. The surface and edge condition of the glass specimens were investigated under the microscope, and one example of SF6® glass is shown in Fig.1 (b).

The composition dependence of glass rheology is not the topic we study in this work. We choose SCHOTT SF6® glass for these experiments mainly due to its low glass transition temperature combined with the good stability of the material properties. The temperature limit for the present HPT setup is ~540 °C due to the softening of the anvil steel Boehler S390 MC around that temperature in combination with the loads applied.

The SCHOTT N-BK7® glass used in our previous work(Ding et al., 2018a; Ding et al., 2018b) with T_g =561 °C is not suitable for the HPT deformation experiments.

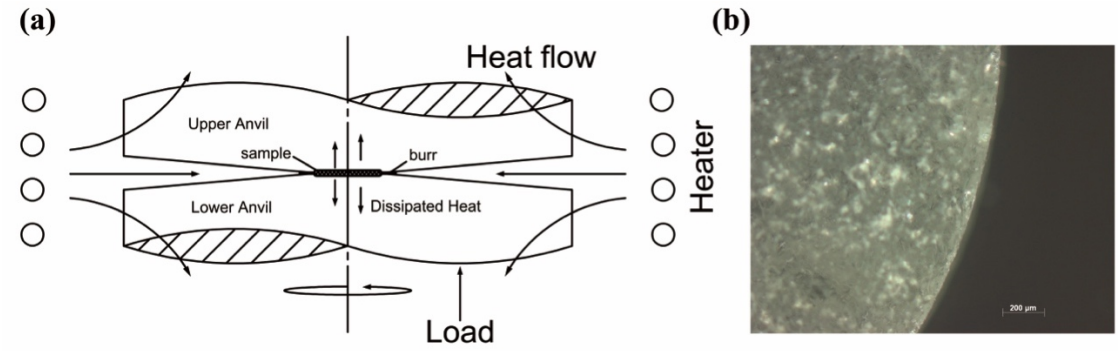

Fig.5.1 *(a) Schematic graph of high-pressure torsion apparatus in this work; (b) Microscope image of the glass sample.*

5.3.2 Test equipment and experimental process

The high-pressure torsion (HPT) apparatus used in these experiments is a Klement HTP pre-series machine, with the same basic design as described in Vorhauer et al. [32] and Wetscher et al. [34], a sketch of the principle of operation of HPT is shown in Fig.5.1 (a). Two anvils are pressed against each other with the (glass) sample in between thus applying a hydrostatic pressure. The contact surfaces between sample and anvil can be both flat (unconstrained HPT), both with identical cavities or with asymmetric cavities (quasi-constrained HPT). The unconstrained HPT configuration is most similar to a classical rheometer, whereas the symmetric cavities are most common and correspond closest to a true hydrostatic loading of the sample. During the initial uniaxial compression, a burr forms in the gap between the anvils on the rim of the cavity providing a sealing of the sample as well as preventing the anvils from touching which results in the measurement of the friction of the anvils instead of the load on the samples. In the present case for a proper formation of the burr, the total depth of both cavities was determined to be approximately 20% smaller than the thickness of the glass sample. With this

experimentally determined value, only a small amount of the material freely flows into the burr during the initial part of the experiment.

After the application of pressure, the lower anvil is rotated at nominal 0.01 rounds per minute (RPM), which causes the sample to transmit a torque on the upper anvil and its holder. A self-built torque-sensor consisting of four strain-gauge half-bridges from HBM connected to two full bridges in averaging configuration is used to measure the torque needed to deform the sample. Before each set of experiments, the raw physical value (mV/V) of the strain-gauge signal was calibrated using a standard Gedore torque-wrench at 50 Nm and 100 Nm, with a limiting precision of 2% without any pressure applied. The calibration was also monitored randomly between experiments. The effect of the hydrostatic loading on the torque signal (zero-shift) was also recorded (it is smaller than one percent) and subtracted from the signal before evaluation.

The hydrostatic load was recorded as the pressure in the piston and as the load transmitted via the sample to an HBM C2A load-cell directly in N. The present machine is designed to provide controlled pressure application from 1-10 GPa, depending on the sample diameter.

In this work, firstly, a set of 6 mm diameter glass samples was used to investigate the pressure range from ~3 GPa to ~7 GPa. A second set, with improved torque-sensor and the cooling system, aimed to achieve lower pressures by using 10 mm samples for pressures from ~1 GPa to ~3 GPa (by automatic loading). Also using 10 mm samples for ~0.3 GPa pressure were obtained by manual loading, bypassing computer control of the pressure.

An important parameter in the present case is the sample temperature: Heating was performed using a Hüttinger induction heater, symmetrically heating the anvils. The temperature control and monitoring were done by using a Sensortherm pyrometer with a control unit capable of detecting temperatures above 75 °C. The control window of the setup is below 0.5 °C. A reference measurement using a thermocouple in a copper disc in place of the sample showed that the sample lags at most two minutes behind the

Pyrometer data (large deviation at low temperatures). The overall uncertainty of the temperature is about ±5 °C.

The procedure of the current experiment was as follows: firstly, both cavities of the two anvils were sandblasted with 250 microns quartz sand. Then, the glass specimen was placed in the lower anvil and lifted to a bare touch of the upper anvil, and the samples were heating to the initial temperatures ranging from 350 ℃ to 496 ℃. After waiting the experimentally determined two minutes, the pressure from 0.3 GPa to 7 GPa was applied via uniaxial loading. Finally, the deformation was started with the nominal speed of 0.01 RPM, which turned out to be 0.0096 RPM as calculated from the data recorded over several minutes.

To verify the reproducibility of the data, for each sample heating cycles were performed, between the chosen temperatures thus checking the consistency per sample. Additionally, the whole experiment was repeated on another sample.

Furthermore, an experiment at room temperature and a pressure of 3 GPa was also performed. In order to be able to compare with measurements in a rheometer and to judge the effect of the burr, also flat anvils were used for one deformation.

To isolate the effect of the pressure on the torque one experiment at 435°C, 10 mm diameter sample was performed, stepwise increasing the pressure from 0.3 to 5.1 GPa once the torque readout stabilized.

5.3.3 Data analysis

For a torsional deformation, the glass sample could be deformed as a viscous flow (Zheng & Mauro, 2017) or via a plastic yielding (Schuh & Lund, 2003).

5.3.3.1 Approach 1: viscous flow

For a viscous flow, the viscosity is constant when the deformation reaches steady state, and the viscous strain rate, stress, and viscosity can be calculated by

$$\dot{\varepsilon}(r) = \frac{2\pi r f}{H} \tag{5.1}$$

$$\tau(r) = \eta\dot{\varepsilon}(r) = \eta\,\frac{2\pi r f}{H} \tag{5.2}$$

$$M_T = \int_0^R 2\pi r \cdot \tau(r) \cdot r dr = \frac{\eta\, \pi^2\, R^4 f}{H} \quad (5.3)$$

$$\eta = \frac{M_T H}{\pi^2 R^4 f} \quad (5.4)$$

where $\dot{\varepsilon}(r)$ is the change of strain with time at a radius *r*, $\tau(r)$ is the shear stress at a radius *r*, η is the viscosity, M_T is the measured torque, *f* is the frequency of the rotation (converted to SI-units via RPM/60), *H* is the thickness of the sample, and *R* is the outer radius of the sample.

5.3.3.2 Approach 2: shear yielding

For a yield deformation, the shear yield stress *Y* is not dependent on the radius, and therefore

$$M_T = \int_0^R 2\pi r \cdot Y \cdot r dr = \frac{2\pi\, R^3 Y}{3} \quad (5.5)$$

$$Y = \frac{3M_T}{2\pi\, R^3} \quad (5.6)$$

And the friction coefficient can be calculated as

$$\mu = \frac{Y}{P} \quad (5.7)$$

Where P is the uniaxial pressure (normal stress).

5.4 Results

The experimental conditions and the measured mechanical data are provided in Table 5-1. The number of the aforementioned repetition stages per experiment and their changes, as well as the resulting deviation of the measured values together with the nominal, identical experimental parameters, are reported in Table 5-1.

Table 5-1 *Experimental conditions and results*

Samples	Glass type	Diameter [mm]	Thickness [mm]	Pressure [GPa]	Temperature [℃]	Torque [N·m]	Viscosity Log_{10}[Pa·s]	Yield stress [GPa]	Repeat times	Note
S1	SF6	6	0.54±0.02	3.3±0.1	435±5	49±1	11.32±0.02	0.87±0.02	4	
S2	SF6	6	0.54±0.02	5.2±0.1	496±5	80±1	11.53±0.02	1.41±0.02	4	
S3	SF6	6	0.54±0.02	4.9±0.1	435±5	81±1	11.53±0.02	1.43±0.02	4	
S4	SF6	6	0.54±0.02	5.0±0.1	350±5	89±1	11.58±0.02	1.57±0.02	4	
S5	SF6	6	0.54±0.02	7.1±0.1	496±5	121±2	11.71±0.02	2.14±0.04	4	
S6	SF6	6	0.54±0.02	6.8±0.1	435±5	115±1	11.68±0.02	2.03±0.02	4	
S7	SF6	6	0.54±0.02	6.5±0.1	350±5	113±2	11.68±0.02	2.00±0.04	4	
S8	SF6	10	0.54±0.02	0.3±0.0	435±5	57±3	10.49±0.02	0.22±0.01	3	Manual
S9	SF6	10	0.54±0.02	1.3±0.1	496±5	111±5	10.78±0.05	0.42±0.02	3	
S10	SF6	10	0.54±0.02	1.1±0.1	435±5	137±2	10.87±0.01	0.52±0.01	3	
S11	SF6	10	0.54±0.02	1.1±0.1	350±5	164±3	10.95±0.03	0.63±0.01	3	
S12	SF6	10	0.54±0.02	2.1±0.1	496±5	144±4	10.90±0.02	0.55±0.02	3	

S13	SF6	10	0.54±0.02	2.1±0.1	435±5	178±2	10.99±0.01	0.68±0.01	3	
S14	SF6	10	0.54±0.02	2.0±0.1	350±5	201±3	11.04±0.01	0.77±0.01	3	
S15	SF6	10	0.54±0.02	3.2±0.1	496±5	206±4	11.05±0.02	0.79±0.02	3	
S16	SF6	10	0.54±0.02	3.0±0.1	435±5	221±3	11.08±0.01	0.84±0.01	3	
S17	SF6	10	0.54±0.02	3.0±0.1	350±5	251±2	11.14±0.02	0.96±0.01	3	
S18	SF6	10	0.54±0.02	3.0±0.1	25	164±2	10.95±0.01	0.63±0.01	2	Room T
S19	SF6	10	0.54±0.02	3.7±0.1	435±5	250±2	11.14±0.01	0.95±0.01	2	
S20	SF6	10	0.54±0.02	5.1±0.1	435±5	307±3	11.23±0.03	1.17±0.01	2	
S21	SF6	10	0.54±0.02	7.4±0.2	435±5	776±9	11.63±0.02	2.96±0.03	1	Anvils touching
S22	SF6	10	0.62±0.02	0.3±0.0	435±5	50±15	10.50±0.12	0.19±0.06	1	Flat anvils

Most importantly, torsional experiments could be performed on SCHOTT SF6® glass under pressures from 0.3 GPa to 7.4 GPa, the work necessary to maintain the deformation could be monitored accurately via the torque measured as shown in Fig.5.2. The experiments at 435 ℃ (black curve) show that the torque increases approximately proportional to the pressure from 137 N·m at 1.1 GPa to 307 N·m at 5.1 GPa. However, in another experiment at a pressure of 7.4 GPa, the measured torque at 435 ℃ increased dramatically high to nearly 776 N·m. Subsequent visual inspection of sample and anvils, showed that the top and bottom anvils had touched together at this high pressure, and a clear deformation band of approximately 18 mm in place of the rims of the cavities had appeared, as is visible in Fig.5.2.

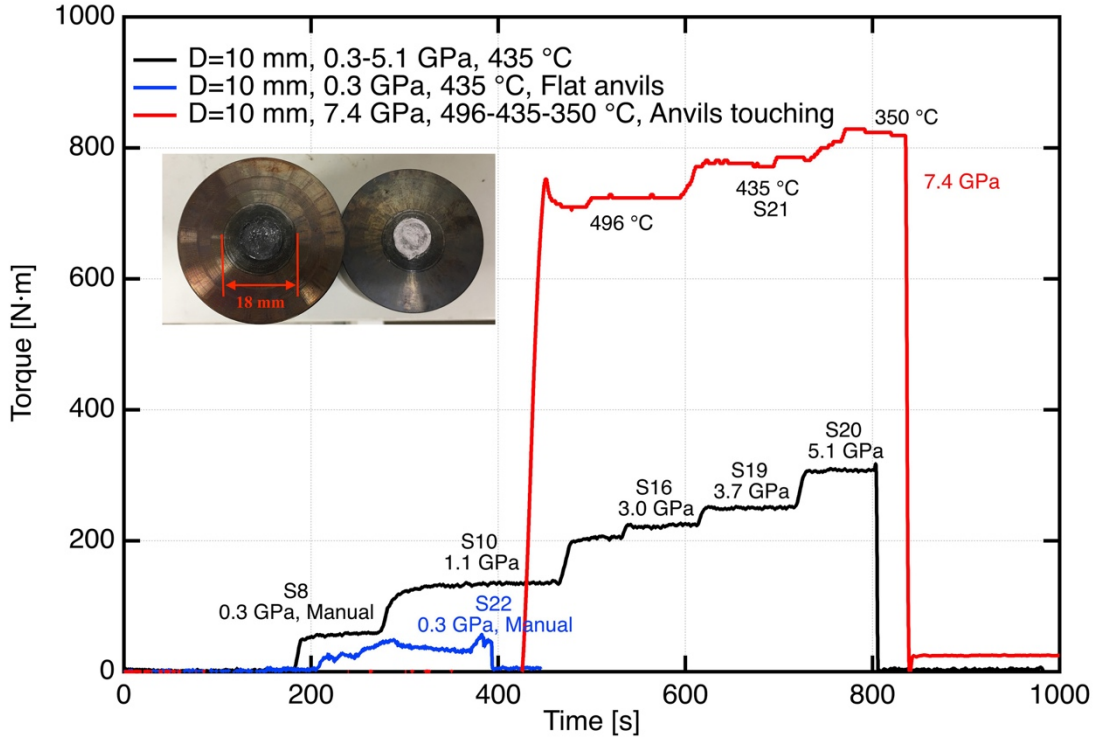

Fig.5.2 *Mechanical torque curves of SF6 glass measured at different pressures and setups. The digital photo shows the status of anvils after the experiment at 7.4 GPa (red curve).*

The bottom piston of the HPT with anvil diameter of 10 mm could automatically lift and smoothly deform the sample at the pressure above 1 GPa. To obtain a lower pressure, the bottom piston was manually lifted until a load was detected by the upper load sensor, corresponding to 0.3 GPa, and subsequently, the deformation was started. To better judge the torque measurements via HPT in the current context, two anvils were machined to flat surfaces, allowing an experiment in the HPT equipment with the ideal rheometry configuration. The flat-

anvil measurement reported in Fig.5.3 reaches a similar torque value as the one measured with the quasi-constrained setup (with burrs). However, the curve also shows that the deformation was not as stable as for the higher pressures, most likely connected with some sliding occurring.

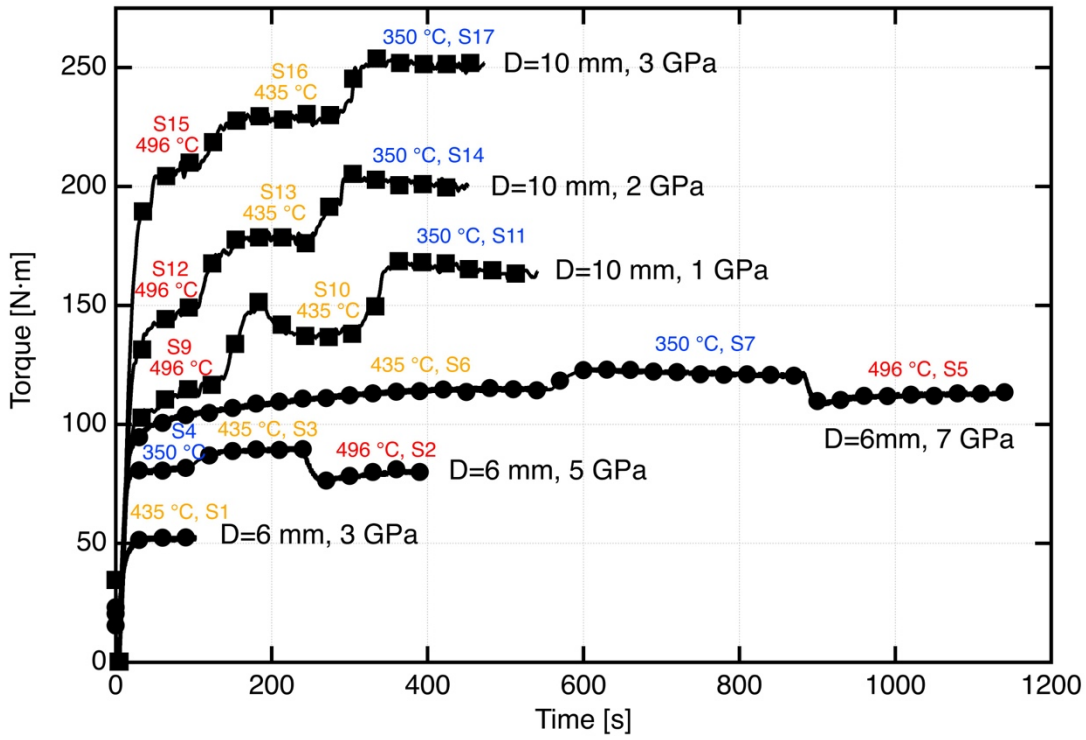

Fig.5.3 *Original mechanical torque data from the HPT measurements of SF6 glass. For all curves, 1 data point out of every 600 points is shown for clarity.*

The raw torque curves from the HPT deformation measurements are shown in Fig.5.3. The deformation experiments at a constant torsional speed of 0.0096 RPM and different temperatures, pressures and anvil diameters reach steady state torques from ~50 N·m to ~275 N·m. To determine the pressure dependence, we conducted automatic loading experiments at uniaxial pressures ranging from ~1 GPa to ~7 GPa. At the same temperature, the torque is approximately increasing linearly with elevated pressure of ~40 N·m/GPa using 10 mm samples and ~15 N·m/GPa for 6 mm samples.

An overview of the temperature dependence is well observable in Fig.5.3. At the same pressure, the temperature reduction from 496 °C to 435 °C is accompanied by a torque increase of around 25 N·m is observed in the setup of 10 mm anvils. The temperature decrease from 435 °C to 350 °C is accompanied by a torque increase of around 27 N·m. However, the

significant temperature change yields only slight influence on the torque measurements in 6 mm setup. Besides, the torque does not even change significantly when the glass sample is quenched to room temperature.

The torsional experiment was also done at room temperature at 3 GPa, during which a big cracking noise was heard at the beginning of the deformation. A clear yielding point in the torque data of approximately 185 N·m is seen in Fig.5.4. After the yielding point, the torque is gradually decreasing to around 164 N·m and reaches steady state. It must be noted that the torque measured at room temperature at 3 GPa is even ~40 N·m lower than at 496 ℃. A pause test was done in this experiment by stopping the rotation of the HPT machine. The torque subsequently decreased gradually, and it recovered to the same level (as before the pause) once the deformation was turned on. After the deformation, a large amount of fine glass powder generated in the anvil (especially the burr area) was observed. A possible explanation of this experiment is discussed in the shear yielding part.

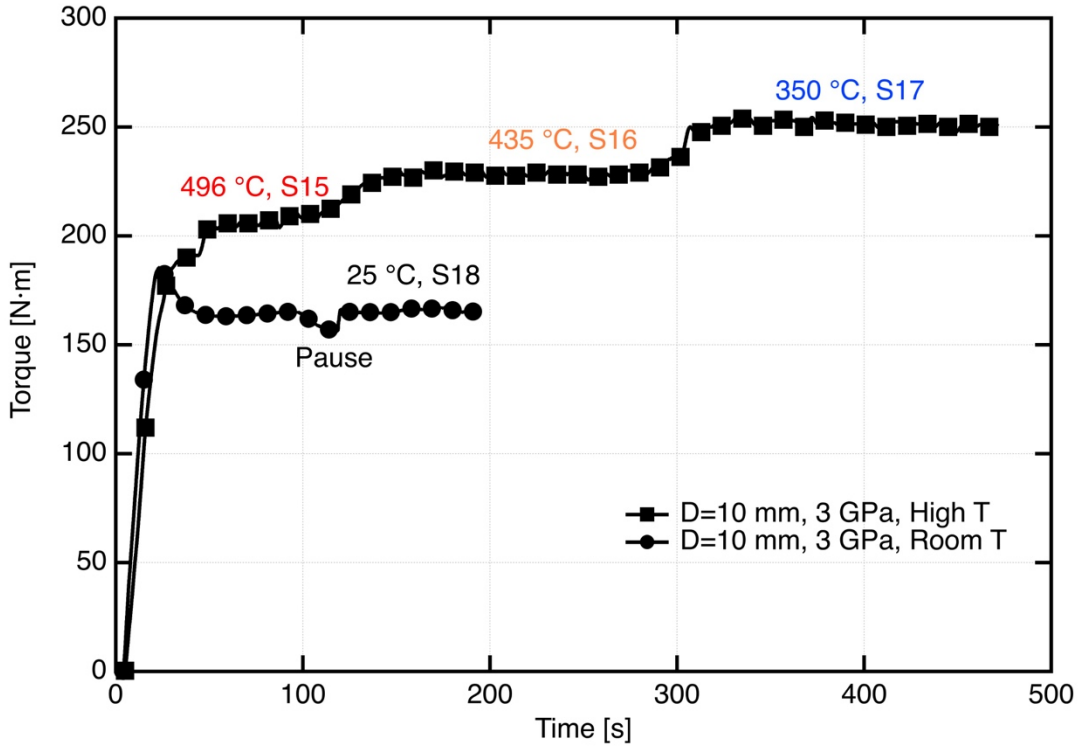

Fig.5.4 *Torque measurement of SF6 glass at room temperature and high temperatures under 3 GPa. For all curves, 1 data point out of every 220 points is shown for clarity.*

5.5 Discussions

5.5.1 Approach 1: viscous flow

Assuming that viscous flow is the predominant deformation mechanism in the present experiments on SCHOTT SF6® glass, the corresponding viscosity was calculated. The 3D plot in Fig.5.5 (a) gives an overview of the temperature and pressure dependence of the viscosity of SF6 glass. Apparently, the viscosity of SF6 glass in HPT is not sensitive to temperature. The temperature change from 350 ℃ to 496 ℃ is accompanied by a maximal viscosity change from 10.8 Log_{10}(Pa·s) to 11.7 Log_{10}(Pa·s) only, which is entirely different to the black curve in Fig.5.5 (b) at ambient pressure, where the change is from 16.2 Log_{10}(Pa·s) to 8.0 Log_{10}(Pa·s).

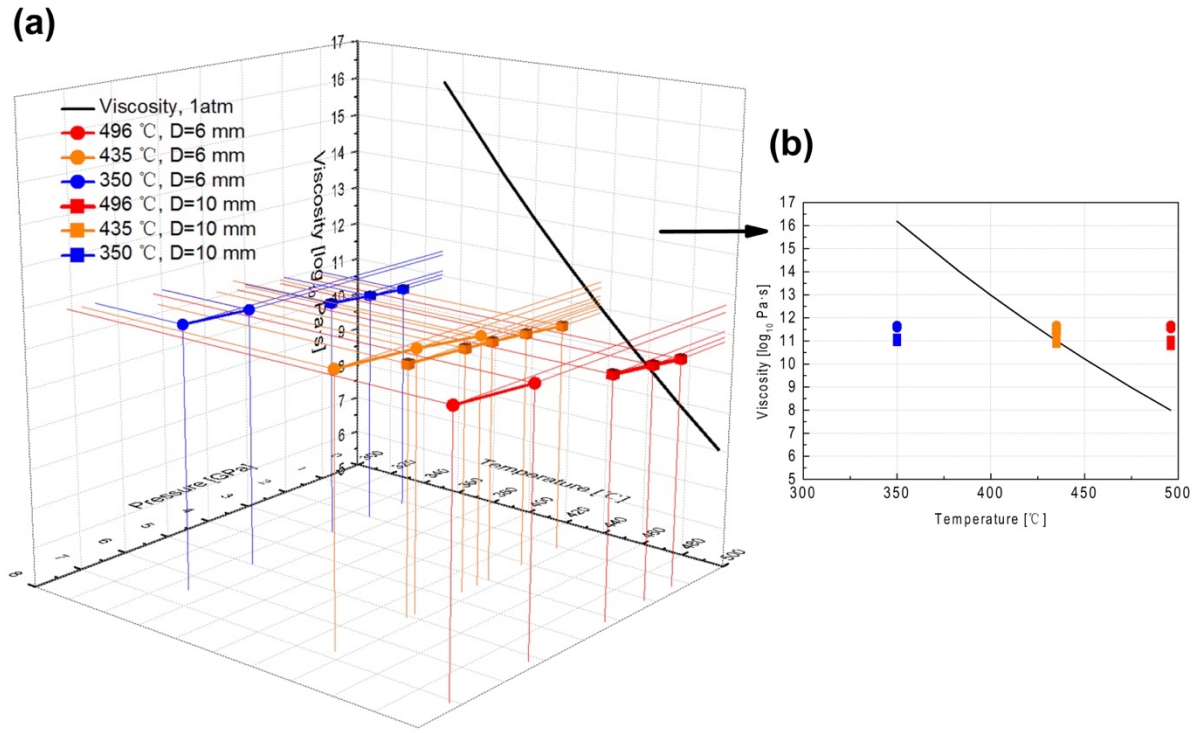

Fig.5.5 *(a) Viscosity-Temperature-Pressure 3D plotting of SF6 glass samples; (b) Temperature dependence of Viscosity of SF6 glass under high pressure compared to 1-atm (projection).*

Looking at the viscosity results in Table 1 and Fig.5.5, a discrepancy in the viscosity of the two different sample diameters is quite apparent. The viscosity of SF6 glass with a diameter of 6 mm at 435 ℃ and 3 GPa is 0.25 Log_{10}(Pa·s) higher than the one with 10 mm diameter. The difference in torque with different samples diameters is not uncommon as the displacements

have the stronger influence on the smaller anvils than on the bigger ones concerning the ratio of sample area to the rim. Indeed, the influence of the pressure on the viscosity is rather small of only approximately 0.1 Log_{10}(Pa·s)/GPa. Specifically, the viscosity of SF6 at 435 ℃ and 1GPa is 10.87 Log_{10}(Pa·s), which is even slightly lower than the viscosity at 435 ℃ at 1-atm of 11.01 Log_{10}(Pa·s).

To answer the question if the viscous flow dominates the HPT deformation of SF6 glass, as well as to explain the experimental data, consider the following two cases:

5.5.1.1 Viscous flow induced by dissipative heating

A significant temperature increase can occur during HPT deformation, depending on the rotation speed (Edalati et al., 2011; Zhilyaev & Langdon, 2014). The high pressure (load) may produce viscous heating, and therefore have similar equivalent viscosities, independent of the ambient parameters. If we assume a pure viscous shear heating, the dissipative heating rate is

$$q_{diss} = \int_0^R 2\pi r \cdot \tau(r) \cdot \dot{\varepsilon}(r) \cdot dr \cdot H = \frac{2\eta\pi^3 R^4 f^2}{H} = 2\pi f M_T \qquad (5.8)$$

which under stationary thermal conditions has to be equal to the dissipative heat loss rate of

$$q_{loss} = q_{diss} = \kappa A \Delta T_{diss} \qquad (5.9)$$

where κ is the heat transfer coefficient depending on the material and cooling rate of anvils, *W/(m²K)*, A=$2\pi R^2$ is the heat transfer area (upper and lower sample surfaces), and $\Delta T_{diss} = T_{sample} - T_{measured}$ is the additional temperature difference between the sample the temperature reference point. We assume a κ of 37 W/(m²K) for all the SF6 glass experiments and calculate the dissipative shear heating induced temperature increase reported in Fig.5.6. The calculated temperature increase is too low for some of the measurements at 350 ℃ and too high for some of the measurements at 496 ℃. Therefore, this simple assumption with a constant κ does not explain all measurement results.

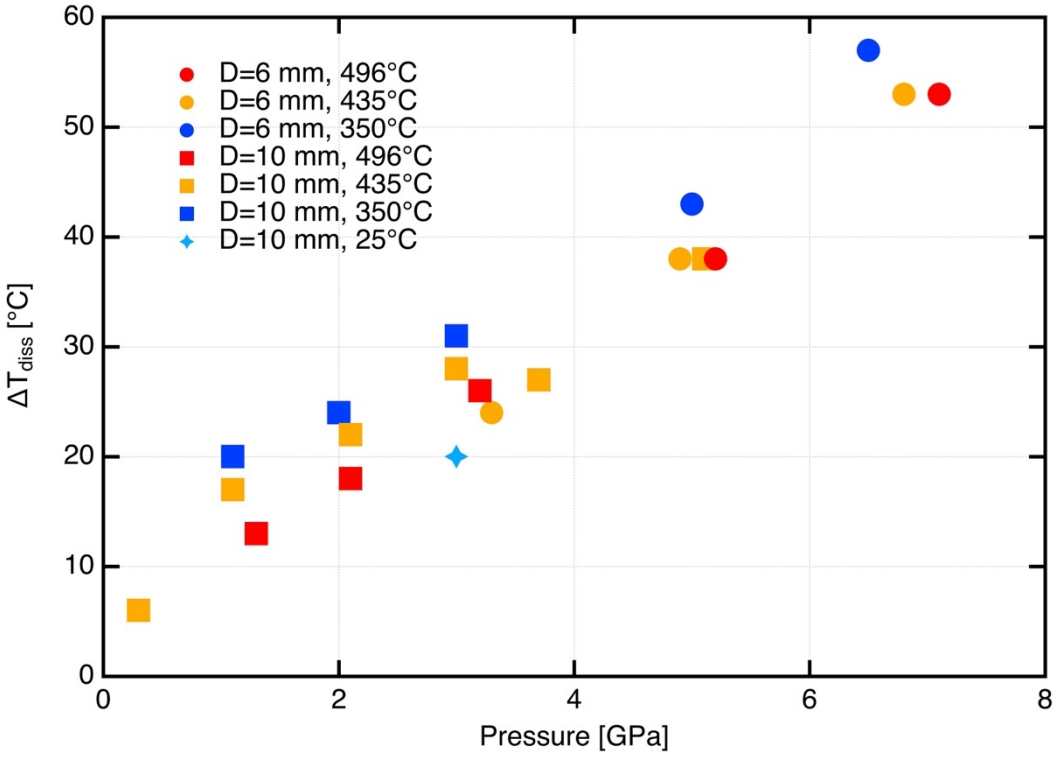

Fig.5.6 *Calculated dissipative shear heating induced temperature increase of SF6 glass as a function of pressure (κ=37 W/(m²K)).*

Additionally, the experiments were performed at a nominal deformation speed of 0.01 RPM. Extrapolating the Results from Edalati et al. (Edalati et al., 2011) and Zhilyaev & Langdon (Zhilyaev & Langdon, 2014) to the speed we applied in this work shows only small heating is to be expected. Using the Vickers hardness HV=3.6 GPa and omega=f=0.0096 RPM for the present case gives only 2 ℃ heating at 2 GPa and 7 ℃ heating at 6 GPa.

5.5.1.2 Viscous flow induced by elastic energy

The elastic energy which is greatly influenced by pressure might also govern the viscous flow of glass in our work. The elastic energy in HPT consists of the elastic shear stress (deviatoric), and the hydrostatic stress (volumetric). E_1 accounts for the shear stress (deviatoric)

$$\frac{1}{H}E_1 = \int_0^R 2\pi r \cdot \frac{1}{2}\sigma_{xy}\delta_{xy} \cdot dr = \int_0^R 2\pi r \cdot \frac{1}{2G}\left(\eta\frac{2\pi r f}{H}\right)^2 \cdot dr = \frac{{M_T}^2}{\pi G R^4} \quad (5.10)$$

where R, H, f, M_T and η are the same as in section 2.3, σ_{xy} is the shear stress, δ_{xy} is the shear strain, G is the shear modulus.

And E_2 accounts for the hydrostatic stress (volumetric). In this work, we assume

$$\frac{1}{V}E_2 = \frac{1}{2}\sigma_{hyd}\varepsilon_{hyd} = \frac{1}{2}\frac{P^2}{K_{ref}} \quad (5.11)$$

where σ_{hyd} is the hydrostatic stress, ε_{hyd} is the bulk strain, P is the hydrostatic pressure, K_{ref} is the reference bulk modulus at ambient pressure.

Thus, we obtain the total elastic energy:

$$\frac{1}{V}E = \frac{1}{V}E_1 + \frac{1}{V}E_2 = \frac{{M_T}^2}{\pi^2 G R^6} + \frac{1}{2}\frac{P^2}{K_{ref}} \qquad (5.12)$$

To assess the equivalent temperature increase ΔT_{elas},

$$E = \rho C_p \, \Delta T_{elas} \qquad (5.13)$$

is used, where ρ is the density measured at room temperature and pressure, and C_p is the heat capacity measured at room temperature and pressure. The resulting ΔT_{elas} as a function of pressure shown in Fig.5.7. The calculated equivalent temperature increase at pressures lower than 3 GPa is smaller than 85 ℃ which cannot explain the data. Therefore, viscous flow activated by elastically stored energy is thus also not the main mechanism for the deformation of SF6 glass via HPT.

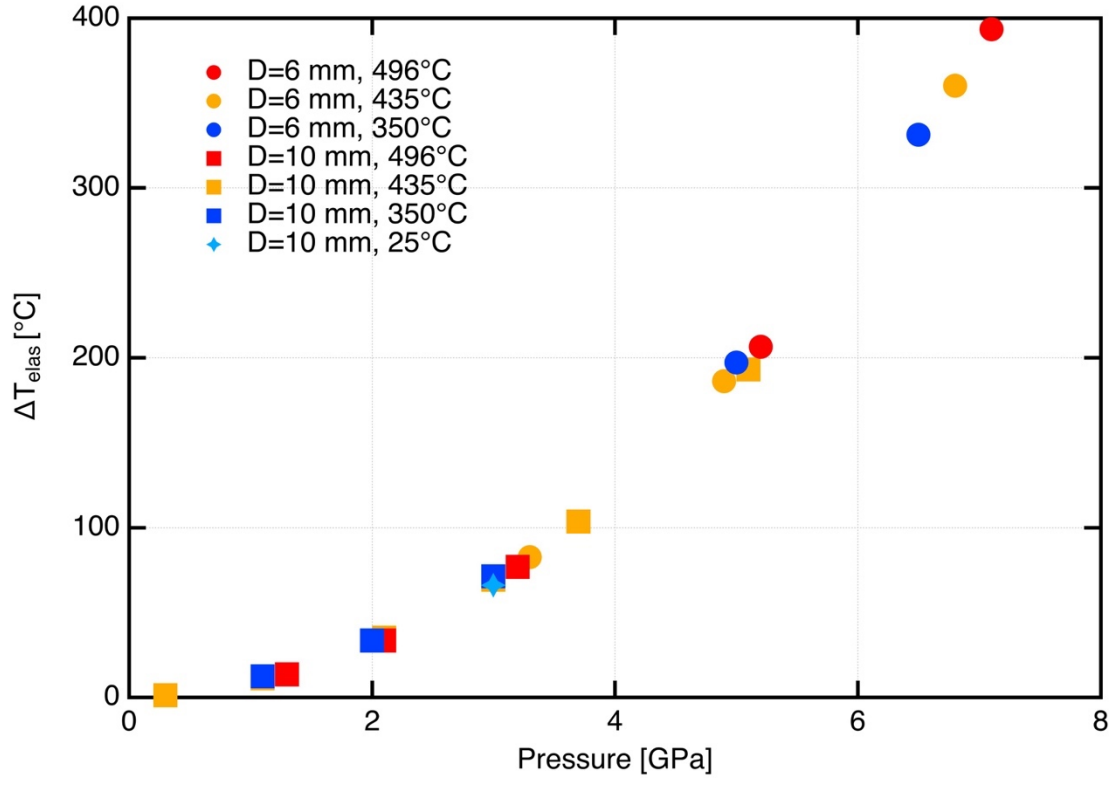

Fig.5.7 *Calculated elastic energy induced temperature increase of SF6 glass as a function of pressure.*

5.5.2 Approach 2: shear yielding

To account for the temperature influence on the yield stress, Raghavan et al. (Raghavan et al., 2015) used the Arrhenius model

$$Y = Y_0 e^{\frac{E_a}{RT}} \quad (5.14)$$

In this work, we extend the Arrhenius equation to Eq. 5.15 by introducing an activation volume as has been reported in other studies (Ding et al., 2018; Jin et al., 2003) to account for the pressure effect.

$$Y = Y_0 e^{\frac{E_a + PV_a}{RT}} \quad (5.15)$$

where Y_0 is a hypothetical yield stress at infinite temperature, E_a is the activation energy, and V_a is the activation volume. To keep the model simple, we apply one set of constant Y_0, E_a and V_a parameters to fit all the yield stress data.

The experiments were performed at the same constant strain rate for two different sample diameters. The apparent activation energy E_a can be determined from a linear fit to the plots in Fig. 8(a). The SF6 glass during HPT deformation exhibited very low activation energy of only around 1 kJ/mol compared to the activation energy of 515 kJ/mol at ambient pressure for viscous flow. Similarly, Fig.5.8(b) is used to obtain the apparent activation volume V_a. The calculated V_a varies from 1.16 cm^3/mol to 2.06 cm^3/mol, which is close to the activation energy of SCHOTT N-BK7® glass of ~2 cm^3/mol reported by Ding et al. (Ding et al.,2018a; Ding et al., 2018b). Moreover, Fig.5.8(b) shows that the yield stress increases with increasing pressure.

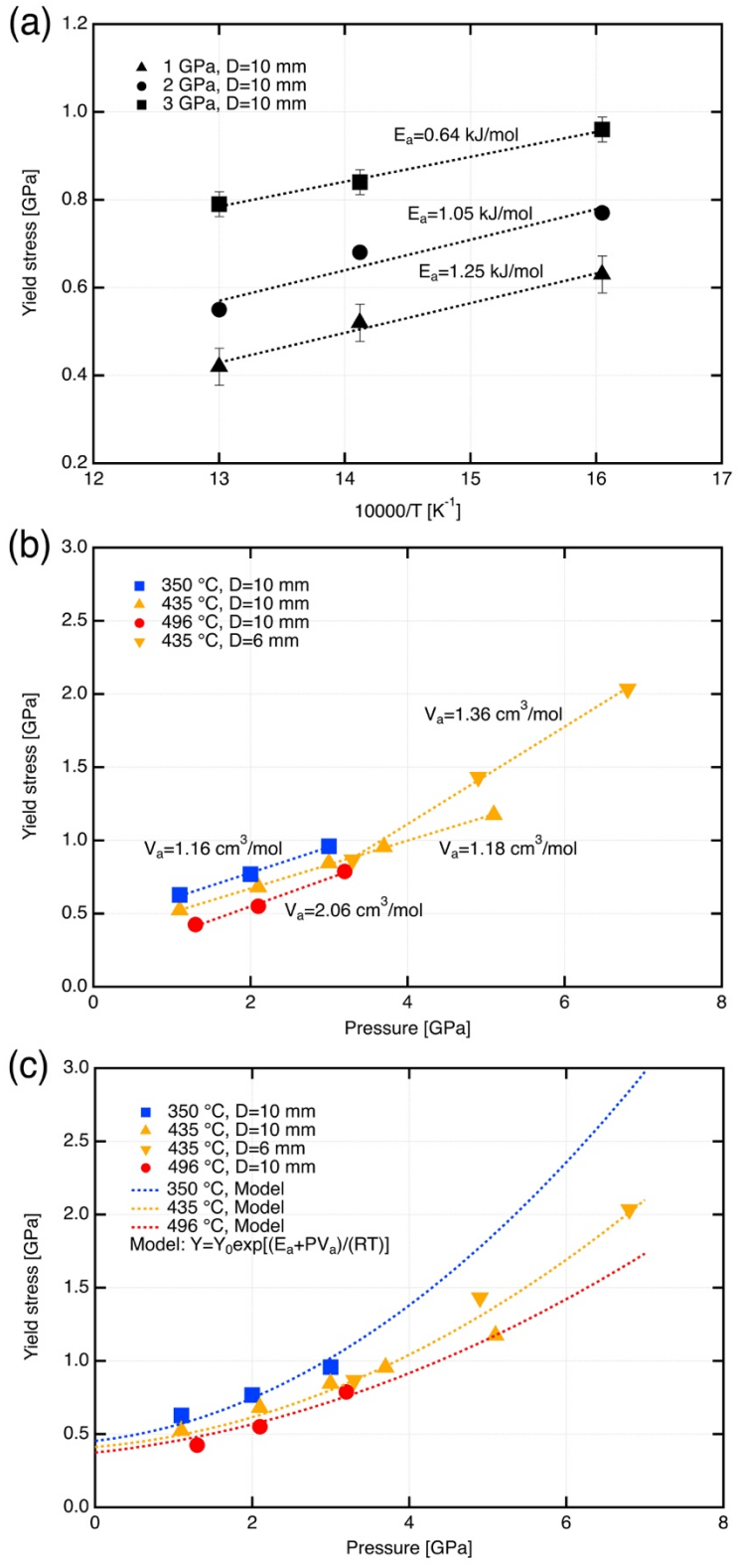

Fig.5.8 *(a) Yield stress of SF6 glass deformed in HPT as a function of pressure to determine the apparent activation volume; (b) Temperature dependence of the yield stress to determine the apparent activation energy of SF6 glass during HPT deformation; (c) Yield stress calculated from the HPT measurements fitted by an Arrhenius type model.*

However, the SF6 glass samples deformed at 435 ℃ under 0.3 GPa and at room temperature at 3 GPa cannot be fitted with the proposed Arrhenius type model. For the former, the low pressure (by manual loading) might not suppress sliding as well as for the higher pressures. For the latter, we recall the big noise heard from the sample deformed at room temperature under 3GPa. The big noise during the high-pressure loading indicates that a brittle fracture occurred, which opening the bulk glass sample and lower the torque. On the other hand, the cracking of glass generates various fine powders in the sample, which might be another important mechanism for glass flow at room temperature. Indeed, the particle size of glass influences the ability of the glass flow (Wong, 2000).

To fit the experimental data, we employ a multidimensional unconstrained nonlinear minimization optimization algorithm (using the MATLAB function fminsearch (Lagarias et al., 1998)), to find the best-fit parameters for the model. Fig. 8(c) displays that the Arrhenius type model can coarsely describe the experimental yield stress calculation with the parameters $Y_0 =$ 0.17 GPa, $E_a = 4.83$ kJ/mol and $V_a = 1.42$ cm^3/mol. The best-fit activation energy is slightly higher than the calculation in Fig. 8(a), and the best-fit activation volume is in agreement with the calculation in Fig.5.8(b). The model also extrapolates the yield stress at ambient pressure decreases with increasing temperatures, with ~0.44 GPa at 350 ℃, ~0.39 GPa at 435 ℃, and 0.37 GPa at 496 ℃, respectively. We note that the fitting is only in coarse agreement with the experimental data, and some slight differences remain in the slope of the experimental data and model, which may result from systematic deviations. Yet the model is better than the other explanations even in its basic version.

5.5.2.1 Pure friction?

Considering that all the deformation experiments exhibit similar activation energy, one other possible reason could be sliding between the glass samples and anvils. The friction coefficient determined according to Eq. 5.7 and plotted in Fig.5.9 apparently decreases with increasing temperature in the 10 mm anvils setup and is thus not a possible explanation for the torques measured. Furthermore, the samples (even for the 0.3 GPa case at least at one sample side) showed well surface characteristics/markings of the anvil, most notably scratches. This is a strong indication that in this area no sliding was present and that thus the overall amount of sliding should not be dominant.

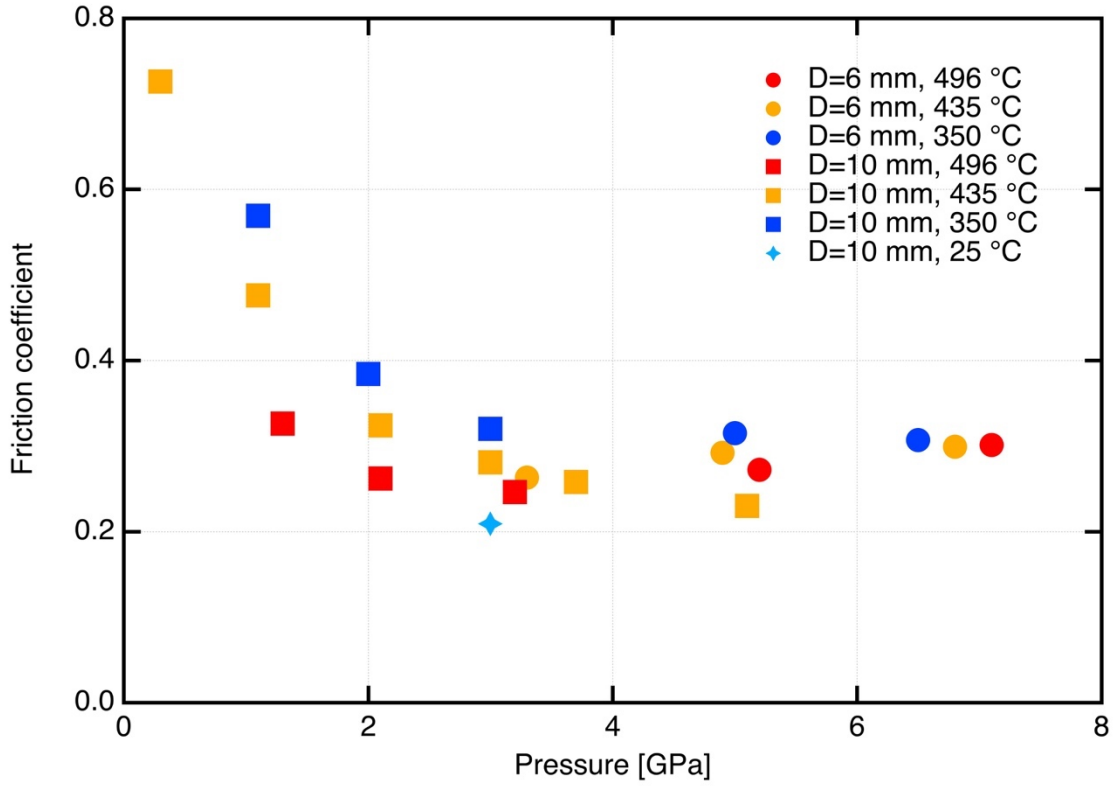

Fig.5.9 *Friction coefficient of SF6 glass as a function of pressure in HPT.*

5.6 Conclusions

Deformation experiments were performed on SCHOTT SF6® in an HPT apparatus under high pressure and different temperatures. From several approaches tested, the mechanism of plastic shear yielding during the HPT experiments on SF6 offers the most likely explanation for the measured results. This yield stress of SF6 glass decreases with increasing temperature and decreasing pressure. An extended Arrhenius model was applied and shown that it can explain the experimental results of SF6 glass, with some short-comings.

5.7 Acknowledgments

Linfeng Ding is funding by the European Union's Horizon 2020 research and innovation program under the Marie Sklodowska-Curie grant agreement N° 642029. The authors thank the technicians and engineers at the SCHOTT machine-shop for the sample preparation.

5.8 References

Adam, G. & Gibbs, J. H. (1965). On the Temperature Dependence of Cooperative Relaxation Properties in Glass-Forming Liquids. *The Journal of Chemical Physics*, 43 (1): 139-146.

Alkorta, J., Martinez-Esnaola, J. M. & Sevillano, J. G. (2005). Absence of one-to-one correspondence between elastoplastic properties and sharp-indentation load-penetration data. *Journal of Materials Research*, 20 (5): 1369-1369.

Avramov, I. (2000). Pressure dependence of viscosity of glassforming melts. *Journal of Non-Crystalline Solids*, 262 (1-3): 258-263.

Bachmaier, A., Kerber, M., Setman, D. & Pippan, R. (2012). The formation of supersaturated solid solutions in Fe-Cu alloys deformed by high-pressure torsion. *Acta Materialia*, 60 (3): 860-871.

Cohen, M. H. & Turnbull, D. (1959). Molecular Transport in Liquids and Glasses. *Journal of Chemical Physics*, 31 (5): 1164-1169.

Cook, R. L., King, H. E., Herbst, C. A. & Herschbach, D. R. (1994). Pressure and temperature dependent viscosity of two glass forming liquids: Glycerol and dibutyl phthalate. *The Journal of Chemical Physics*, 100 (7): 5178.

Demetriou, M. D., Launey, M. E., Garrett, G., Schramm, J. P., Hofmann, D. C., Johnson, W. L. & Ritchie, R. O. (2011). A damage-tolerant glass. *Nature Materials*, 10 (2): 123-128.

Ding, L., Thieme, M., Demouchy, S., Kunisch, C. & Kaus, B. J. P. Effect of pressure and temperature on viscosity of a borosilicate glass. *Journal of the American Ceramic Society*, 0 (0).

Ding, L., Buhre, S., Kunisch, C. & Kaus, B. (2018). Pressure dependence of density and structural relaxation of glass near the glass transition region. *Journal of the American Ceramic Society*, 101 (3): 1149-1158.

Donovan, P. E. (1989). A Yield Criterion for Pd40ni40p20 Metallic-Glass. *Acta Metallurgica*, 37 (2): 445-456.

Edalati, K., Miresmaeili, R., Horita, Z., Kanayama, H. & Pippan, R. (2011). Significance of temperature increase in processing by high-pressure torsion. *Materials Science and Engineering a-Structural Materials Properties Microstructure and Processing*, 528 (24): 7301-7305.

Fulcher, G. S. (1925). Analysis of recent measurements of the viscosity of glasses. *Journal of the American Ceramic Society*, 8 (6): 339-355.

Grassia, L. & Simon, S. L. (2012). Modeling volume relaxation of amorphous polymers: Modification of the equation for the relaxation time in the KAHR model. *Polymer*, 53 (16): 3613-3620.

Greet, R. J. & Turnbull, D. (1967). Test of Adam-Gibbs Liquid Viscosity Model with O-Terphenyl Specific-Heat Data. *Journal of Chemical Physics*, 47 (6): 2185-2190.

Hodge, I. M. (1994). Enthalpy Relaxation and Recovery in Amorphous Materials. *Journal of Non-Crystalline Solids*, 169 (3): 211-266.

Inoue, A., Shen, B. L., Koshiba, H., Kato, H. & Yavari, A. R. (2003). Cobalt-based bulk glassy alloy with ultrahigh strength and soft magnetic properties. *Nature Materials*, 2 (10): 661-663.

Jin, H. J., Gu, X. J., Wen, P., Wang, L. B. & Lu, K. (2003). Pressure effect on the structural relaxation and glass transition in metallic glasses. *Acta Materialia*, 51 (20): 6219-6231.

Lagarias, J. C., Reeds, J. A., Wright, M. H. & Wright, P. E. (1998). Convergence properties of the Nelder-Mead simplex method in low dimensions. *Siam Journal on Optimization*, 9 (1): 112-147.

Lee, E. H. & Radok, J. R. M. (1960). The Contact Problem for Viscoelastic Bodies. *Journal of Applied Mechanics*, 27 (3): 438-444.

Mauro, J. C., Yue, Y. Z., Ellison, A. J., Gupta, P. K. & Allan, D. C. (2009). Viscosity of glass-forming liquids. *Proceedings of the National Academy of Sciences of the United States of America*, 106 (47): 19780-19784.

Nanzai, Y. (1993). Molecular Kinetics of Yield Deformation and Ductile Fracture in Polymer Glasses. *Progress in Polymer Science*, 18 (3): 437-479.

Paterson, M. (1990). Rock deformation experimentation. *Geophysical monograph*: 187-194.

Peter, K. (1970). Densification and flow phenomena of glass in indentation experiments. *Journal of Non-Crystalline Solids*, 5 (2): 103-115.

Raghavan, R., Harzer, T. P., Chawla, V., Djaziri, S., Phillipi, B., Wehrs, J., Wheeler, J. M., Miehler, J. & Dehm, G. (2015). Comparing small scale plasticity of copper-chromium nanolayered and alloyed thin films at elevated temperatures. *Acta Materialia*, 93: 175-186.

Schuh, C. A. & Lund, A. C. (2003). Atomistic basis for the plastic yield criterion of metallic glass. *Nature Materials*, 2 (7): 449-452.

Schulze, F., Behrens, H. & Hurkuck, W. (1999). Determination of the influence of pressure and dissolved water on the viscosity of highly viscous melts: Application of a new parallel-plate viscometer. *American Mineralogist*, 84 (10): 1512-1520.

Shang, H. X. & Rouxel, T. (2005). Creep behavior of soda-lime glass in the 100-500 K temperature range by indentation creep test. *Journal of the American Ceramic Society*, 88 (9): 2625-2628.

Simon, S. L., Park, J. Y. & McKenna, G. B. (2002). Enthalpy recovery of a glass-forming liquid constrained in a nanoporous matrix: Negative pressure effects. *European Physical Journal E*, 8 (2): 209-216.

Sperry, L. & JD, M. (1968). Pressure dependence of viscosity of B_2O_3. *PHYSICS AND CHEMISTRY OF GLASSES*, 9 (3): 91-95.

To, T., Célarié, F., Roux-Langlois, C., Bazin, A., Gueguen, Y., Orain, H., Le Fur, M., Burgaud, V. & Rouxel, T. (2018). Fracture toughness, fracture energy and slow crack growth of glass as investigated by the Single-Edge Precracked Beam (SEPB) and Chevron-Notched Beam (CNB) methods. *Acta Materialia*, 146: 1-11.

Tribone, J. J., Oreilly, J. M. & Greener, J. (1989). Pressure-Jump Volume-Relaxation Studies of Polystyrene in the Glass-Transition Region. *Journal of Polymer Science Part B-Polymer Physics*, 27 (4): 837-857.

Turnbull, D. & Cohen, M. H. (1970). On the Free- Volume Model of the Liquid- Glass Transition. *The journal of chemical physics*, 52 (6): 3038-3041.

Vaidyanathan, R., Dao, M., Ravichandran, G. & Suresh, S. (2001). Study of mechanical deformation in bulk metallic glass through instrumented indentation. *Acta Materialia*, 49 (18): 3781-3789.

Vorhauer, A. & Pippan, R. (2004). On the homogeneity of deformation by high pressure torsion. *Scripta Materialia*, 51 (9): 921-925.

Williams, M. L., Landel, R. F. & Ferry, J. D. (1955). The Temperature Dependence of Relaxation Mechanisms in Amorphous Polymers and Other Glass-Forming Liquids. *Journal of the American Chemical Society*, 77 (14): 3701-3707.

Wong, A. C. Y. (2000). Characterisation of the flowability of glass beads by bulk densities ratio. *Chemical Engineering Science*, 55 (18): 3855-3859.

Xi, X. K., Zhao, D. Q., Pan, M. X., Wang, W. H., Wu, Y. & Lewandowski, J. J. (2005). Fracture of brittle metallic glasses: Brittleness or plasticity. *Physical Review Letters*, 94 (12).

Xu, W., Edwards, D., Wu, X., Stoica, M., Calin, M., Kühn, U., Eckert, J. & Xia, K. (2013). Promoting nano/ultrafine-duplex structure via accelerated α precipitation in a β-type titanium alloy severely deformed by high-pressure torsion. *Scripta Materialia*, 68 (1): 67-70.

Zheng, Q. J. & Mauro, J. C. (2017). Viscosity of glass-forming systems. *Journal of the American Ceramic Society*, 100 (1): 6-25.

Zhilyaev, A. P., Nurislamova, G. V., Kim, B. K., Baro, M. D., Szpunar, J. A. & Langdon, T. G. (2003). Experimental parameters influencing grain refinement and microstructural

evolution during high-pressure torsion. *Acta Materialia*, 51 (3): 753-765.

Zhilyaev, A. P. & Langdon, T. G. (2014). Reassessment of temperature increase and equivalent strain calculation during high-pressure torsion. *6th International Conference on Nanomaterials by Severe Plastic Deformation (Nanospd6)*, 63.

Chapter 6

6. Conclusions and perspectives

6.1 Conclusions

In this thesis, experiments and models were applied to study: (i) the volumetric relaxation of glass after high-pressure treatment near the glass transition region in Piston-cylinder apparatus; (ii) the deviatoric uniaxial deformation of glass under high pressure in Paterson press; (iii) the deviatoric torsional deformation of glass in high-pressure torsion apparatus. The main results and findings are briefly summarized below.

- The effects of high pressure on density and volume recovery of SCHOTT N-BK7® glass near the glass transition region has been measured and quantitatively described in this work by applying the static high-pressure in Piston-cylinder apparatus. A simplified and effective pressure cell (2#) together with an experimental process is developed to compress glass at high pressures around the transition region using a piston-cylinder apparatus. Glass samples can be effectively densified in the piston cylinder apparatus with an approximately linear increase in density at increasing pressure. A mathematical model with two internal parameters is developed that describes the volume recovery of all samples with a single set of parameters.
- The deviatoric deformation experiments in uniaxial compression on SCHOTT N-BK7® glass were performed at temperatures near the glass transition temperature (561 °C) and at confining pressures of 100 to 300 MPa in Paterson press. The main results of this part are: The viscosity of SCHOTT N-BK7® glass increases linearly with increasing pressure at ~0.1 $\log_{10}$(Pa·s)/100 MPa in the range of confining pressure investigated. The pressure dependence of viscosity measured in this study (~0.1 $\log_{10}$(Pa·s)/100 MPa) is consistent with the latest two-internal-parameter relaxation model. At the same temperature and the same pressure, the viscosity measured in this study is approximately +1.0 $\log_{10}$(Pa·s) higher than in (Ding et al., 2018). The reason for this discrepancy has not been identified clearly. The mechanical data can be overall fitted by a Maxwell viscoelastic model with two parallel elements.
- The deviatoric torsional deformation experiments were performed in high-pressure torsion (HPT) apparatus to deform the SCHOTT SF6® glass subjected to pressures from 0.3 GPa to 7 GPa and temperatures from 25 ℃ to 496 ℃. Results show that the plastic yield deformation was occurring during the HPT experiments on the SF6 glass at elevated temperature from 350 ℃ to 496 ℃. The yield stress of SF6 glass decreases with increasing temperature and decreasing pressure. An extended Arrhenius model with one set of parameters, namely infinite yield stress Y_0=0.17 GPa, activation energy E_a=4.83 kJ/mol and activation volume V_a=1.42 cm^3/mol, can explain the experimental results well.

6.2 Limitations and perspectives

6.2.1 Limitations

There are still some limitations in this work:

(1) The experimental process for the study on the volumetric flow glass can be improved. For example, ① the heating temperature of high-pressure treatment in Piston-Cylinder apparatus can be lower than 700 ℃, and the thermal holding time also can be shorter than 24 hours. Based on the model, the N-BK7 glass is viscous enough at 580 ℃ under 1.5 GPa, and a thermal holding of 2 hours is enough for glass to reach the equilibrium; ② the thermal holding time for volume recovery can be shorter than 72 hours. Based on the experimental results, 24 hours is enough for all the compressed glass samples in this work reach the equilibrium state at 525 ℃.

(2) The 2-internal-parameter relaxation model can be extended by introducing multi fictive temperatures and fictive pressures with better fitting. The MATLAB function fminsearch can be applied to find the best-fit parameters.

(3) More Maxwell model elements (e.g., 3-5) can be tested on fitting the mechanical results from Paterson press.

(4) At the same temperature and the same pressure, the viscosity measured from the deviatoric flow (Chapter 4) is approximately +1.0 $\log_{10}$ (Pa·s) higher than in the volumetric flow (Chapter 3). The reason for this discrepancy has not been identified clearly.

6.2.2 Perspectives

Much work is still needed in the future for a better understanding of the pressure dependence of the rheology of glass. Possible future research should cover the following topics:

(1) The hydrostatic pressure condition was questioned by the reviewers in the study of the volumetric flow of glass using the Piston-cylinder apparatus with the solid medium pressure cell (NaCl). The gas medium high-pressure apparatus is known to generate the most hydrostatic high-pressure, therefore, apply the gas medium apparatus (e.g., Paterson press) to study the volumetric flow of glass and check the quality of this work will be interesting. The first step results suggest that the state in Chapter 3 is hydrostatic predominantly.

(2) The model in Chapter 5 can be developed to more complex one to predict the yielding stress of glass at room temperature under high pressure. Much work can be done by connecting the viscoelasticity and yield stress on glass-forming materials. For example, the HPT tool can be developed with much lower torsional speed to separate the viscous flow and plastic yielding of glass.

Appendix 1

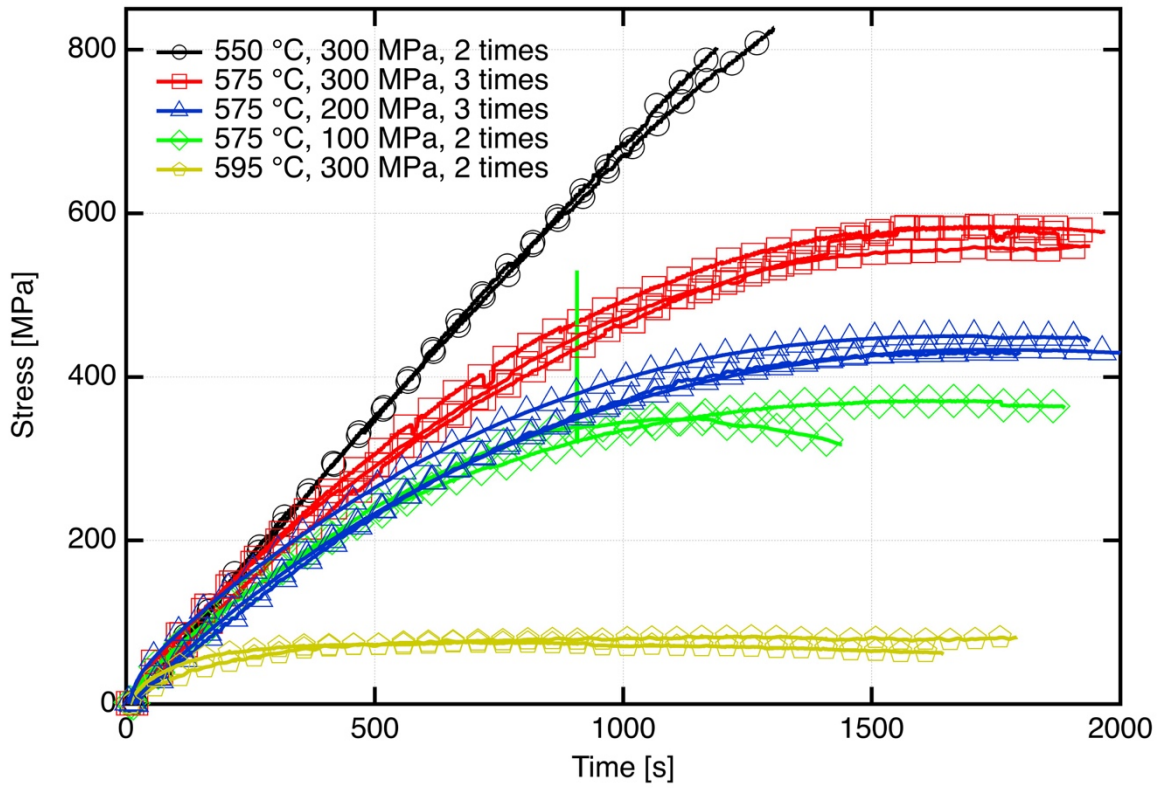

Fig. S1 *The stress-time curves of the experiments. Identical color is used for the repeated experiments with the same experimental conditions.*

Acknowledgement

This project has received funding from the European Union's Horizon 2020 research and innovation program under the Marie Sklodowska-Curie grant agreement N° 642029, CREEP. I greatly appreciate that I had the chance to join the CREEP Innovative Training Network. The CREEP network is an excellent platform for training and career development.